


For Reference

NOT TO BE TAKEN FROM THIS ROOM

Ex LIBRIS
UNIVERSITATIS
ALBERTAENSIS





Digitized by the Internet Archive
in 2022 with funding from
University of Alberta Library

<https://archive.org/details/Betty1977>

THE UNIVERSITY OF ALBERTA

DEVELOPMENT AND CHARACTERIZATION OF CORRELATION
INSTRUMENTATION FOR CHEMICAL MEASUREMENTS

by



KEITH ROGER BETTY

A THESIS

SUBMITTED TO THE FACULTY OF GRADUATE STUDIES AND RESEARCH
IN PARTIAL FULFILMENT OF THE REQUIREMENTS FOR THE DEGREE
OF DOCTOR OF PHILOSOPHY

DEPARTMENT OF CHEMISTRY

EDMONTON, ALBERTA

SPRING, 1977

ABSTRACT

Many hardware and software processing operations carried out on chemical data can be classified as correlation operations. These include such processes as signal-to-noise ratio enhancement using lock-in detection, autocorrelation, digital filtering, transversal filtering, differentiation, signal detection using matched filtering, and pattern recognition. Recent advances in solid-state electronics and in computer technology have facilitated both the hardware and software implementation of correlation data processing operations. It is shown in this study that such technological developments allow the evolution of powerful and inexpensive systems for the correlation processing of chemical data.

Lock-in amplification, which involves the cross-correlation of a periodically modulated signal with a reference waveform of the same frequency, is one of the most common signal measurements used in the chemical laboratory. In the first part of this study, it is shown that the conventional design of a lock-in amplifier can be enhanced and simplified with a single integrated circuit known as a phase locked loop. Then a new type of integrated circuit is described that is uniquely suited to the development of autocorrelation

instrumentation. Autocorrelation is an effective signal processing technique for recovering both the amplitude and frequency of a periodic signal buried in noise. A noisy sine wave signal ($S/N < 0.2$) can easily be recovered using the autocorrelator.

A particularly effective way of detecting and quantifying a specific spectral pattern in a complex spectral signal is to cross-correlate the signal with the sought-for spectral pattern. A hardware cross-correlator based on a specially designed transient recorder was built and used in conjunction with a diode array spectrometer to measure the atomic emission of several elements in an inductively coupled plasma. The correlation approach provides a unique lock-and-key measurement that allows a highly automated and selective analytical measurement.

A number of correlation signal processing operations can be performed using software-based digital filters. It is shown that a Fourier domain digital filter (applied to the Fourier transform of a signal) based on a simple trapezoidal function forms a particularly versatile approach that can approximate the processing capabilities of the popular correlation filters developed by Savitzky and Golay. Finally, it is shown that correlation filters such as those of Savitzky and Golay can be implemented on signals in real time by

using a new and powerful integrated circuit known as a tapped analog delay line. This device stores and makes available in parallel form a short sampled segment of an input waveform. The characteristics and applications of this device to the correlation (transversal) filtering of analog signals in real time are discussed and illustrated in detail.

ACKNOWLEDGEMENT

I would like to acknowledge the understanding and assistance given by Dr. G. Horlick.

TABLE OF CONTENTS

	<u>Page</u>
CHAPTER	
I. INTRODUCTION	1
What is Correlation?	2
Cross-Correlation	9
Convolution	10
Fourier Transformation	11
Correlation Instrumentation	14
II. LOCK-IN AMPLIFICATION	18
Background	18
Experimental	26
Results and Discussion	27
III. AUTOCORRELATION: THE SERIAL ANALOG MEMORY . .	38
Background	38
Serial Analog Memories	40
Experimental	46
Results and Discussion	56
Conclusion	64
IV. CROSS-CORRELATION I: A HARDWARE CORRELATOR . .	66
Background	66
The Transient Recorder	71
Experimental	89
Inductively Coupled Plasma	89
Chemicals	90
Instrumentation	90
Readout System	94
Results and Discussion	96
Conclusions	110
V. DIGITAL FILTERING	113
Background	113
A. The Fourier Transform Route	115
Experimental	115
Results and Discussion	119
B. Frequency Response of Savitzky- Golay Filter Functions	129

	<u>Page</u>
CHAPTER	
VI. CROSS-CORRELATION II: THE TAPPED ANALOG DELAY LINE	138
Background	138
Experimental	140
Results and Discussion	142
Conclusions	164
VII. SUMMARY	166
BIBLIOGRAPHY	168
APPENDIX I	174
APPENDIX II	180

LIST OF TABLES

<u>Table</u>	<u>Description</u>	<u>Page</u>
I	Lock-In Amplifier Linearity and Dynamic Range	31
II	Operating Conditions of ICP and Spectrometer	91
III	Generation of TAD Resistor Values from Savitzky-Golay Weights	158

LIST OF FIGURES

<u>Figure</u>	<u>Description</u>	<u>Page</u>
1.	Autocorrelation of sine and square waves.	5
2.	Generalized autocorrelation.	7
3.	Convolution and correlation.	12
4.	Block diagram of a correlator.	15
5.	Block diagram of a lock-in amplifier.	20
6.	Block diagram of a phase locked loop.	22
7.	Block diagram of the Signetics 561 phase locked loop.	25
8.	Circuit diagram for a lock-in amplifier based on the Signetics 561 phase locked loop.	28
9.	Circuit diagram for a lock-in amplifier based on Figure 5b.	33
10.	Log-log plots of output vs input for "referenceless" lock-in amplifiers.	36
11.	Block diagram of the Serial Analog Memory.	42
12.	Simple block diagram of the autocorrelator.	45
13.	Block diagram of the autocorrelator.	47
14.	Circuit diagram of the autocorrelator.	51
15.	Log-log plots of output vs input for the SAM and autocorrelator.	59
16.	Recorder output of autocorrelation functions.	63
17.	Cobalt, nickel and iron spectra.	68
18.	Cross-correlation of line spectra.	69
19.	Block diagram of hardware correlator.	72
20.	Block diagram of transient recorder.	74

<u>Figure</u>	<u>Description</u>	<u>Page</u>
21.	Circuit diagram of transient recorder.	76
22.	Transient recorder with waveform subtraction.	81
23.	Memory subdivision and background subtraction capabilities of transient recorder.	86
24.	Use of transient recorder pretrigger.	87
25.	Circuit diagram of hardware correlator.	92
26.	Output vs input of hardware correlator for sine wave signals.	95
27.	Correlator output and software peak area for calcium standards.	100
28.	Correlator output vs chromium concentration for 2.16 sec integration time.	102
29.	Correlator output vs chromium concentration for 14.4 sec integration time.	103
30.	Spectrometer output for chromium solutions.	104
31.	Effect of stripping an interfering species.	109
32.	Direct cross-correlation and Fourier domain filtering.	114
33.	Fourier domain digital filters.	118
34.	Second derivative and "deconvolution" Fourier domain filters.	120
35.	Removal and analysis of high frequency noise from a spectral signal.	122
36.	Removal of fixed frequency noise and minimization of quantization noise on spectral signals.	123
37.	Resolution enhancement of spectral signals.	126

<u>Figure</u>	<u>Description</u>	<u>Page</u>
38.	Savitzky-Golay filters and their frequency responses, filters I to VI.	131
39.	Savitzky-Golay filters and their frequency responses, filters VII to XI.	132
40.	Frequency response of a Savitzky-Golay filter and an RC low pass filter.	134
41.	Transversal filter.	139
42.	TAD transversal filter.	141
43.	Output vs input of the TAD.	143
44.	Frequency and phase responses for symmetrical exponential filter.	148
45.	Full range frequency and phase responses of symmetrical exponential filter.	149
46.	Frequency and phase responses of one-sided exponential filter.	151
47.	Resymmetrization of phase shifted peaks.	153
48.	Frequency response of first derivative filter.	156
49.	Frequency responses of theoretical and actual second derivative filters.	162
50.	Block diagram of the SERDEX module.	175
51.	Circuit diagram of SERDEX implementation.	177

LIST OF PHOTOGRAPHIC PLATES

<u>Plate</u>	<u>Description</u>	<u>Page</u>
1.	Autocorrelation of sine, triangular and square waves.	57
2.	Autocorrelation of noisy sine waves.	61
3.	Normal and memory subdivision modes of the transient recorder.	85
4.	Use of the correlator for calcium determination.	98
5.	Correlation with a stripped reference.	107
6.	Application of a symmetrical exponential TAD transversal filter.	145
7.	Application of a TAD transversal filter to "differentiation" of a square wave.	155
8.	Second derivative resolution enhancement.	160

CHAPTER I

The technique of correlation has long been a ubiquitous part of the acquisition and treatment of scientific data. An early worker in the field of communications was Lee (1), who later reviewed the topic in detail (2). In chemistry, there have been several general treatments of correlation techniques (3-6) as well as a large number of detailed applications. Correlation, and the related techniques of convolution and Fourier transformation, can be implemented by instruments as conceptually simple as the lock-in amplifier, or as complex and expensive as the hardware correlators available from companies such as Hewlett-Packard. It is also possible to perform correlations on a digital computer. The use of correlation methods has, however, been limited both by a lack of understanding of the technique, and, because of the frequent requirement to store and manipulate arrays of data, by the lack or high cost of the equipment required. Lately, the remarkable progress made in integrated-circuit technology has made devices available that can enable correlations to be performed simply and inexpensively by hardware, while the advent of the minicomputer and now the microcomputer has greatly increased the facility of software correlations. Because of the tremendous power of correlation

techniques to perform a wide variety of operations, and because of the universality of application of the resulting instrumentation, the purpose of this work is to simplify the use of correlation for the measurement of chemical data, both by the design of old instrumentation in new ways and by the design of new instrumentation and techniques that can extract information in different ways. The resulting instrumentation can be used for tasks that vary from signal-to-noise ratio enhancement or resolution enhancement, to matched filtering and pattern recognition. Initially, however, a brief introduction to the mathematics of correlation, convolution, and Fourier transformation will be given. This discussion will be based in part on material presented elsewhere (3, 6-8).

What is Correlation?

Correlation is a computational technique for determining the coherence within a signal, or between two signals. Mathematically, it is generally expressed as the correlation integral:

$$C_{ab}(\tau) = \lim_{t \rightarrow \infty} \frac{1}{2t} \int_{-t}^{+t} a(t)b(t \pm \tau) dt \quad (1)$$

where $C_{ab}(\tau)$ is the correlation function of the two signals $a(t)$ and $b(t)$, while τ is their relative displacement. Evaluation of this integral requires either a hardwired processor that might be analog or digital or both, or a digital computer. The calculation thus may be based either on a continuous function over the interval $+t$ to $-t$, or on a sampled function. In the latter case, the correlation integral is usually expressed by a sum:

$$C_{ab}(\tau) = \sum_t a(t)b(t \pm n\Delta t) \quad (2)$$

$$n = 0, 1, 2 \dots$$

where Δt is the sampling interval. This definition requires that the displacement only occur as an integral multiple of the sampling interval.

Two different correlation operations can be identified. If $a(t)$ and $b(t)$ are identical (i.e. if $a=b$), an autocorrelation function is obtained by application of Equation 1. Thus autocorrelation indicates whether coherence exists within a signal. In contrast, a cross-correlation function, produced if $a(t)$ and $b(t)$ are different, shows the similarities between two signals.

To illustrate the process of correlation consider the autocorrelation of a sine wave as shown in

Figure 1a. In the first frame the sine wave is multiplied by itself in phase, i.e. $\tau=0^\circ$. The result as illustrated is a sine^2 wave. To complete the evaluation of the autocorrelation function at this relative displacement the average value of the sine^2 wave must be determined (see Equation 1). The dashed line indicates this value. This first point of the autocorrelation is plotted in the lower part of Figure 1a and represents the mean square value of the original sine wave.

In the successive frames of Figure 1a the evaluation of the autocorrelation function at τ values of 90° , 180° , and 270° is illustrated. From the plot of the autocorrelation function C_{aa} in Figure 1a it should be apparent that the autocorrelation operation applied to any sinusoidal wave of indeterminate phase converts it to a cosine wave. Thus phase information contained in the original sine wave is lost. However, the amplitude and frequency (or period) of the autocorrelation function are unambiguously related to those of the original sine wave. The period of the two are identical while the amplitude of the autocorrelation function is the mean square of the original sine wave.

The autocorrelation function of any periodic waveform will display similar characteristics since any such waveform, as can be shown by Fourier analysis, is

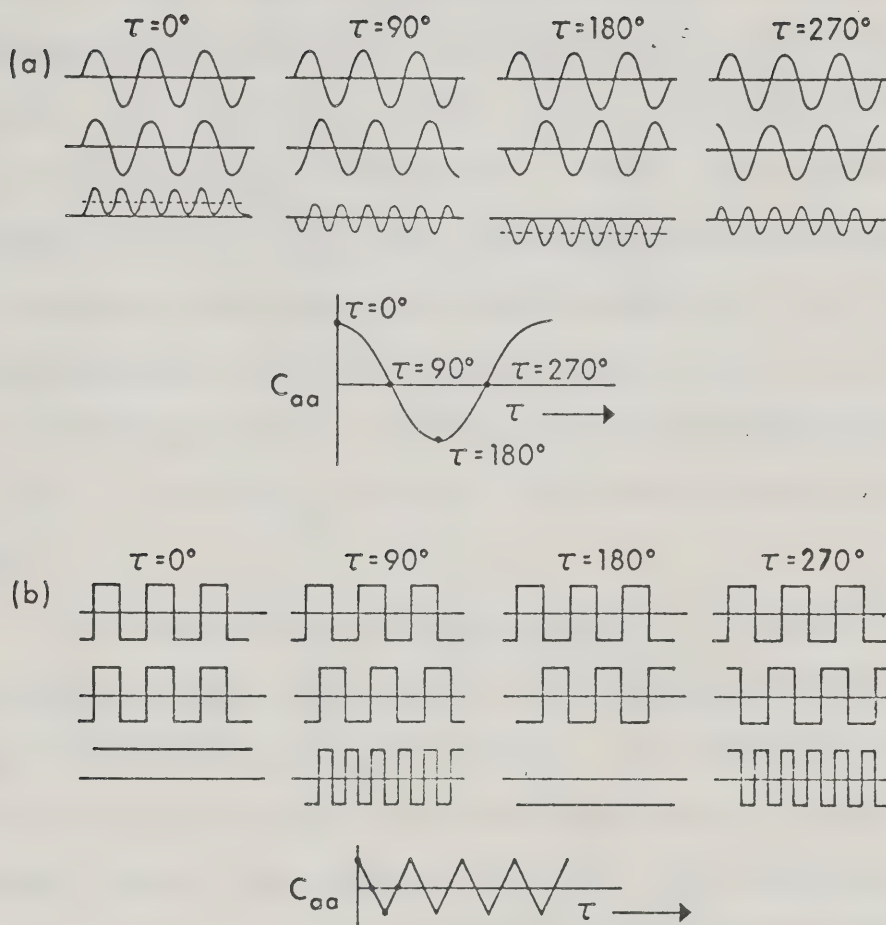


Figure 1. (a) Autocorrelation of a sine wave. (b) Autocorrelation of a square wave.

just a combination of a number of sine waves, each with its own amplitude and phase characteristics. But, as mentioned above, although frequency and amplitude information about the original waveform is carried in the autocorrelation function, the phase information in the original signal is lost. This fact is emphasized by the autocorrelation function of a square wave generated as shown in Figure 1b. The triangle wave autocorrelation function contains the same frequencies (i.e. sine wave components) as the original square wave, however, in the triangular wave all the sine wave components are in phase at $\tau=0^\circ$ and produce a different summation wave shape.

Autocorrelation of non-periodic or random (noise) waveforms produces markedly different results from those obtained for periodic waves. To understand this, we need only recognize again that any wave, whether periodic or not, is composed of sine wave components. Each of these components, when autocorrelated, will produce a cosine wave beginning at $\tau=0$. When many such components are present in a parent waveform, the resulting autocorrelation will just be the sum of the autocorrelation functions of the components. Four such autocorrelation images are shown in Figure 2a. A true random waveform (white noise) contains all frequencies. The cosine autocorrelation images of all these frequen-

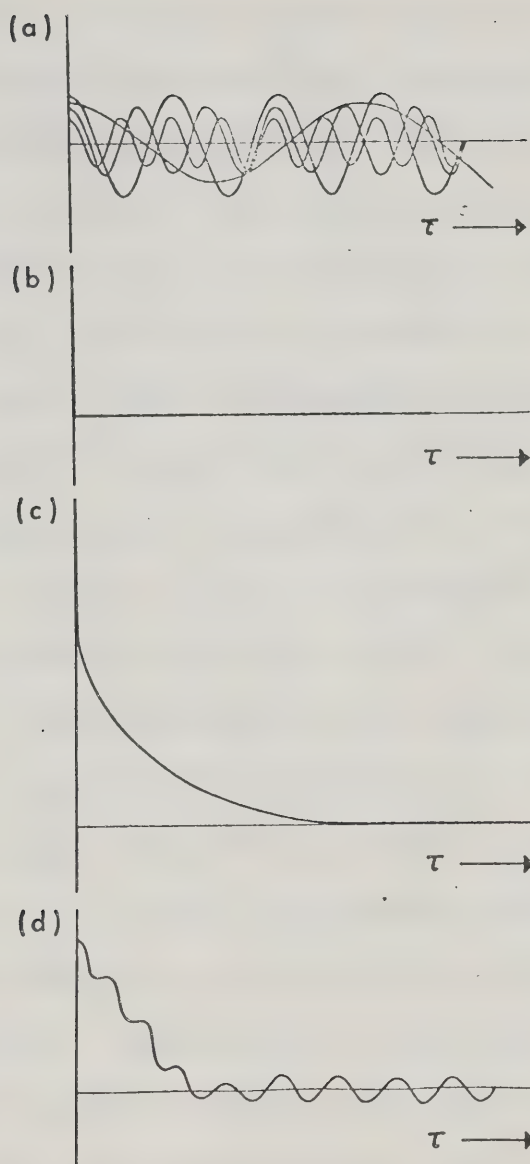


Figure 2. (a) Cosine autocorrelation images. (b) Autocorrelation function of ideal random noise. (c) Autocorrelation function of bandlimited random noise. (d) Autocorrelation function of a noisy sine wave.

cies reinforce at $\tau=0$ to produce a value equal to the mean square of the original random signal and at any point beyond $\tau=0$ they destructively interfere to produce a time averaged value of zero (see Figure 2b).

In order to obtain this ideal autocorrelation function of random noise, the bandwidth of the noise must be infinite. Of course, no process in nature is truly random. Real random waveforms are "band-limited" and do not produce a single spike upon autocorrelation but instead a shape such as portrayed in Figure 2c. The functional form is a decaying exponential (for low pass filtered random noise) whose width is inversely proportional to the bandwidth of the noise waveform.

When the autocorrelation functions of bandlimited random noise (Figure 2c) and of periodic signals (Figure 1) are compared it is clear how autocorrelation can be a powerful technique for the extraction of periodic signals from noise. Random noise contributes to the autocorrelation function only at very small values of τ . A periodic signal, in contrast, will continue to contribute even at very large values of τ . The autocorrelation function of a noisy sinusoid is shown in Figure 2d. The amplitude and frequency of the periodic signal buried in noise can be determined simply by examining the autocorrelation function at a location well removed from the central ($\tau=0$) peak. These points

will be further discussed in Chapter III.

Cross-Correlation

In contrast to autocorrelation, cross-correlation examines the coherence between two different signals. This coherence can only exist when the same frequencies are present in both waveforms. For example, the cross-correlation of a sine wave with a square wave of the same frequency produces an output sine wave since the fundamental frequency of the square wave is the only one that is common to both. Furthermore, although an autocorrelation is symmetrical about $\tau=0$ and shows a maximum at that point, a cross-correlation is generally asymmetrical and does not necessarily maximize at $\tau=0$: in the example given of a sine wave and a square wave the phase angle of the output sine wave depends on the phase difference between the two inputs. The behaviour of the cross-correlation function is also different if the inputs contain random noise. The cross-correlation of two different random signals is itself random and will therefore have a zero time average. Hence, it may not be necessary to displace the two inputs to obtain an output to which noise does not contribute, as long as the two input frequencies are in phase; i.e. scanning may not be necessary.

A further advantage of cross-correlation over

autocorrelation is that the output amplitude is dependent upon the amplitudes of two different signals, and thus can be adjusted merely by adjusting the amplitude of one of the inputs. If the amplitude of this reference waveform is maintained constant, the amplitude of the output signal will be linearly dependent on the amplitude of the other sought-for input, in contrast to autocorrelation where a squared dependence of output amplitude to input must exist. Of course, it is now necessary to generate the reference waveform by some means.

Further examples of cross-correlation will be given in Chapters II, IV, and VI.

Convolution

The points that have been introduced are sometimes more well known under the heading of convolution. However, convolution, which occurs during any operation involving signal generation or measurement, can be considered as merely a special type of correlation. The mathematical expression of convolution is

$$\text{Con}_{ab}(\tau) = \lim_{t \rightarrow \infty} \frac{1}{2t} \int_{-t}^{+t} a(t)b(-t \pm \tau) dt \quad \dots \quad (3)$$

Comparison of (3) and (1) shows that the only difference between correlation and convolution is the appearance of a minus sign before the t in the b function; i.e. this function is inverted left-to-right before the multiplication is performed. An example of this inversion can be seen in Figure 3 (from Reference 3). If a step function is applied to an instrument such as a chart recorder which has a response function that is an exponential decay, the recorder output will be observed to be distorted by the instrument. Application of the correlation integral to the system yields an output step function whose leading edge curves upward. We know that recorders do not respond in this way to step input signals; rather, the leading edge must curve downwards. Reversing the recorder response function, i.e. performing a convolution rather than a correlation, produces the desired output form. Of course, if the instrument response function was symmetrical, correlation and convolution would produce identical results.

Fourier Transformation

A final topic intimately related to correlation and convolution is Fourier transformation. The advent of the digital computer and the Fast Fourier Transform (FFT) has allowed the ready implementation of Fourier transform approaches to data processing. It can be

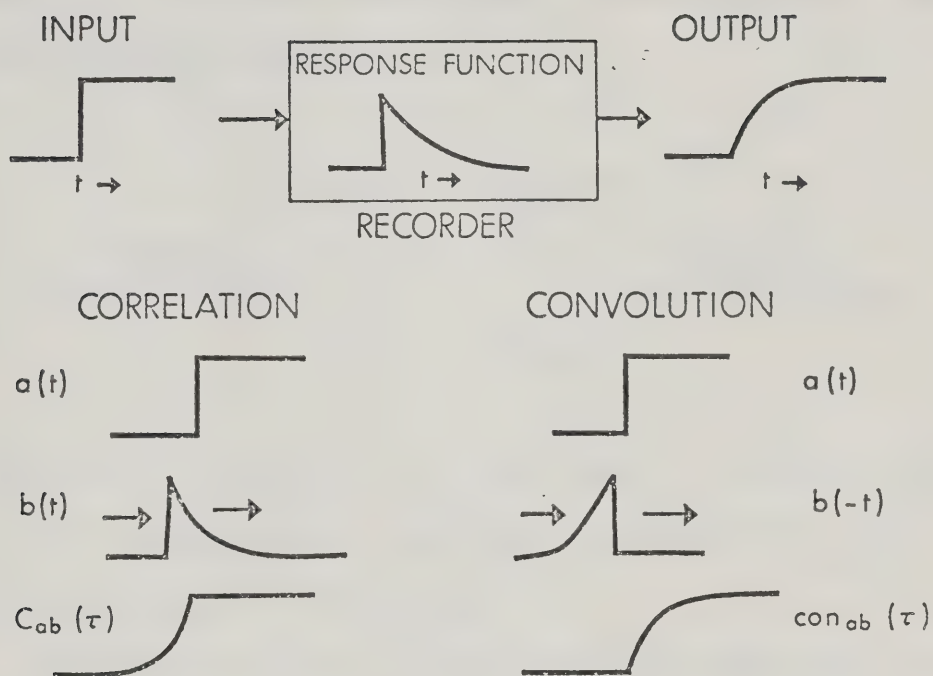


Figure 3. Convolution and correlation of a step waveform with an exponential instrument response function.

shown that the correlation of two functions a and b is equivalent to the multiplication of the Fourier transforms of the functions and inverse transformation of the result to give the correlogram. Schematically, this can be represented as

$$a(t) \quad * \quad b(t) = C_{ab}(\tau) \quad (4)$$

$$\begin{array}{ccccc} \downarrow & \text{Fourier} & \downarrow & \uparrow & \text{Inverse} \\ & \text{Transformation} & & & \text{Fourier} \\ & & & & \text{Transformation} \\ A(f) & \times & B(f) & = & C_{AB}(f) \end{array} \quad (5)$$

The asterisk in Equation 4 is here used to represent the operation of correlation; Equation 4 is therefore simply a shorthand notation of Equation 1.

Since correlation and Fourier transformation are so intimately related, it is instructive to consider the Fourier process in more detail. The basic equation is

$$a(t) = \int_{-\infty}^{+\infty} A(f) e^{2\pi i t f} df \quad (6)$$

The inverse Fourier transform is

$$A(f) = \int_{-\infty}^{+\infty} a(t) e^{-2\pi i t f} dt \quad (7)$$

Functions $a(t)$ and $A(f)$ therefore constitute a Fourier

transform pair, and are equivalent representations of each other. If the function $a(t)$ is a linear function of time, as are many chemical signals (chart recorder output, etc.), then the Fourier transform $A(f)$ will be a linear function of frequency, time^{-1} . This particular use of the term frequency should be distinguished from that normally encountered in optical spectroscopy; for that reason, the function $A(f)$ will generally be referred to here as the Fourier domain signal.

An interesting property of the Fourier transformation is that functions of complex appearance in the time domain often appear remarkably simple in the Fourier domain, and vice-versa. For this reason, it is often useful to consider the Fourier domain representation of a function, as will be shown in Chapters V and VI.

Correlation Instrumentation

A block diagram of an instrument that performs a direct implementation of the correlation equation (Equation 1) is shown in Figure 4. The inputs to the correlation are a signal (function a of Equation 1) and a reference (function b of Equation 1). Often, the reference must undergo some type of processing (such as τ variation) and might even be stored in the reference processor, which may be quite complex. The signal and processed reference are multiplied and then integrated

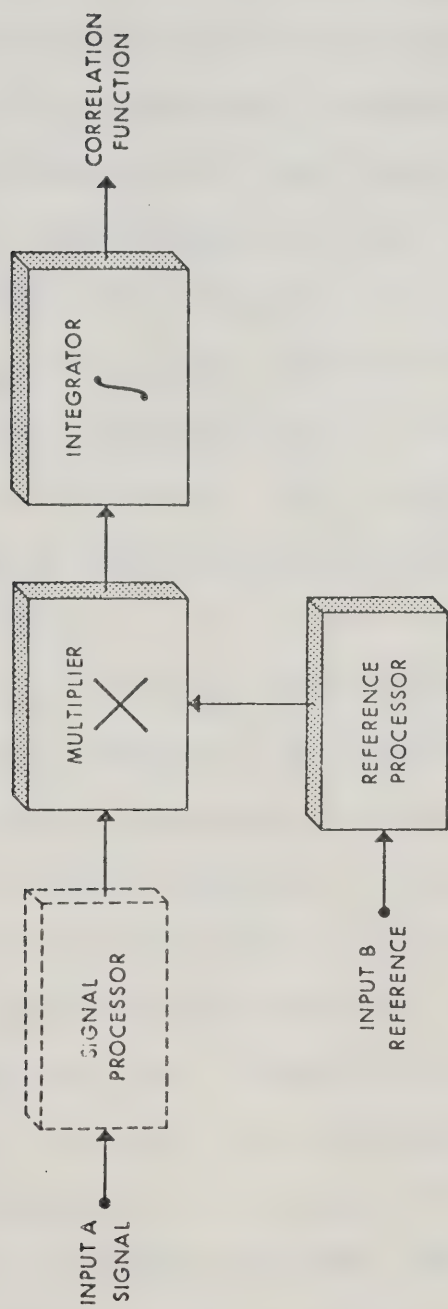


Figure 4. Block diagram of a correlator.

to give the output correlation function (c of Equation 1). The integrator of the hardware correlator may also have to be quite complex. It may also be necessary to have a signal processor (dotted in Figure 4). This block diagram may represent both a hardware correlator, in which case the reference processor might be a phase shifter and comparator (see Chapter II) and the signal processor a tuned amplifier; or a software correlator, in which case the reference and signal processors might be A/D converters and a digital computer would perform the shifting, multiplication, and integration operations. The functions a and b might be identical, in which case an autocorrelation would be performed (see Chapter III).

In this thesis, we will examine several ways of implementing Equation 1 by instruments that perform the functions diagrammed in Figure 4. In Chapter II, a versatile lock-in amplifier will be discussed in which the realization of Figure 4 is very simple. In Chapter III, an autocorrelator based on a Serial Analog Memory (SAM) which acts as a temporary storage device will be discussed, in which the implementation of Figure 4 is extremely complex. In Chapter IV, a cross-correlator based on a transient recorder that stores the reference signal (function b of Equation 1) will be discussed, in which the implementation of Figure 4 is also quite

complex. Chapter V will discuss the Fourier transform realization of Equation 1 by a digital computer; and Chapter VI will discuss the direct evaluation of Equation 1 by a Tapped Analog Delay Line (TAD), which allows the implementation of Figure 4 in an extremely simple but powerful way. Applications to be discussed in this thesis include signal-to-noise ratio enhancement, matched filtering, and resolution enhancement as applied to spectral signals.

CHAPTER II

LOCK-IN AMPLIFICATION

Background

One of the simplest, yet most powerful, instruments based on the principle of correlation is the lock-in amplifier (9), which is one of the most common and effective instruments used in the chemical laboratory for the measurement of noisy signals (5, 10-14). A measurement in which a lock-in amplifier is utilized involves three main operations: amplitude modulation of a carrier wave with the desired signal information, selective amplification and synchronous AM demodulation. The amplitude modulation step is implemented at some specific point in the experimental system and the lock-in amplifier carries out only the last two steps.

The key step in a lock-in amplifier measurement and that step which gives the technique its name is synchronous AM demodulation (10). Synchronous demodulation involves multiplication of the modulated carrier wave by a reference signal of exactly the same frequency as the carrier wave and phase-locked to the carrier wave at 0° phase shift. Demodulation is completed by averaging the output of the multiplication step, usually with a low-pass filter. Lock-in amplification is thus essentially a cross-correlation at $\tau=0$, since it involves

the operations of multiplication and integration.

A block diagram of a conventional lock-in amplifier is shown in Figure 5a. Two channels are normally provided, one to process the signal (amplitude modulated carrier) and one to process the reference. In almost all lock-in amplifier measurement systems, the phase locked reference signal is generated at the amplitude modulation step in the experimental system. For example, in systems where modulation is implemented by chopping a primary light beam with a mechanical chopper, a reference signal can be obtained by using an auxiliary light source and detector combination or from the signal used to drive the chopper. The reference signal as generated at the modulation step is phase-locked to the carrier frequency but it is not, in general, locked at 0° . Thus a phase shifter is required on the reference channel in order that the relative phase of the reference can be adjusted with respect to the carrier. This phase shifter performs the τ variation of the cross-correlation process. The comparator in the reference channel converts the reference to a bipolar square wave before it is applied to the four quadrant multiplier. Selective or tuned amplifiers are also normally included on each channel.

The conventional design of the lock-in amplifier (Figure 5a) can be enhanced and simplified with a

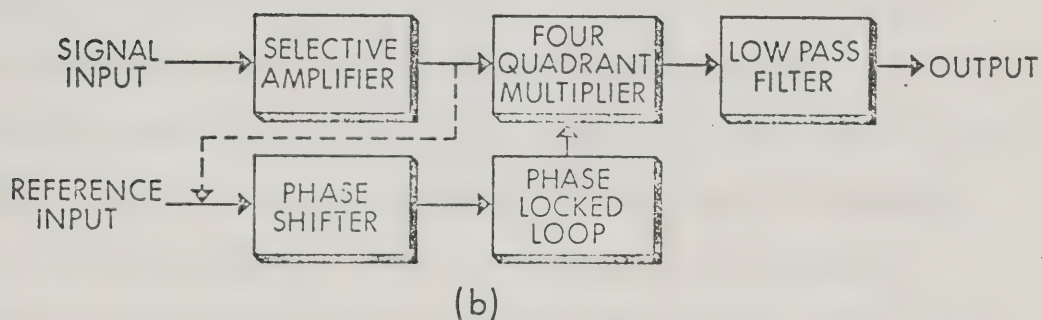
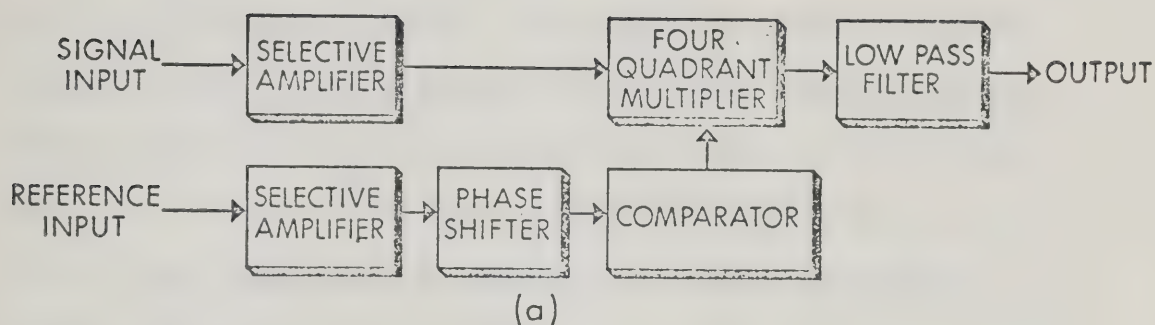


Figure 5. Block diagram of a lock-in amplifier, (a) conventional approach, (b) with a phase locked loop in the reference channel.

versatile circuit known as a phase-locked loop (10, 15, 16). A block diagram of a phase-locked loop (PLL) is shown in Figure 6. It consists of three main parts; a phase comparator, a low pass filter, and a voltage controlled oscillator (VCO). A number of types of phase-locked loops are available from several manufacturers. Among these are the Signetics 561, 562, and 565 PLL's and RCA's CD4046 PLL, all of which are available in 16 or 14 lead dual-in-line packages at very reasonable costs (~\$10.00).

In the basic PLL as shown in Figure 6, the phase comparator compares the phase and frequency of the input frequency with the VCO output and generates an error voltage proportional in sign and magnitude to the phase and frequency difference of the input frequency and the VCO output. This error signal is applied through a low pass filter to the VCO control input and drives the VCO output until the VCO output is exactly the same frequency as the input frequency; i.e., the VCO output becomes locked to the input frequency. The relative phase difference between the input frequency and the VCO output when the loop is locked depends on the exact nature of the phase comparator and, in general, on the value of the input frequency with respect to the free running VCO frequency. In some commercial PLL's (RCA CD 4046) the circuit can be set up so that the phase

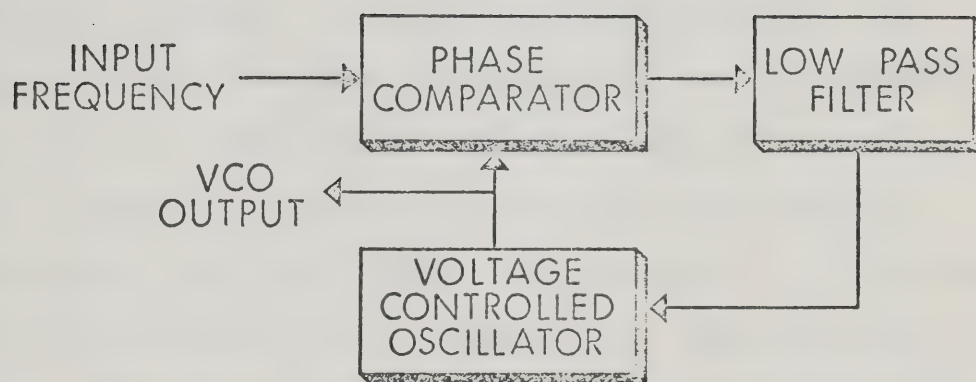


Figure 6. Block diagram of a phase locked loop.

difference is a constant 0° in the lock range, independent of the value of the input frequency. With most others, the phase difference varies anywhere from 0° to 180° over the lock range.

The common applications of the PLL include FM demodulation, frequency multiplication and construction of tracking filters. In connection with lock-in amplifiers, the standard PLL can be usefully incorporated into the reference channel. As shown in Figure 5b, both the selective amplifier and the comparator can be replaced by a PLL. In addition to replacing these components, the PLL provides automatic tracking of the carrier frequency. For this feature the PLL must be of the type that maintains lock at 0° phase shift over the lock range. The phase shifter block is still necessary because the reference, as generated at the modulation step in the experiment, is seldom exactly in phase with the carrier wave. In addition, relative phase shifts are easily introduced in the signal amplification channel before the four quadrant multiplier.

The Signetics 561 phase locked loop is a uniquely versatile circuit element for application to lock-in amplifier measurements. The 561 includes, in addition to a PLL, a multiplier and a low pass filter which can be used for synchronous AM demodulation applications. Thus this simple 16 pin integrated circuit contains al-

most all of the function blocks of a lock-in amplifier. A block diagram of the 561 PLL is shown in Figure 7. In its simplest configuration the only additional circuit block needed to build a complete lock-in amplifier is a phase shifter in the reference channel.

The standard lock-in amplifier as used in scientific measurements normally has separate signal and reference channel inputs. However, the utilization of a phase locked loop in the reference channel allows an interesting modification of this standard approach. The phase locked loop can be used to generate an appropriate reference signal for synchronous AM demodulation from the amplitude modulated carrier wave. This is accomplished by connecting the signal (amplitude modulated carrier) to *both* the signal and reference channels as shown by the dashed line in Figures 5b and 7. The VCO output of the PLL is a square wave, phase locked to the signal, and hence an appropriate reference for synchronous AM demodulation. This removes the need to generate a reference signal at the modulation step and the need to transmit the reference from the experiment to the lock-in amplifier. A fundamental limitation of this approach is that a double sideband modulated carrier (1) cannot be accurately demodulated as phase information will be lost in demodulating such a carrier with a ref-

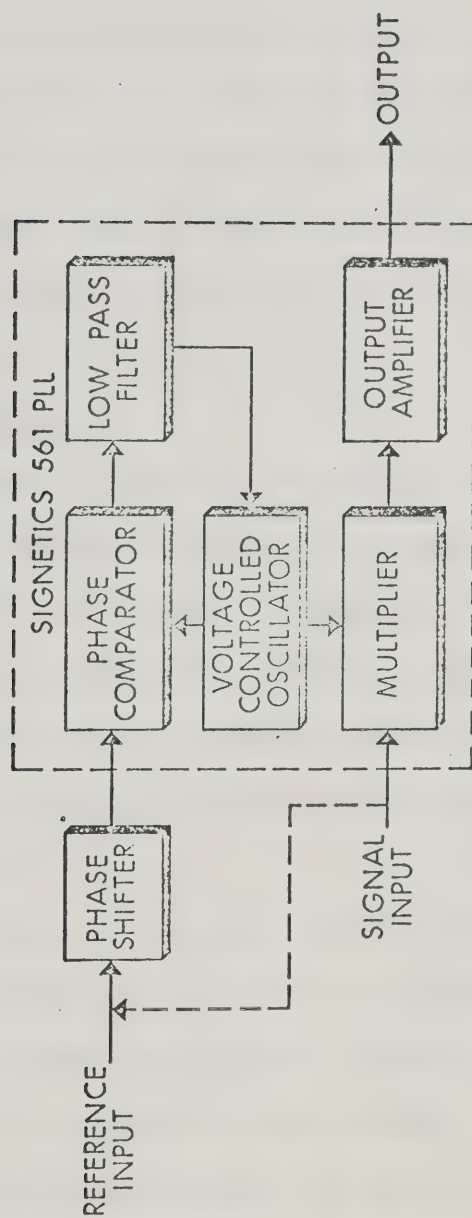


Figure 7. Block diagram of the Signetics 561 phase locked loop.

erence signal generated from itself. However, in the vast majority of lock-in amplifier measurements, AM modulation is employed and no difficulties will be encountered using this approach.

In the following sections the performance and characteristics of lock-in amplifiers based on Figures 5b and 7 are discussed and illustrated. The amplifiers are tested both in the "referenceless" mode and with separate signal and reference channel inputs.

Experimental

All circuits were wired on the Heath Analog-Digital Designer (ADD). The operational amplifiers used were the standard units provided with the ADD unit. The lock-in amplifier based on the 565 PLL requires an external four quadrant multiplier. An Analog Devices 426A four quadrant multiplier was used for this purpose (\$45.00).

The input test signals were provided by a Heath model EUW-27 sine-square wave generator (SSWG) and a General Radio Type 1390-B Random Noise Generator was used as the source of the noise. The random noise had a bandwidth extending from 20 Hz to 20 kHz. Noisy signals were simulated by summing the sine wave signal from the SSWG and the output of noise generator with an operational amplifier.

AC measurements of the input values were made using a Hewlett Packard Model 400EL AC voltmeter, and output dc levels from the lock-in amplifier were measured using a DANA Model 5400/015 DVM. The DANA is a successive approximation type DVM with a sample and hold front end. The aperture time of the sample and hold amplifier is 50 nsec.

Results and Discussion

As mentioned in the introduction, the Signetics 561 phase locked loop integrated circuit incorporates essentially all of the functional blocks necessary for a lock-in amplifier. The complete circuit for a lock-in amplifier constructed using the Signetics NE 561 phase locked loop is shown in Figure 8. It consists of four main sections; a tuned input amplifier on the signal channel (OA1), a phase shifter on the reference channel (OA2), the 561 PLL, and a low pass filter on the output (OA3). The tuned amplifier on the signal channel (10) has a nominal center frequency of 1000 Hz, a Q of about 2.5, and unity gain. The phase shifter (17) on the reference channel provides a variable phase shift of up to 180° with unity gain.

Complete details on the operation of the 561 PLL are available from Signetics. Only those connections pertinent to this application will be discussed. Also

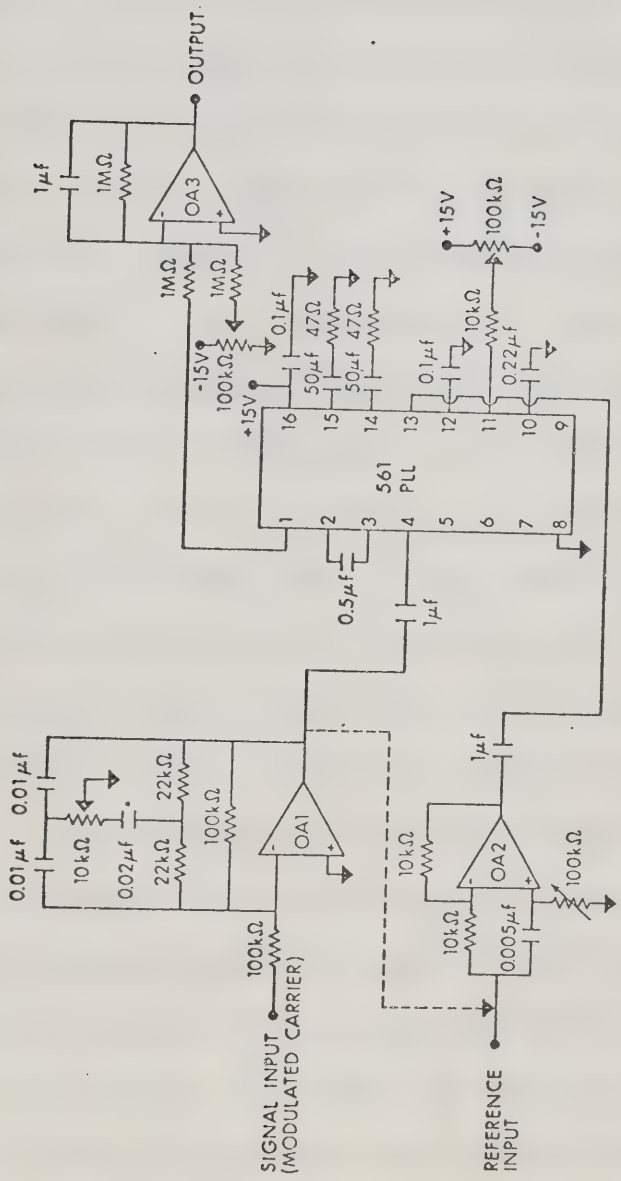


Figure 8. Circuit diagram for a lock-in amplifier based on the Signetics 561 phase locked loop.

it will be useful to refer to Figure 8 during this discussion. The $0.5\ \mu\text{f}$ capacitor between pins 2 and 3 sets the VCO free running frequency. This value was chosen to give a nominal free running frequency of 1000 Hz. Pin 13 is the input to the phase comparator and thus is the reference channel input to the PLL. The $50\ \mu\text{f}$ capacitors and $47\ \Omega$ resistors connected to pins 15 and 14 control the amount of low pass filtering in the phase locked loop. The potentiometer connected to pin 11 is an offset adjustment with which the phase of the VCO frequency can be adjusted relative to the input reference frequency. Both this offset control and the phase shifter (OA2) were used to set the 0° phase shift condition between the signal and reference channels. The capacitors connected to pins 16, 12, and 10 simply provide ac grounds and decoupling at these terminals.

The AM input to the multiplier on the chip is pin 4 and thus this is the signal channel input. Pin 1 is the demodulated AM output. This output can be passively low pass filtered by connecting a capacitor from pin 1 to ground. However, we choose to use an external active low pass filter with a 1 sec time constant (OA3). The output dc level at pin 1 is about +10.5 V when no input signal is applied at pin 4; thus some form of zero adjustment on the output is desirable. This is provided by the potentiometer connected to OA3.

The input tuned amplifier and the output low pass filter on the signal channel were both set for unity gain. Thus in this test circuit the only gain in the signal channel is that provided by the PLL. The gain was about 25 calculated on the basis of the average dc level of the demodulated AM output divided by the rms value of the input sine wave. This limits the maximum input signal to about 80 mV before the multiplier on the 561 begins to saturate.

The lock-in amplifier shown in Figure 8 was first tested with separate signal and reference channels. The input signal was a sine wave obtained from the sine-square wave generator. The square wave output of the SSWG was used as the reference. Reliable locking could easily be achieved with a reference signal as small as 1 mv p-p. The minimum input signal to the phase comparator for lock, as specified by the manufacturer, is 100 μ V.

The linearity and dynamic range of the lock-in amplifier in this configuration were evaluated by measuring the slope of the log-log plot of output vs input. The slopes of these plots for different noise levels are summarized in Table IA and all are very close to unity. For a 4.36 mV rms sine wave input the AM demodulated output was 111 ± 8 mv when 160 mv rms of random noise was added to the sine wave and 112 ± 18 mv when 500 mv was

TABLE I

Lock-In Amplifier Linearity and Dynamic Range
(Separate Signal and Reference Channels)

A. For the circuit shown in Figure 8

<u>Input Signal Range (mV, rms)</u>	<u>Order of Magnitude Change</u>	<u>Noise Level (mV, rms)</u>	<u>Slope of Log-Log Plot for Output vs Input</u>
2.45 - 77.5	1.5	residual	1.01 ± 0.01
4.36 - 43.6	1.0	residual	1.013 ± 0.006
4.36 - 43.6	1.0	160	1.016 ± 0.008
4.36 - 43.6	1.0	500	0.978 ± 0.002

B. For the circuit shown in Figure 9

2.45 - 2450	3.0	residual	0.992 ± 0.003
2.45 - 2450	3.0	160	0.999 ± 0.002
2.45 - 2450	3.0	500	0.988 ± 0.004
24.5 - 2450	2.0	2400	0.998 ± 0.004

present. The standard deviations were calculated from 10 measurements of the output made with the DANA DVM. The time constant on the low pass filter was 1 sec. These data indicate that the circuit is quite effective in enhancing the signal-to-noise ratio of the input signal.

The circuit for a lock-in amplifier based on the block diagram given in Figure 5B is shown in Figure 9. The signal channel consists of a tuned amplifier (OA1), a four quadrant multiplier, and a low pass filter (OA4). The reference channel consists of a phase shifter (OA2 and OA3) and a conventional phase locked loop IC (Signetics 565) as depicted in Figure 6. The two stages of phase shift simply provide a greater degree of flexibility in setting the phase as well as the capability of shifting the relative phase over a total of about 360° .

Again complete details on the 565 PLL can be obtained from Signetics (16). The capacitor to ground from pin 9 and the resistance to +15 V from pin 8 set the free running frequency of the VCO which in this case was 1000 Hz. The $0.5 \mu\text{f}$ capacitor from pin 7 to +15 V controls the loop low pass filtering and the $0.001 \mu\text{f}$ capacitor between pins 7 and 8 is for decoupling. Pins 2 and 3 are the external inputs to the phase comparator and, hence, the reference input. The voltage divider network is necessary in order to bias pins 2 and 3 for proper operation of the chip from a single power supply.

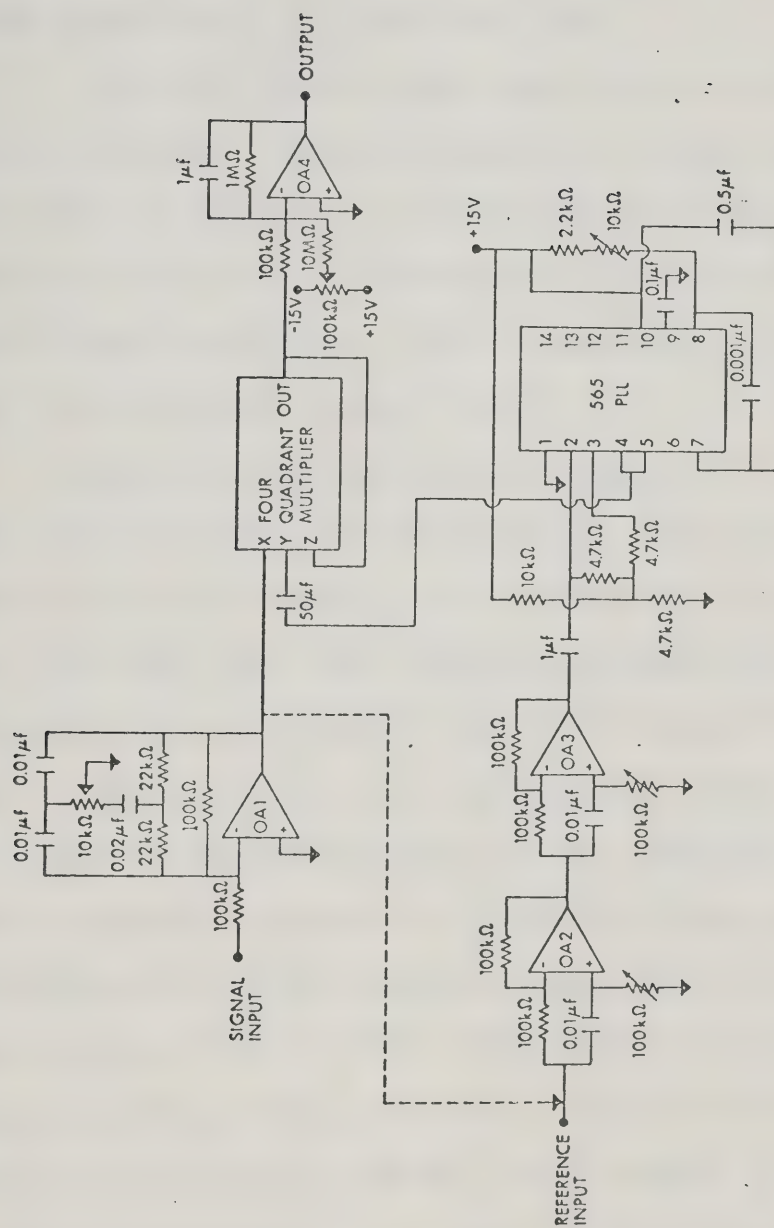


Figure 9. Circuit diagram for a lock-in amplifier based on Figure 5b.

Pin 4 is the VCO output which is the phase locked reference output to the four quadrant multiplier. It must also be connected to pin 5, which is the internal input to the phase comparator, to close the loop.

The only gain in this particular circuit occurs at the multiplier. The VCO output is a square wave with an amplitude of about 5 V. The multiplier output is $XY/10$. This gain of $1/10$ is counteracted by using an active low pass filter which has a gain of 10; thus, the overall gain of the signal channel is 5.

The linearity and dynamic range of this lock-in amplifier was measured as described for the first circuit and the data are summarized in Table IB. It can be seen from the data that the lock-in amplifier has excellent linearity over a dynamic range of 3 orders in magnitude, even in the presence of a considerable amount of noise. The improved dynamic range over the previous circuit occurs primarily because the external four quadrant multiplier has better dynamic range than the on-chip multiplier of the 561 PLL. The signal-to-noise ratio improvement was also excellent. For a 7.7 mV rms sine wave input buried in 500 mV rms of random noise (20 Hz to 20 kHz bandwidth) the output dc level was 37 ± 4 mV, the standard deviation again being calculated from 10 measurements.

Both of the lock-in amplifier circuits were also

tested in the "referenceless" mode discussed earlier. In this case, the reference input was obtained from the signal channel as shown by the dashed line in Figures 8 and 9. The ability of the PLL's to lock on a low level signal is an important asset for this application. The linearity and dynamic range data were measured as before and the results are shown in Figure 10a for the lock-in amplifier given in Figure 8 and in Figure 10b for the amplifier in Figure 9. In both cases (solid line) the "referenceless" configuration works essentially as well as the conventional configuration for the residual noise case. The least squares slopes for the solid lines in Figures 10a and 10b are 1.01 ± 0.01 and 1.02 ± 0.01 .

At high noise levels, the linear dynamic range is reduced because the loop cannot lock as effectively on the noisy reference. The phase adjustment on a lock-in amplifier is set to maximize the AM demodulated output. Any jitter of the optimal phase position as caused by the noise will decrease the output signal as shown in Figure 10. However, even though the linear dynamic range of these "referenceless" configurations is reduced at low signal-to-noise ratios, the circuits can be used at moderate noise levels. For example the amplifier shown in Figure 9 has a linear response at signal levels greater than ~ 100 mV rms even in the presence of 500 mV rms random noise. In many practical measurement situations

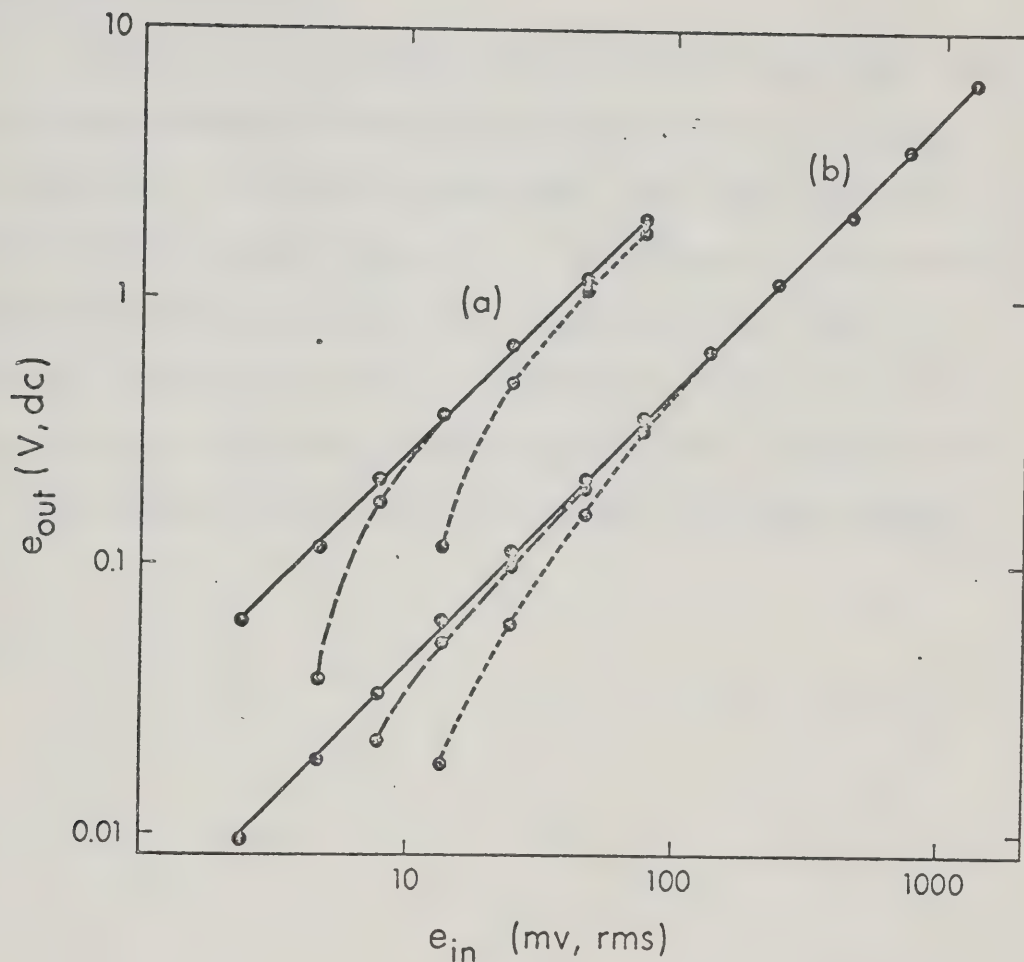


Figure 10. Log-log plots of output vs input for the "referenceless" configurations of the circuits given in Figure 8, (a) and Figure 9, (b). The solid line is the residual noise case, the dashed line for 160 mv rms random noise present on the input signal and the dotted (short dash) line for 500 mv rms.

the noise levels are not this high and the "referenceless" mode of these lock-in amplifiers should be a viable and useful configuration.

Finally, it is clear that a lock-in amplifier need not be considered an expensive component of a measurement system. As already mentioned, the PLL's used in these circuits costs about \$10. Depending on the quality, analog multiplier prices range from about \$10 for 4% accuracy to about \$50 for 1% accuracy. Thus, including the necessary OA's the circuits shown here can easily be built for about \$50 to \$100 excluding the power supply.

CHAPTER III

AUTOCORRELATION: THE SERIAL ANALOG MEMORY

Background

In the previous chapter, we saw how lock-in amplification is basically a single-point cross-correlation at $\tau=0$. It does, however, require that a reference signal be available, or that the received signal be sufficiently noise free that it itself can be used to obtain the reference. Autocorrelation, on the other hand, has the fundamental advantage that a reference is not required. However, in the process of autocorrelation all phase information is lost, and the output is not a linear function of the input.

One interesting application of autocorrelation has been in the measurement of the shot noise from a photomultiplier tube (18-22). Shot noise arises from the quantum nature of light, and the amplitude of the noise current is proportional to the square root of the light intensity. Accordingly, the mean square of the shot noise current (shot noise power) should yield a plot that is directly proportional to light intensity. Shot noise power can be obtained by squaring the shot noise component of the AC coupled signal and low-pass-filtering the result, i.e. an autocorrelation at $\tau=0$. Several workers have used this technique successfully to measure

photocurrents (18-22).

Construction of a scanning autocorrelation, on the other hand, allows the extraction of more information than that available at only $\tau=0$. The field of photon correlation spectroscopy involves the autocorrelation of the intensity fluctuations of a Doppler broadened Rayleigh scattered laser line (23-25). The autocorrelation function of a signal is the Fourier transform of its power spectrum (23). Determination of an autocorrelogram can allow measurement of several flow-related parameters. Representative papers have dealt with such measurements as that of the diffusion coefficients and electrophoretic mobility of bovine serum albumin (26), a study of electrokinetic phenomena (27, 28), and the determination of macromolecular diffusion coefficients (29). To achieve the speed required in these measurements (~ 20 MHz) the autocorrelation is often performed on a "digital clipped," i.e. binary, input signal (30-31).

Another interesting use of autocorrelation involves the measurement of chemical kinetic parameters by the autocorrelation of the noise due to random concentration fluctuations of reactants and products involved in chemical equilibria. Concentration fluctuations can be measured by such techniques as conductivity and fluorescence intensity (32, 33) and kinetic parameters then deduced from the autocorrelogram. In the words of Feher

and Weissman (32), the result involves "the personal satisfaction of using rather than fighting noise."

Although autocorrelation techniques have been employed in these and other fields with considerable advantage and success, their use has unfortunately been somewhat limited primarily by a lack of effective methods and instrumentation for the rapid, automatic evaluation of autocorrelation functions. Present developments in certain large scale integrated circuits such as diode arrays, charge coupled devices, and bucket brigade devices are now beginning to provide very inexpensive devices capable of sophisticated real time correlation operations (34). These integrated circuits can be generally classified as discrete time analog signal processing devices. One such device is a serial analog memory (35). When operated as a variable analog delay line it allows real time autocorrelation processing of noisy periodic signals, and the real time evaluation of autocorrelation functions such as those depicted in Figures 1 and 2. The key circuit element is a serial analog memory that is operated as a variable analog delay line.

Serial Analog Memories

A few years ago self-scanning linear photodiode arrays became available in small integrated circuit packages. These devices have been widely used as electronic

image sensors in industrial and scientific applications (36, 37). These sensors consist of a linear array of silicon photodiodes. Each photodiode is connected to the output line by a FET switch. The FET switches are controlled by a single bit that is shifted through a shift register that is integrated on the same chip.

Functionally the self-scanning linear array of photodiodes can be considered as an *analog* shift register with parallel optical inputs and a serial electrical output. Diode array devices are now available with serial electrical input and output. A wide variety of powerful real time analog data handling and processing operations can be implemented with these devices (34).

One type of device, available from Reticon Corp., 910 Benicia Ave., Sunnyvale, CA 94086, is called a serial analog memory (SAM) (35). A block diagram of a SAM-128V serial analog memory is shown in Figure 11. The SAM consists of three basic subunits: a "dynamic" 128 point serial analog memory, a readin 128 bit digital shift register, and an independent readout 128 bit digital shift register. The complete SAM-128V comes in a single 16 pin integrated circuit package. The maximum clocking rate is specified at 5 MHz, S/N at 40 dB (1 part in 100), and total harmonic distortion at 3.5%.

With the SAM an analog input signal can be sequentially sampled and stored on a series of storage capacitors.

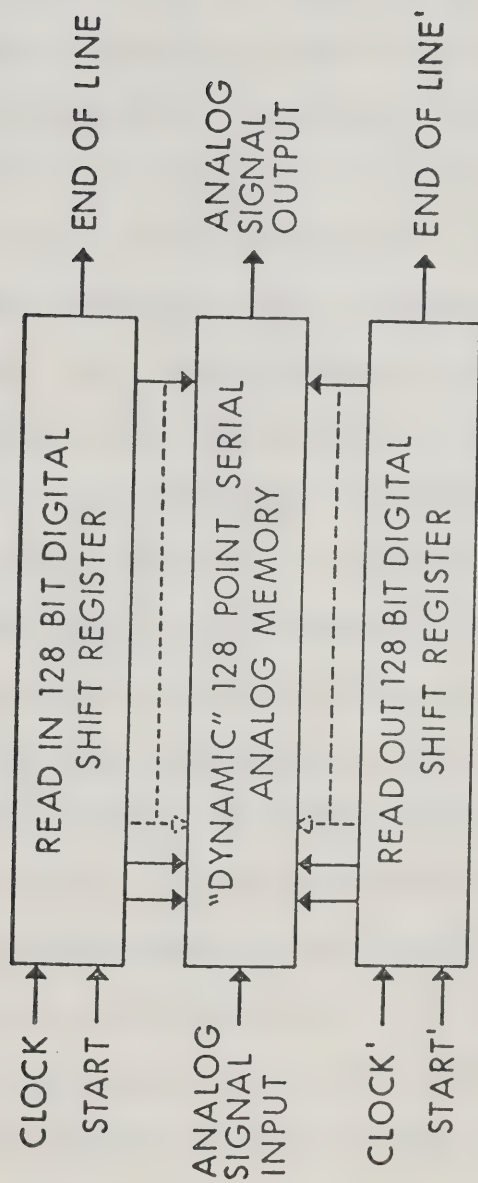


Figure 11. Block diagram of the serial analog memory.

Both aperture and acquisition times are specified at 25 nsec. The stored signal values can be read out in sequence either immediately, or after some delay. The readout rate can be the same as the readin rate or the signal can be read out with a new time base and, hence, either compressed or expanded. Each memory capacitor (reversed biased PN junction) has a FET buffer stage, thus readout is non-destructive. However, with this device the retention time without degradation (because of leakage, i.e. "dark" current) is 40 msec at room temperature. Thus the memory is really a "dynamic" memory requiring periodic refreshing. A more recent version of the SAM has a retention time of 5 sec.

The serial analog memory is potentially an extremely powerful circuit element for incorporation into correlation instrumentation. For example, this single integrated circuit, with appropriate clocking circuitry, can function as a transient recorder. Many types of hardware correlators utilize transient recorders, as will be shown in Chapter IV. In addition, this particular serial analog memory possesses some features that make it uniquely applicable to binary sequence correlation. Readout, as mentioned above, is controlled by the readout shift register. If a bit exists in the n th stage, the n th cell will be read out. Thus if a specific binary sequence is clocked into the readout shift register, the

output will be the summation of the products of the binary sequence and the stored analog information. Thus, this application amounts to the rapid cross-correlation of a stored analog signal with a moving sequence of binary pulses. Such correlations are applicable to pattern detection.

In this chapter, we will discuss the application of the SAM to the design and construction of an autocorrelator. A block diagram of the autocorrelator is shown in Figure 12. The input signal to be autocorrelated is sent simultaneously to the serial analog memory, and to one input of an analog multiplier. The output of the serial analog memory is connected to the second input of the analog multiplier. The output of the analog multiplier is integrated to complete the autocorrelation.

The serial analog memory is operated functionally as a variable analog delay line. The readin and readout clock rates are identical but the readout cycle is sequentially delayed, providing the shifting operation necessary in the evaluation of the autocorrelation function. It is important to emphasize that with the architecture of the SAM it is possible to have *zero* delay, i.e. readout simultaneous with readin, as well as any other delay in units of clock period. Thus the serial analog memory is *not* simply an analog shift register. In a true shift register zero delay cannot be achieved,

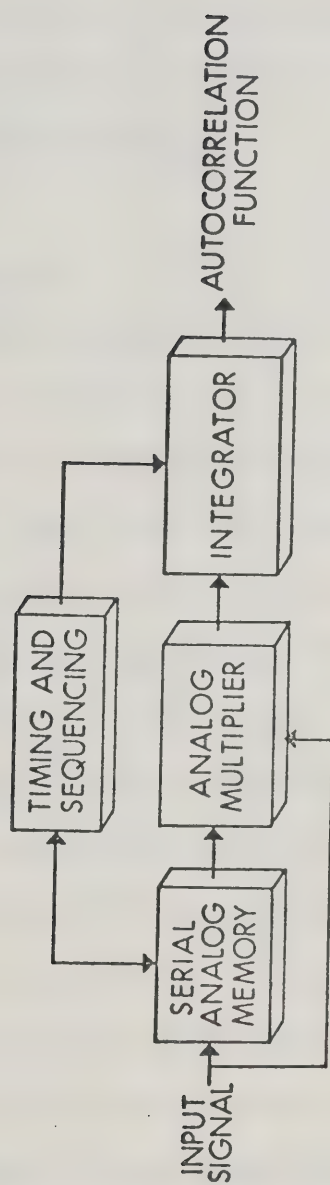


Figure 12. Simple block diagram of the autocorrelator.

as the first sample must be clocked completely through the register before it can be readout. Conventional transient recorders based on ADC's, digital shift registers, and DAC's, and another circuit manufactured by Reticon called a serial analog delay (SAD) both have this limitation and, hence, could not be used in this autocorrelator design.

Experimental

The complete block diagram of the autocorrelator is shown in Figure 13. It should be noted that the SAM-128V was mounted on an SC-128V evaluation circuit card available from Reticon. The input and output lines shown on the block diagram are those of this circuit card. The card contains TTL to MOS interfaces and generates the proper two phase clocks necessary for the readin and readout shift registers.

To properly sample a repetitive analog signal with the SAM it was necessary to synchronize data acquisition, i.e. clocking, with an external start pulse which was, in general, asynchronous to the SAM clock. The master clock frequency was four times that of the readin and readout clock; therefore the maximum jitter of the SAM clock with respect to the signal start was one-quarter of the clock period.

Reception of the external start pulse started the

readin and readout clocks and caused a readin bit to be loaded into the SAM, thereby initiating data acquisition. The generation of the readout sequence was controlled by the modulo 128 counter. At $\tau=0$ (no delay), this counter was set to 127 and thus the first clock pulse to this counter loaded a readout bit, thereby clocking data out of the SAM simultaneously with its acquisition. After 128 clock pulses, the clock to the modulo 128 counter was shut off and a pulse applied to the scaler. After a total of 260 clock pulses, the readin-readout clock was shut down and another start pulse awaited.

Scanning was accomplished by the scaler and reset control. After a selectable number of scans as set by the modulus of the scaler (1 to 1000), the scaler triggers the reset control, which quickly resets the counter to zero on the count of two, giving a count sequence of 0, 1, (2) \rightarrow 0, 1, 2, 3.... Therefore, when the 128 clock pulses to the modulo 128 counter were terminated, the counter held a count of 125 instead of the original 127. Thus, when the next data acquisition sequence began, a readout bit was not loaded into the SAM until two clock pulses after the readin bit, which introduces a delay of two clock pulses in the readout of the data. In this manner, an automatic scan of the delay (τ) from zero to 126 clock pulses in steps of two was accomplished, giving a total of 64 different delays. At

the maximum possible delay a minimum of 259 clock pulses were required to clear all circuitry. For some reason, perhaps associated with the SAM or the circuit card, it was not possible to successfully sequence the scanning action one clock pulse at a time and hence generate a 128 point autocorrelation function.

The delayed output was fed through a buffer amplifier referenced to the 5 volt common of the SAM and then to a four quadrant analog multiplier (Analog Devices 426A) whose other input was the original undelayed signal. When a readout sequence was initiated integration was started on a gated integrator. This integration continued for the appropriate time interval, then the value of the integral was transferred to a sample-and-hold amplifier and the integrator was reset. A low-pass filter on the output of the sample-and-hold amplifier suppressed switching transients and allowed averaging of a large number of repetitive evaluations of the correlation function at a given delay (i.e. the scaler set at modulo-1000). This allowed plotting of the autocorrelation function on an ordinary strip chart recorder. For real time display of the autocorrelation function on an oscilloscope the scaler was set to modulo-1. The RC time constant of the low pass filter for recorder output was ~ 0.1 sec and for oscilloscope output ~ 0.1 msec.

Integration of the multiplier output was terminated

at the finish of either the readin cycle or the readout cycle, depending on whether or not the signal was periodic. For a sine wave input the waveform arriving after the input has been sampled and stored has the same form as the section that was sampled. Thus integration can be initiated by the start readout pulse and terminated when the readout cycle is complete. However, for a more complex non-periodic waveform autocorrelation should only be performed where the delayed and original waveforms actually overlap in time. For such waveforms integration is terminated by the completion of the readin cycle. The circuit is designed to operate in either of these modes. For example, if a sine wave was autocorrelated as a non-periodic waveform the autocorrelation function had the form of a damped cosine wave, its amplitude decreasing to almost zero where the signal and delayed signal overlapped by only two clock pulses.

A complete schematic of the autocorrelator is shown in Figure 14. The master clock gate is formed by FF1, FF2, and FF3. Assume that Q of FF1 is 0, i.e. FF1 has been reset. This sets FF2, and resets FF's 3, 4, 5, and the first (upper) modulo 128 counter. The arrival of a trigger pulse will then toggle FF1, this freeing FF's 2, 3, 4, 5 and the upper modulo 128 counter. Further start pulses cannot toggle FF1 ($K=0$) until the circuit has been rearmed. The first 1→0 transition of the master

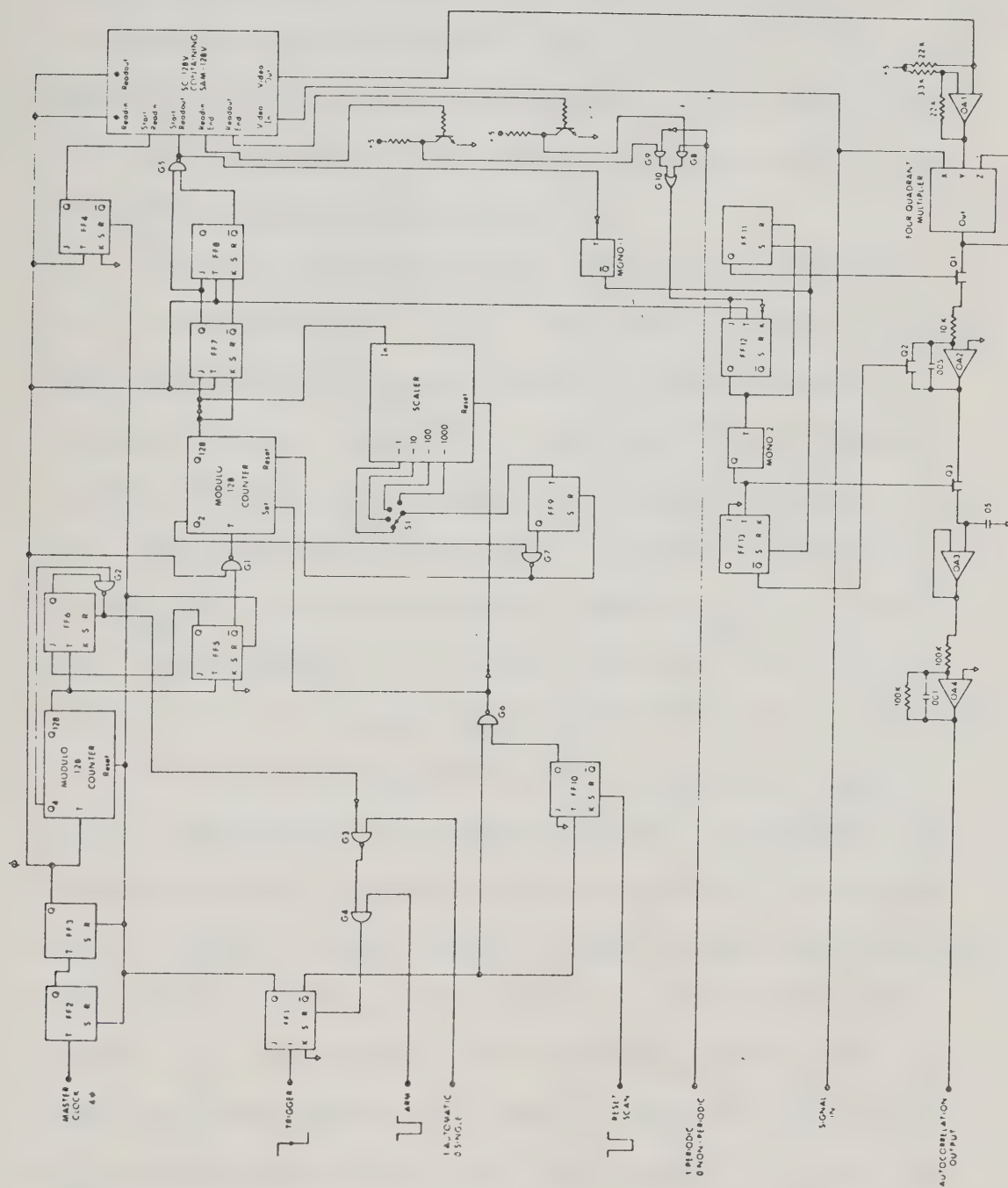


Figure 14. Circuit diagram of the autocorrelator.

clock will toggle FF2 to 0, thus toggling FF3 (ϕ) from 0 to 1. Once freed, FF2 and FF3 simply divide the master clock frequency by four. The input start pulse generator is formed by FF4. The first 1 \rightarrow 0 of ϕ toggles FF4 to 1; subsequent transitions are ignored ($K=0$). Thus, Q of FF4 is 0 for one and only one 0 \rightarrow 1 transition of ϕ , and therefore loads a single start bit.

The output start pulse generator is formed by FF's 7 and 8 and G5. FF's 7 and 8 form a shift register that transfers \bar{Q}_{128} of the second (lower) modulo 128 counter. Assume that FF's 7 and 8 are initially both 0, and that the lower modulo 128 counter has been set to 127. The first 0 \rightarrow 1 transition of ϕ will be inverted by G1 ($\bar{Q}_{FF5}=1$) and will therefore toggle Q_{128} to 0, which will be presented to K of FF7. The next 1 \rightarrow 0 at ϕ will toggle FF7 to 1, making the output of G5 a 0. A further 1 \rightarrow 0 at ϕ will now toggle FF8 to 1, making the output of G5 a 1. Therefore, the output of G5 is also 0 for one and only one 0 \rightarrow 1 transition of ϕ , and only one readout bit is loaded. Note, however, that if the lower counter has been set to 127, the readout bit will be loaded exactly one clock pulse later than the readin bit; this point will be referred to later. The 0 \rightarrow 1 transition of Q_{128} at the 64th 0 \rightarrow 1 of ϕ will be reflected in 0's at both FF7 and FF8 on the 65th 1 \rightarrow 0.

The 128 pulse gate is formed by the upper

modulo-128 counter, FF5, and G1. The 128th 1→0 transition of ϕ toggles Q_{128} and thus FF5, closing G1. It was necessary to operate the two modulo 128 counters on opposite clock phases to avoid timing problems associated with this closure. Once toggled to 1, FF5 was locked ($K=0$) but FF6 was freed ($J=1$). Assume that FF6 is originally 0. The 256th 1→0 of ϕ will toggle Q_{128} of the upper modulo-128 counter for the second time, thus toggling FF6 to 1. The 260th clock pulse toggles Q_4 of the upper modulo-128 counter to 1; this causes the output of G2 to be zero until FF6 is reset. In the AUTOMATIC mode, the momentary 0 from G2 will also reset FF1 through G3 and G4, thus shutting off ϕ and restarting the operating sequence. Therefore, the upper modulo-128 counter, FF5, and FF6 form the modulo-260 counter.

Scanning is controlled by the scaler, S1, FF9, and G7. Assume that FF9 is originally 0. The 1→0 transitions of Q_{128} of the lower modulo-128 counter are inverted and counted by the scaler. With S1 in the position shown ($\div 1$), each 127→0 of the lower counter will toggle FF9 to 1. Two clock pulses later, Q_2 will be a 1, causing the output of G7 to be zero until FF9 is reset. This momentary zero resets the lower counter and causes the count sequence already described. Connecting the input of G7 to Q_1 rather than Q_2 will cause the counter to scan one clock pulse at a time; however, the SAM could

not be made to so scan.

The scanning action may be started with $\tau=0$ by setting FF10. When FF1 is reset and a trigger pulse awaited, the output of G6 will be 0, thus setting the lower counter to 127 and resetting the scaler. The toggling of FF1 by a trigger pulse will then toggle FF10 to 0 thus making the output of G6 a 1 and freeing both the lower counter and the scaler. FF10 will then remain in the 0 state ($J=0$) until set again.

Integration of the product of the original and delayed signals is controlled by Mono-1, Mono-2, and FF's 11, 12, and 13. Assume FF12 is initially in the 1 state. The initiation of the readout sequence at the 0 \rightarrow 1 of G5 is inverted and used to toggle Mono-1. This sets FF's 11 and 13, thus closing Q1 and opening Q2. OA2 then begins to integrate the multiplier output. Assume the circuit is in the PERIODIC mode. The appearance of a MOS 1 level from Readout End one clock pulse before the termination of readout is converted to a TTL zero and presented to J of FF12. The next 1 \rightarrow 0 of ϕ signals the end of data readout and toggles FF12 to 0. This resets FF11, opens Q1, and toggles Mono-2, thus connecting the integrator output to the sample-and-hold (OA3) through Q3. After a sample has been taken ($\sim 20 \mu\text{sec}$), Mono-2 toggles FF13, thus closing Q2 and resetting the integrator. One clock pulse after readout is terminated,

Readout End becomes a MOS 0. This is converted to a TTL 1 and causes FF12 to become 1 one clock pulse later.

At several points in this discussion, it has been necessary to assume initial states for several flip-flops. The timing of the circuit is such that, after a maximum of 259 clock pulses from power on, the FF's must be in the state assumed. The number 259 is the total of 2 clock pulses to establish the state of FF's 7 and 8, 128 more to finish readin, a maximum delay of 127 (for scanning one clock pulse at a time) and 2 more clock pulses to clear FF12.

It was mentioned earlier that the output start bit was loaded one clock pulse later than the input start bit. Nevertheless, it was possible to have readout simultaneous with readin ($\tau=0$) under these circumstances, due either to some peculiarity of the SAM or of the sequencing circuitry. It was also mentioned that scanning was possible only in two clock pulse delays. However, at power on, the circuit would either scan in delay sequence 0, 2, 4, ..., 126 or in sequence 1, 3, 5, ..., 127. Once the power was on, the scanning mode (even or odd) was fixed. Attempts to obtain a 128 point autocorrelation function by timing phasing variations were unsuccessful. All results reported here are for the even scanning mode, so that a zero delay was obtained.

Results and Discussion

Examples of several input and output waveforms for the autocorrelator are shown in Plate 1. The input waveform and delayed segment are shown in column I for sine, triangular and square waves (all 8 kHz). The corresponding output autocorrelation functions (scaler set to modulo-1) as they are displayed in real time on the oscilloscope are shown in column II. The time base for the autocorrelation function photographs was 10 msec/div. Thus these autocorrelation functions are computed in about 52 msec. The break in each of the autocorrelation function photographs indicates automatic restart of the autocorrelator on application of another start pulse.

It is clear from the photographs that the serial analog memory is not distortion free. The delayed signal segments stored in the SAM show some significant amplitude distortions. In addition distortion can be observed in the autocorrelation functions, particularly that for the square wave which should be a triangular wave. As the signal delay was slowly scanned from zero to 126, three different types of distortion could be observed. These have been labeled as fixed pattern noise, step distortion, and breathing.

1. Fixed pattern noise. As the delay is slowly scanned, a noise pattern is superimposed upon the de-

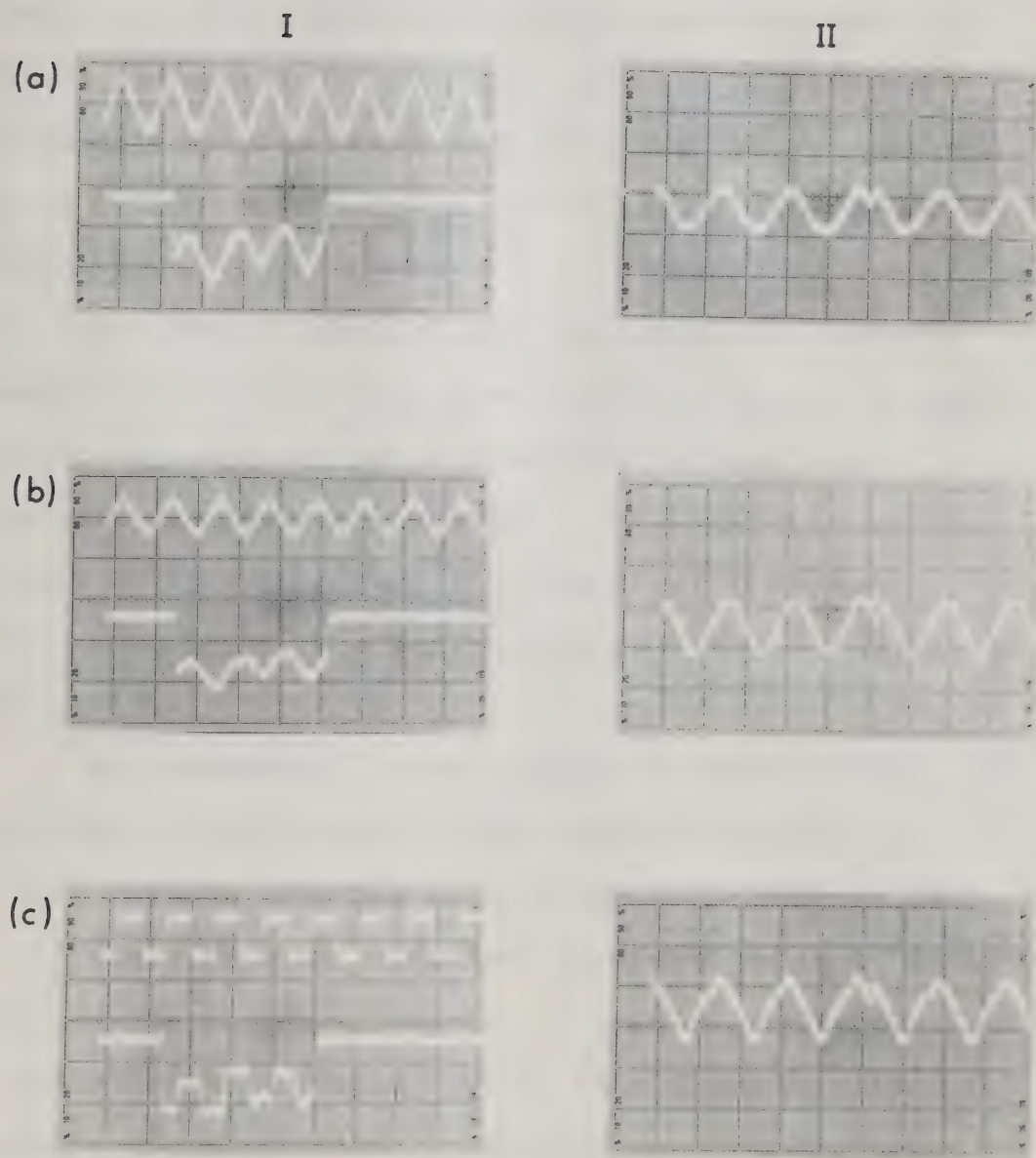


Plate 1. Autocorrelation of sine, triangular and square waves.

layed signal and scans with it; i.e. the noise pattern is unaffected by the delay. The major probable cause of this type of distortion is diode-to-diode non-linearity. Such distortion has also been observed in Reticon photodiode arrays (37). The two spikes that are clearly visible about halfway along the delayed signal in column Ib are an example of this type of distortion.

2. Step distortion. As the delay is slowly scanned from zero to 126, a visible step occurs in the delayed waveform and moves along the delayed waveform as a function of the delay. This step is most clearly visible in Column Ic. The first (leftmost) square wave cycle is clearly lower than the two rightmost cycles.

3. Breathing. As the delay is slowly varied, the amplitude of the delayed signal changes such that it is at a maximum when the delayed signal is exactly 180° out of phase with the undelayed generator output. Therefore, as the delay varies, the delayed waveform "breathes" up and down in amplitude. It is this distortion that is probably the major cause of the asymmetry in the autocorrelation functions.

The input-output amplitude characteristics of the SAM and the autocorrelator are shown in Figure 15. For an 8 kHz sine wave input with a p-p amplitude ranging

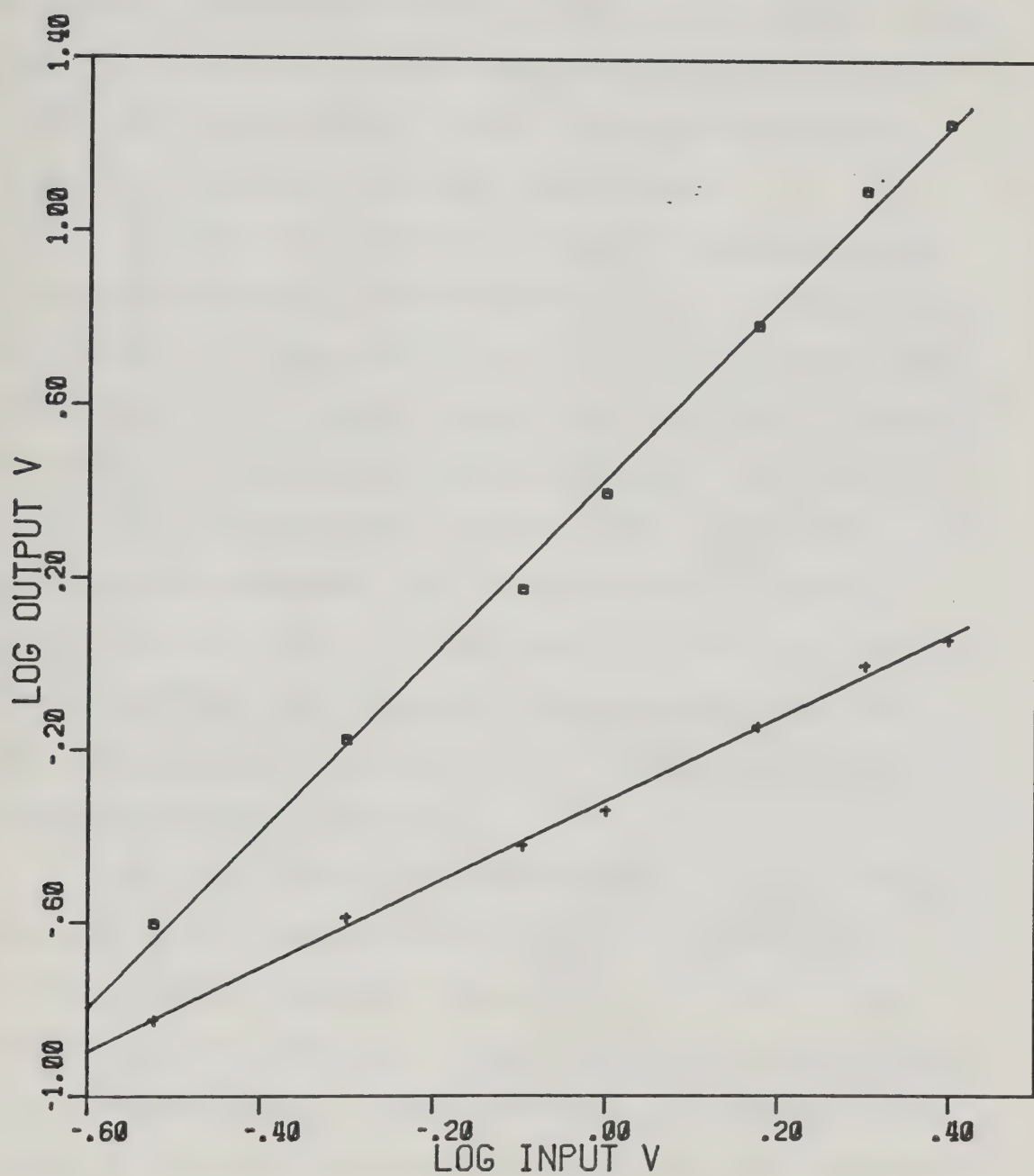


Figure 15. Log-log plots of output vs input for the serial analog memory (crosses) and autocorrelator (squares).

from 0.3V to 3.0V (one order of magnitude) the slope of a log-log plot of SAM output vs SAM input is 0.97 ± 0.02 and for a log-log plot of autocorrelator output vs SAM input the slope is 2.05 ± 0.05 . The SAM was just beginning to saturate with the 3V p-p input.

In order to test the ability of the autocorrelator in processing a noisy periodic signal, random noise was added to a sine wave signal. A 1.1V p-p sine wave with about 3V p-p added random noise is shown in column I of Plate 2a along with a delayed segment. The random noise was obtained from a General Radio Type 1390-B random-noise generator and had a bandwidth extending from 5 Hz to 20 kHz. It can clearly be seen in Plate 2a that the delayed noisy signal segment originates from the beginning of the upper trace although, as before, some distortion is evident.

The sine wave is somewhat difficult to visually discern in the original signal trace. However, the autocorrelation function computed in one cycle of the autocorrelator (52 msec) clearly reveals the periodicity of the noisy input. If the sine wave amplitude is reduced to 0.5V p-p the waveforms shown in Plate 2b result. By reducing the input amplitude by about a factor of two, the autocorrelation function amplitude drops by about a factor of 4. Now it is even difficult to see any periodicity in the autocorrelator output although the

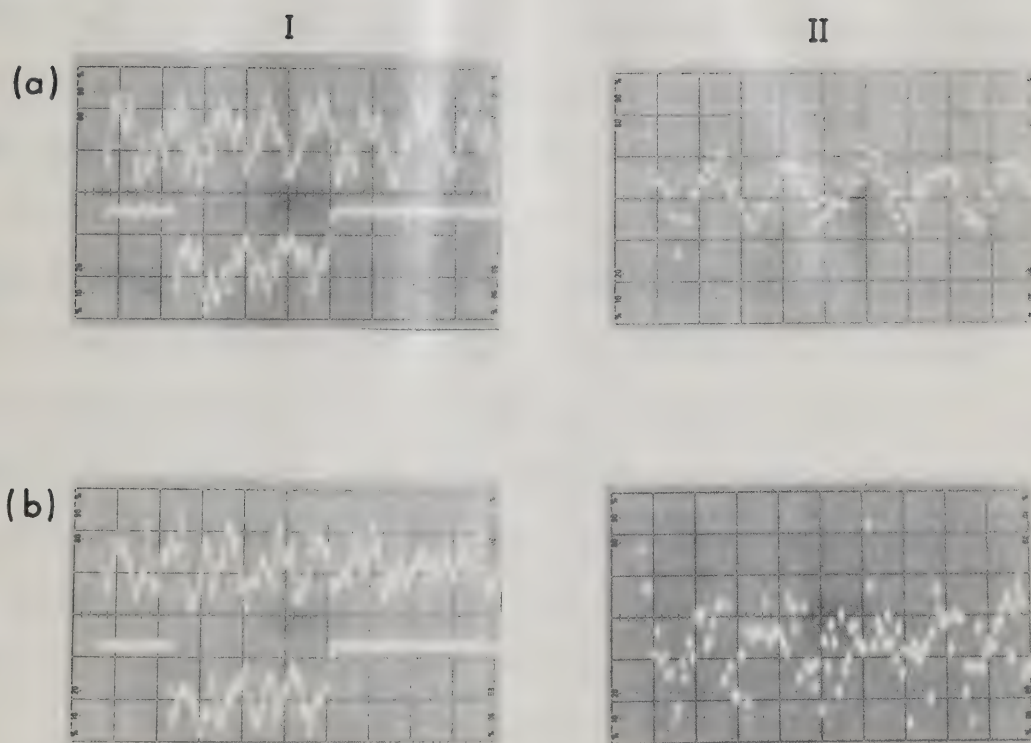


Plate 2. Autocorrelation of noisy sine waves.

relatively large $\tau=0$ peak caused by the random noise is visible.

As mentioned in the experimental section it is possible to time average the autocorrelation function by repeated evaluation and integration of the autocorrelation function at one specific τ value. This also allows plotting of the autocorrelation function on a strip chart recorder. The autocorrelation function obtained when the scaler is set at modulo-1000 and the time constant of the output low pass filter to 0.1 sec is shown in Figure 16a. Now the period and amplitude of the autocorrelation function can easily be measured. Remember the input signal is that shown in the upper trace of Plate 2b, column I. For comparison, the autocorrelator output in this mode for a noise free sine wave input is shown in Figure 16b. The total plotting time for each of these waveforms was 52 sec.

It should be noted that the autocorrelation function provides a convenient means of determining the signal-to-noise ratio of the original waveform (3). The value of the autocorrelation function at $\tau=0$ is just the mean square of the original signal plus noise, while the peak amplitude of the autocorrelation function at values removed from $\tau=0$ is equal to the mean square of the signal alone. For an alternating waveform the mean square value is directly proportional to the power of

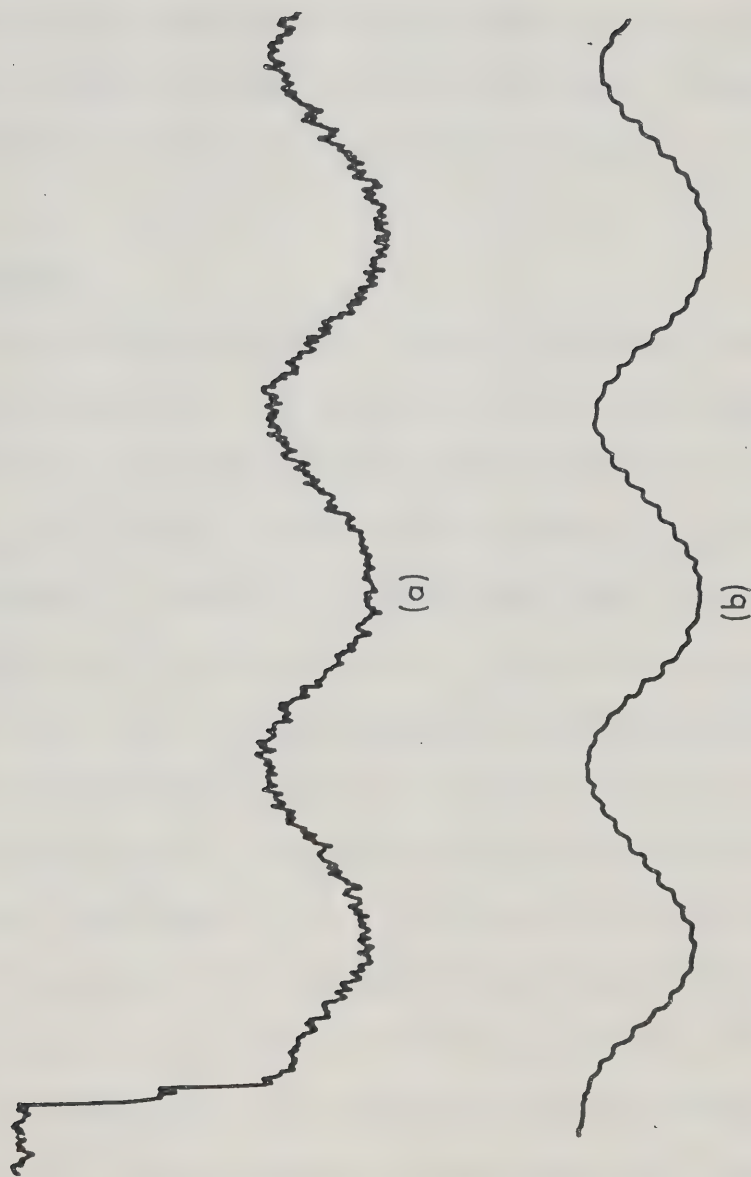


Figure 16. Recorder output of autocorrelation functions,
(a) noisy sine wave, (b) noise free sine wave.

the alternating waveform. Thus the signal-to-noise power ratio can be calculated from the mean square of the signal divided by the difference between the $\tau=0$ value ($S+N$) and the mean square of the signal. On this basis the signal-to-noise power ratio in the original noisy sine wave calculated from its autocorrelation function (Figure 16a) is about 0.2.

Conclusion

This autocorrelator was not directly applied to a chemical signal. The primary aim of this study was to point out the availability and applicability of devices such as the serial analog memory to correlation measurements. Hieftje (7) has shown that correlation techniques can be advantageously applied to measurements where lock-in amplifiers are typically employed. Since lock-in amplification is widely used in analytical instrumentation, the correlation approach has potential wide applicability as instrumentation becomes more readily available to implement correlation analysis. Devices such as the SAM are sure to promote this development. In addition, the autocorrelation approach to processing a noisy periodic signal does not require a reference signal as is necessary for lock-in detection. It would be possible, for example, to measure the amplitude of an input signal by adjusting the delay such that

observations were recorded at a local maximum (or minimum) well separated from the peak at $\tau=0$ (see Figure 16). This would provide data similar to that provided by a lock-in amplifier, but without a reference.

Application of the SAM to chemical measurements is by no means limited to autocorrelation. Both transient recorders and cross-correlation instruments could be constructed using serial analog memories. The construction of a transient recorder using a device related to the SAM, a serial analog delay (SAD), has already been reported (38). Many additional applications are outlined in literature available from Reticon. Reticon has also announced the availability of a second-generation device, the SAM-128LR, that allows retention of information for up to 5 seconds at 25°C, and has a dynamic range of 70 dB. This and further improvements in the construction of these devices can be expected to lead to both increased performance and lower cost.

CHAPTER IV

CROSS-CORRELATION I: A HARDWARE CORRELATOR

Background

Although lock-in amplification is a cross-correlation technique, only continuous signals may be handled by the simple lock-in amplifier of Chapter II. The autocorrelator of Chapter III may be applied to repetitive signals that are not necessarily continuous, but provides an output amplitude that is not linearly related to input amplitude. If a reference signal is readily available, a linear relationship of output with input may be provided by cross-correlation. In fact, depending upon the type of reference provided, cross-correlation allows selective extraction of information from a signal. If the reference is a noise-free version of the signal, the type of operation known as matched filtering is performed, and results in optimization of the signal-to-noise ratio for peak height measurement (39-43). Matched filtering has been used by Miller (39) by cross-correlating noisy decaying exponentials with a noise-free reference.

Cross-correlation may also be used to obtain a criterion of identification for signals consisting of a series of peaks, since a large value of the cross-correlation function at $\tau=0$ is indicative of similarity between signal and reference (3). This procedure is a

type of pattern recognition (45). With binary spectra, the application of Equation 2 results in an AND-sum (46,47).

An example of the application of cross-correlation to emission spectra is shown in Figures 17 and 18 (from Reference 8). Figure 17 shows emission spectra of Co, Ni, and Fe in the region of 3430 to 3500 Å. The spectra were excited using an O₂-H₂ flame and recorded photographically. The plots of Figure 17 are the result of digitizing the output of a scanning densitometer (8).

The Co spectrum was chosen as the sought-for spectral information. The Co, Ni, and Fe spectra were then cross-correlated with the Co spectrum to provide the patterns shown in Figure 18 (from Reference 8). Figure 18A shows the autocorrelation of the Co spectrum. There is a large maximum at $\tau=0$ as expected, indicating the similarity of the two spectra. The remaining pattern contains information about relative peak separations and is not easily interpretable. Also, since the pattern is an autocorrelation, it is symmetrical about $\tau=0$.

The result of cross-correlating the Co with the Ni and Fe spectra is shown in Figures 18B and 18C. Here, there is no distinct maximum at $\tau=0$ indicating that the two spectra in each case are dissimilar. In addition, the cross-correlation patterns are quite complex and not symmetrical.

The large maximum at $\tau=0$ of Figure 18A and the

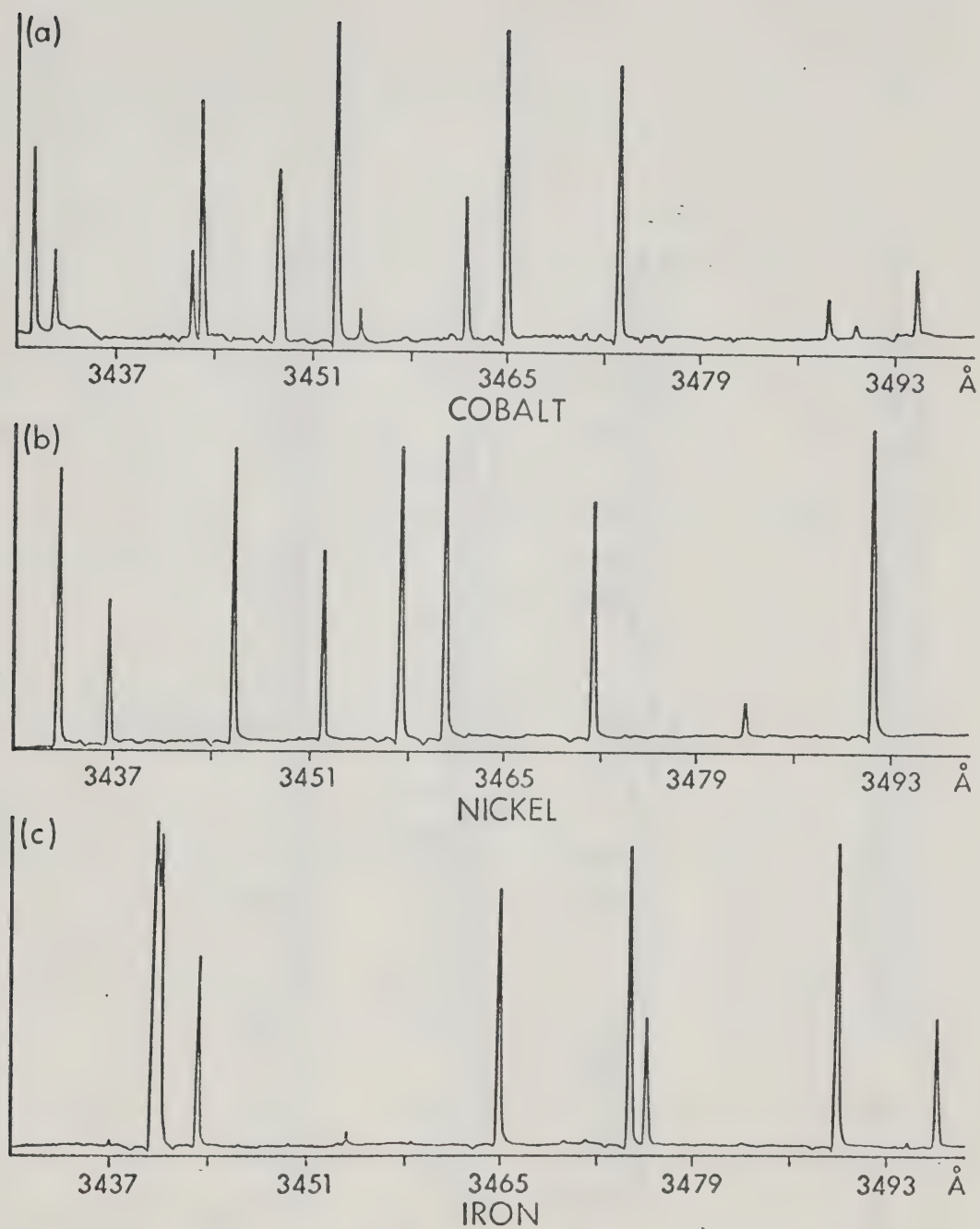


Figure 17. Cobalt, nickel and iron spectra.

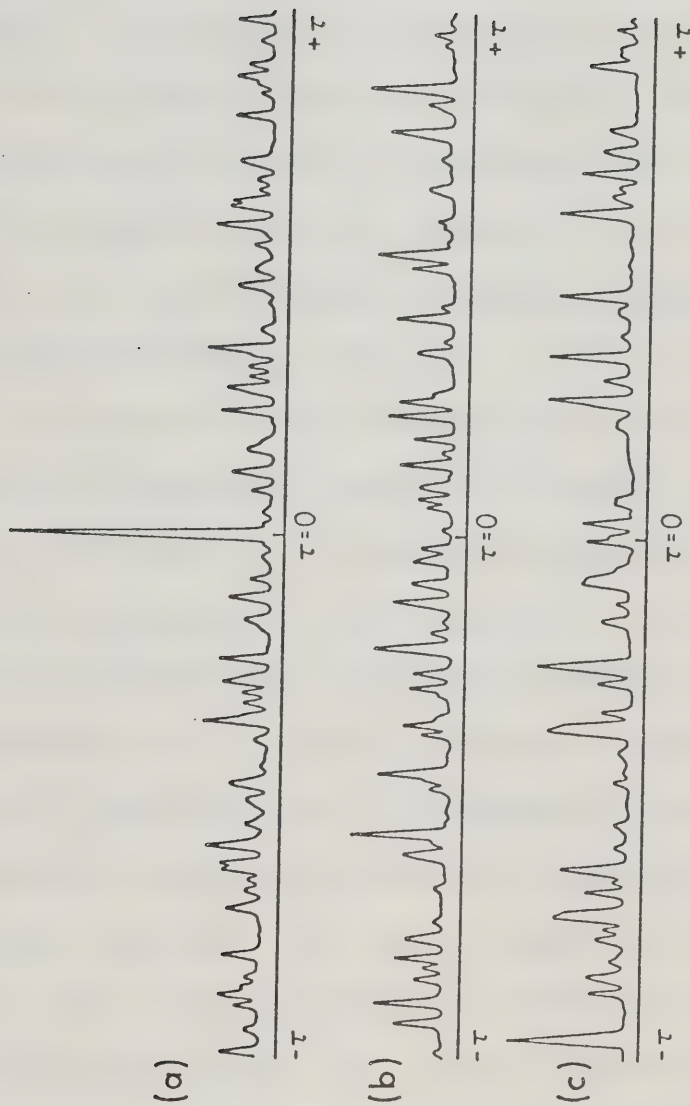


Figure 18. Cross-correlation functions for Co and Co (a), Co and Ni (b), and Co and Fe (c) spectra.

small maximum of Figures 18B and 18C suggest that cross-correlation at $\tau=0$ of a raw spectrum with a reference spectrum of the sought-for element may be used to determine the concentration of the reference element in a complex matrix with a relatively low chance of interference. In addition, there should be a significant increase in signal-to-noise ratio due to the matched filtering operation (8). Beech has used cross-correlation for quantitative NMR analysis with digitized NMR spectra (48) and obtained a signal-to-noise ratio enhancement of about tenfold.

In order for the cross-correlation approach to detection of spectral peaks to be useful, it is necessary to have some method of obtaining information at several different wavelengths simultaneously. An instrument that readily supplies such information is the diode array spectrometer (37). In this chapter, cross-correlation at $\tau=0$ of the output of a diode-array spectrometer with a reference spectrum stored in a specially designed transient recorder (49) will be used to quantitatively measure the atomic emission of elements in an inductively-coupled plasma (ICP) (50). This approach represents a unique "lock-and-key" procedure to the measurement of atomic emission, since only those elements having spectral peaks at wavelengths identical to those of the reference spectrum can contribute to the correlation integral.

A block diagram of the hardware correlator is shown in Figure 19. The output of the diode array spectrometer is connected both to the input of the transient recorder and also to one input of the multiplier/integrator. The output of the transient recorder is connected to the other input of the multiplier/integrator. A reference spectrum is stored in the transient recorder by measuring the emission of a concentrated solution of the element to be determined. The raw array output and the stored reference are then multiplied point by point and integrated over the wavelength range covered. The output voltage is thus proportional to the mutual areas of the signal and reference, with contributions from all peaks of the reference in the wavelength region covered.

It is important to note that this instrument is based on a particular design for a transient recorder, that itself performs some of the sequencing required and also allows background subtraction (49). The construction and operation of this transient recorder will now be discussed.

The Transient Recorder

Transient recorder has become the generic name for a simple digital data acquisition instrument consisting of an analog-to-digital converter, a digital memory, and a digital-to-analog converter (49) (see

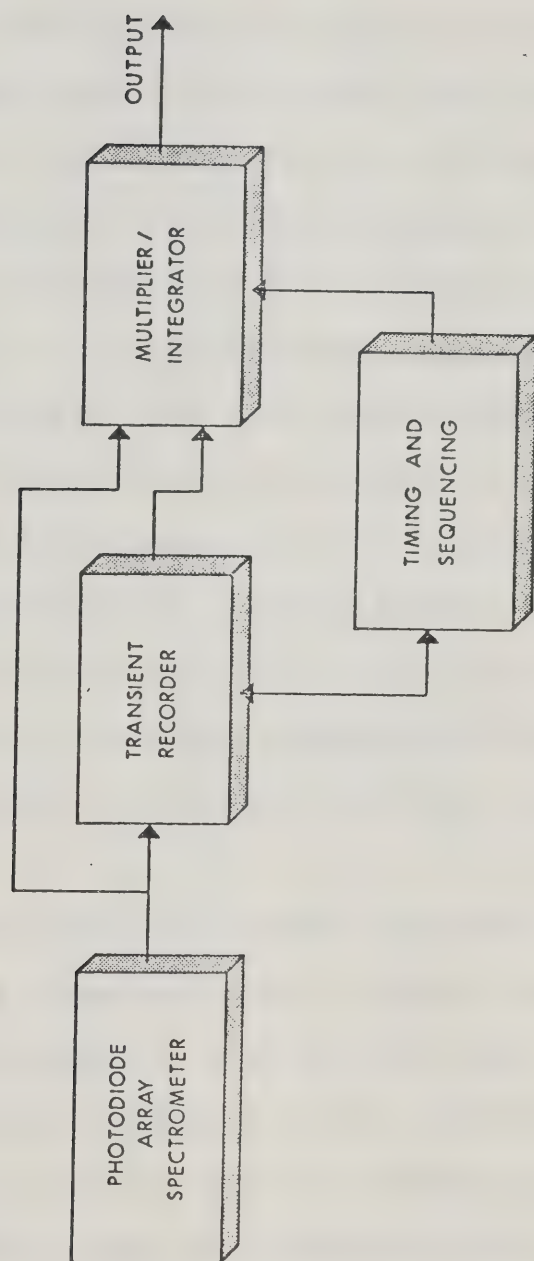


Figure 19. Block diagram of hardware correlator.

Figure 20) although names such as time-domain conversion system (51) and data logger (52) have also been used. Such an instrument is widely applicable to the acquisition and processing of laboratory signals and is frequently used to either obtain data at high speed and read it out later at slow speed, say on a laboratory recorder, or to obtain data at a low speed and read it out at high speed to an oscilloscope or to a computer. Some basic designs have been presented in the literature (10, 51, 52) and transient recorders are available commercially from such manufacturers as Biomation, Princeton Applied Research Corporation and Nicolet Instrument Corporation. In recent years components for the main subsystems (ADC, digital memory, and DAC) have become available at very reasonable costs. With these components, a transient recorder can be built for at least a factor of ten less cost than most commercial systems.

The transient recorder described here can be built for a component cost of about \$300. This design uses a 1024 word (10 bit) digital shift register memory. Unique control circuitry allows subdivision of the memory into several units of variable and arbitrary length. Very often it is necessary to subtract a background from a laboratory signal. Circuitry is provided for synchronized feedback of previously stored information

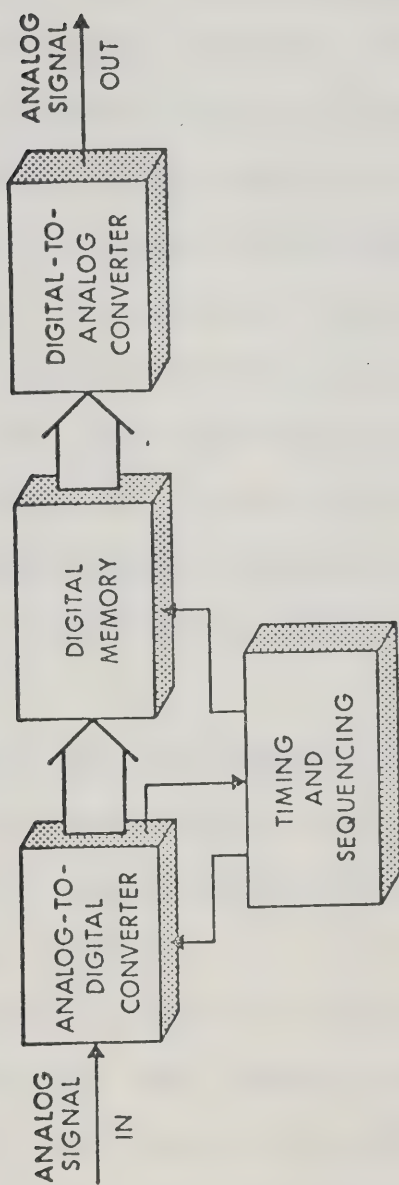


Figure 20. Block diagram of transient recorder.

(i.e. a background scan) to an input difference amplifier which background subtracts an incoming signal. This circuitry is extendable to numerous other data processing operations such as division (ratio), log ratio, multiplication, and addition. Finally, the design includes the sequencing for a versatile pretrigger system. Pretrigger refers to the ability of a transient recorder to acquire data "before" the arrival of an instrumental trigger pulse. In actuality the transient recorder is allowed to free run (continuously acquire data) and the trigger pulse then functions as a stop pulse. The design presented here allows precise variation of the pretrigger delay (number of points obtained before the arrival of a trigger pulse) from zero to 1023 in units of one.

Although the final design differs considerably from that of Korte and Denton (51) and has several additional features, their circuit was a great aid in the initial design stages.

A schematic diagram of the transient recorder is shown in Figure 21. The analog-to-digital converter (Model ADC-10Z) and digital-to-analog converter (model DAC-10Z-3) were both obtained from Analog Devices. The ADC-10Z is a 10-bit successive approximation ADC with a conversion time of 20 μ sec. The DAC-10Z-3 is also 10 bits with a settling time of 5 μ sec. A wide variety of

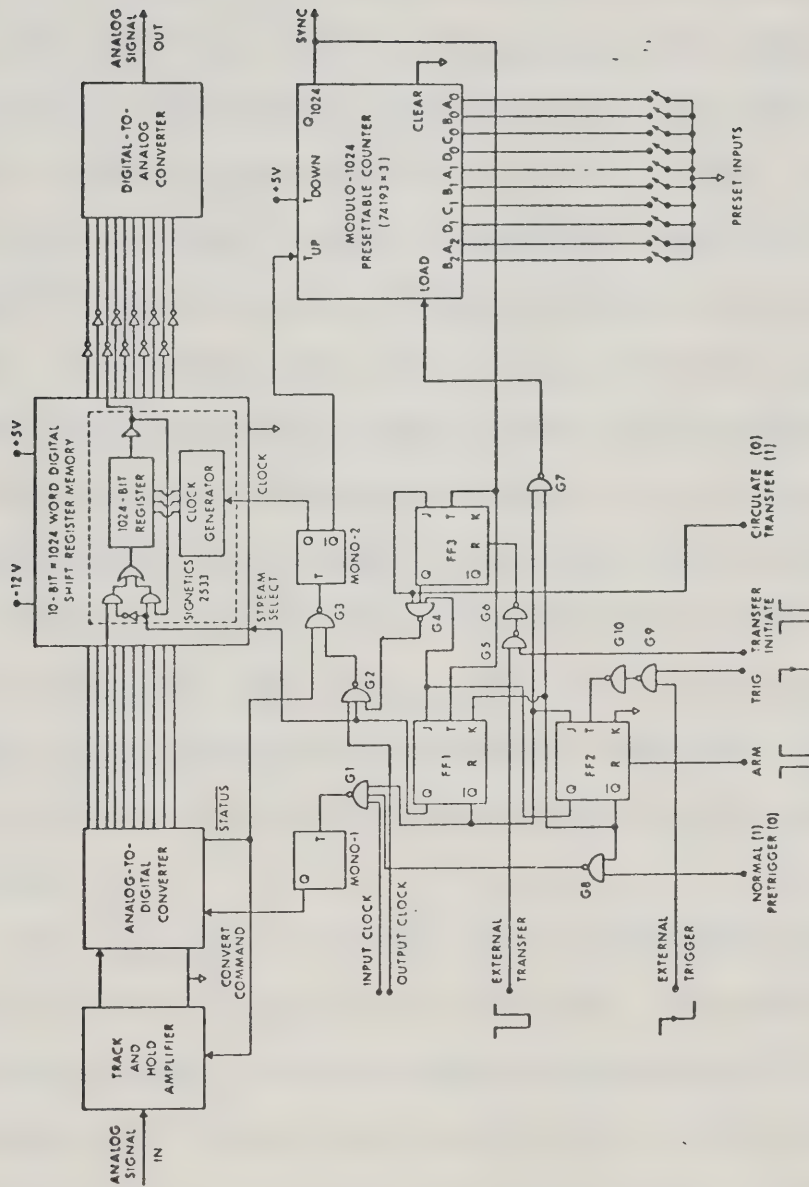


Figure 21. Circuit diagram of transient recorder.

conversion modules could be used other than these depending on the desired specifications of the transient recorder.

The 10-bit by 1024 word digital shift register memory was built up from ten Signetics 2533 1024-bit static shift registers. These registers are TTL compatible and can be clocked from dc to 1.5 MHz. Again a wide range of shift register integrated circuits could be utilized for the memory section of the transient recorder. For example hex 32-bit, dual 128-bit, quad 80-bit and dual 256-bit are some of the configurations available for static shift registers. Static registers are recommended over dynamic registers unless high speed (10 MHz) is required. The rest of the circuit is the timing and sequencing block and the key subsystem is the modulo-1024 presettable counter. It consists of three 74193 presettable 4-bit binary up-down counters.

The transient recorder was breadboarded using a Heath EU-801 Analog-Digital Designer. The ADC and DAC were each mounted on cards which plugged directly into the Heath unit. The 10-bit by 1024 word shift memory was also built on a single card that plugged into the Heath unit. The standard Heath cards and modules were used for the rest of the circuitry.

The operation of the circuit will first be dis-

cussed in its NORMAL mode for the simple acquisition of 1024 data points after application of a trigger pulse. Assume that FF1 is in the 0 state ($Q=0$) and that FF2 is ARMED (reset, $Q=0$). This puts the circuit in a READY condition. In this condition the preset count (assume 0) is automatically loaded (output of G7=0) and the arrival of a trigger pulse is awaited. Upon application of a trigger pulse either manually or externally from an experiment FF2 is toggled to the 1 state ($Q=1$) opening gate G1. Note that any subsequent trigger pulses are ignored ($K=0$ of FF2) until the circuit is rearmed.

When gate G1 is opened, the input clock fires mono-1 (set for about 200 nsec) thereby initiating analog-to-digital conversion. The $\overline{\text{STATUS}}$ output of the ADC controls the track-and-hold amplifier and fires mono-2 (set for about 400 nsec) at the end of a conversion, which writes a new word into the memory. Pulses from \overline{Q} of mono-2 are applied to the count-up input of the presettable modulo-1024 counter. The overflow pulse occurring at the Q1024 output toggles FF1 to the 1 state ($Q=1$), thus closing gate G1 and stopping data acquisition. Note that upon completion of data acquisition FF1 is locked in its 1 state by the connection to K from \overline{Q} of FF2 and that FF2 is inhibited from undergoing a 0 \rightarrow 1 transition by the connection to J from \overline{Q} of FF1. The reasons for these interconnections will be presented later.

Two output modes are provided in the circuit, CIRCULATE and TRANSFER. The CIRCULATE mode is for repetitive output (oscilloscope) and the TRANSFER mode (push button or external control) is for non-repetitive output (recorder). When data acquisition is terminated the circuit may be in either mode. For normal operation when acquiring data we set the output mode to CIRCULATE and the output clock to a high frequency (50-100 kHz). With this arrangement the acquired waveform is automatically displayed on the oscilloscope immediately after data acquisition is terminated (i.e. when FF1 is toggled to the 1 state). In the CIRCULATE mode (0), the output of G4 must be a 1 and this, with the 1 at the Q of FF1, opens gate G2 and puts the memory (stream select = 1) in the recirculate mode. Note that in this mode FF3 is locked in the "0" state by the J connection. The output of the tenth bit of the counter (Q1024) is used to trigger the oscilloscope for trace synchronization.

If, during the CIRCULATE mode, the TRANSFER mode (1) is selected, the next 1→0 transition from Q1024 will toggle FF3 causing the output of G4 to be a 0 and closing G2, thus ceasing data circulation. At this time the memory output will contain the first word of storage. If the TRANSFER INITIATE switch is then momentarily depressed or if a momentary 0 is applied to the EXTERNAL TRANSFER line, FF3 will be reset and the data will

circulate once, again stopping with word number one at the memory output. This mode is used for recorder output (with a slow output clock) or for synchronizing readout of the transient recorder with an experiment.

Now, let's assume that the transient recorder is in its CIRCULATE mode (oscilloscope) and that we want to take in some new data. The circuit can be put into the READY condition by applying an ARM pulse. This resets FF2, unlocking FF1 from its 1 state so that the next 1→0 transition at Q1024 toggles it to the 0 state, closing gate G2 and ceasing data circulation. Note that until FF1 toggles to the 0 state FF2 cannot accept a trigger pulse because of the connection to J from \bar{Q} of FF1. Thus an ARM pulse puts the circuit in a READY condition with the memory output, and hence DAC output, containing the first word of the previously acquired data. This important feature allows modification of new data input to the transient recorder by previously acquired data. For example, the difference between a new signal and a previously acquired signal can be obtained simply by including a difference amplifier in a feedback loop between the output and the input (see Figure 22). This arrangement allows background subtraction of signals acquired from a photodiode array spectrometer.

It is possible, in the NORMAL mode, to acquire less than 1024 points. If the counter is preset to 512,

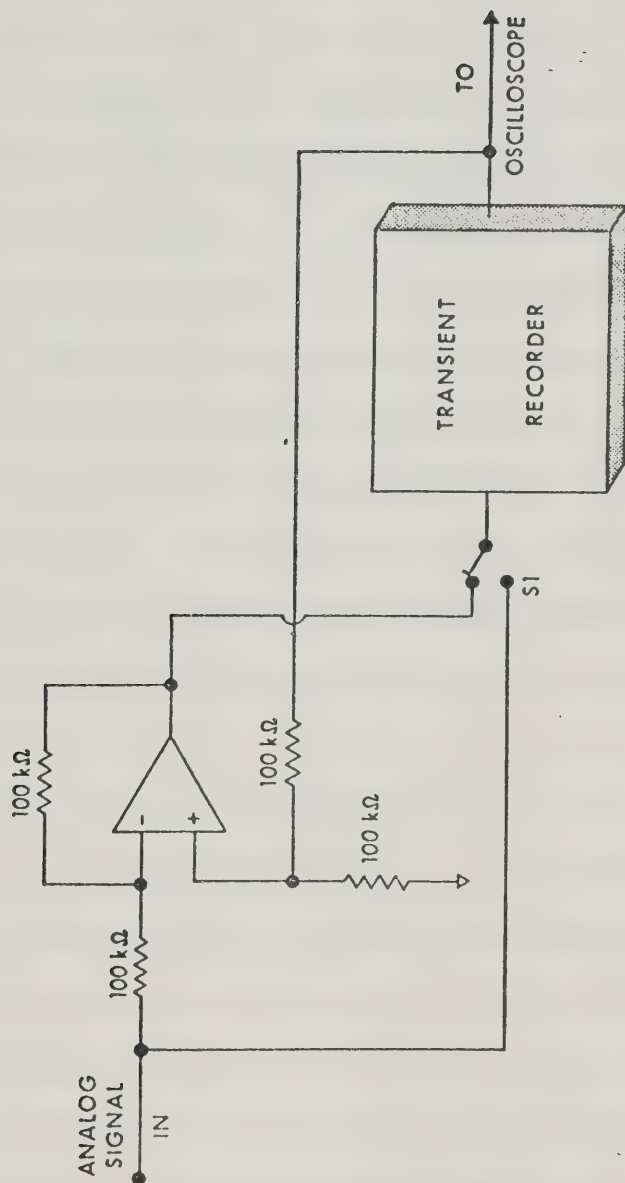


Figure 22. Transient recorder with waveform subtraction capability.

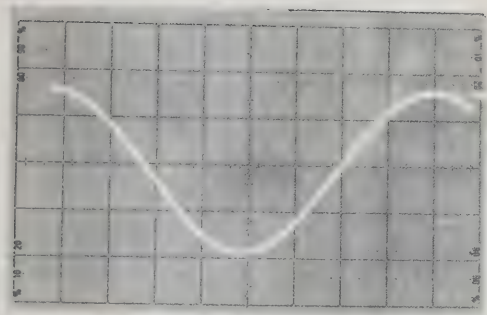
then only 512 points are acquired. Upon termination of data acquisition (in the CIRCULATE mode) the circuit still displays 1024 points as the LOAD function is only activated in the READY condition. If, after acquiring and displaying 512 points, the circuit is put in the READY condition by arming it, a second 512 point waveform can be acquired so that two independent 512 point signals can occupy the memory. This amounts to dividing the memory into two segments. If the counter is set to 768 (1024-256) then 256 points would be acquired and four such waveforms could be stored in the memory. Thus, by appropriate manipulation of the presettable counter the memory can be subdivided into several units of variable and arbitrary length. This very flexible memory subdivision adds considerably to the capability of the transient recorder.

As mentioned earlier the circuit can also be operated in a PRETRIGGER mode. In the PRETRIGGER mode the output of gate G8 is a 1 so that data acquisition starts as soon as the circuit is in the READY condition. In this condition the output of gate G7 is a 0 which overrides the counting function of the presettable counter. The circuit stays in this free running mode, continuously acquiring data until a trigger pulse is received. Application of a trigger pulse frees the counter and allows it to count up from its preset condition to 1024. The Q1024

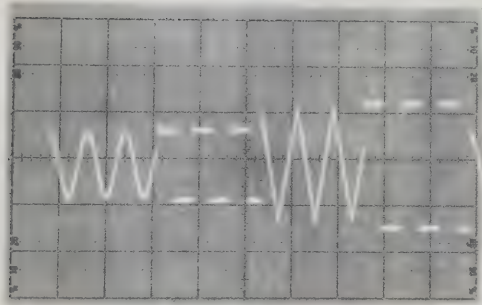
output terminates data acquisition in the normal way. Thus, if the counter is preset to 0 the shift register memory will contain 1024 samples of the input signal occurring after the trigger (start) pulse; if preset to 512, it will contain 512 samples acquired before the trigger pulse and 512 samples acquired after the trigger pulse. With this design the pretrigger delay can easily be varied from zero to 1023 in units of one using the preset inputs.

The operation of the transient recorder is shown in Plate 3 and Figures 23 and 24. Memory subdivision is illustrated in Plate 3. A full 1024 point acquisition is shown in Plate 3a, four 256 point acquisitions in Plate 3b and three acquisitions of 192, 320 and 512 points are shown in Plate 3c. Memory subdivision and background subtraction are both illustrated in Figure 23. The memory was subdivided into four 256 point segments. The first segment contains an optical spatial pattern as measured with a 256 element photodiode array (37). This array has a strong sinusoidal fixed pattern background noise. This can be subtracted out using the system shown in Figure 22 and the result is stored in the second segment of memory (Figure 23b). The array background is stored in segment 3 (Figure 23c) and the signal stored in segment 4 (Figure 23d) is the result of subtracting two repetitions of the signal in 23a. The

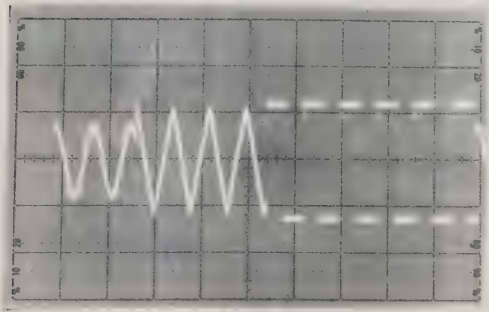
Plate 3. Oscilloscope photographs illustrating normal and memory subdivision modes of the transient recorder. (a) Full 1024 point acquisition. (b) Four successive 256 point acquisitions of independent signals. (c) 192, 320 and 512 point acquisitions.



(a)



(b)



(c)

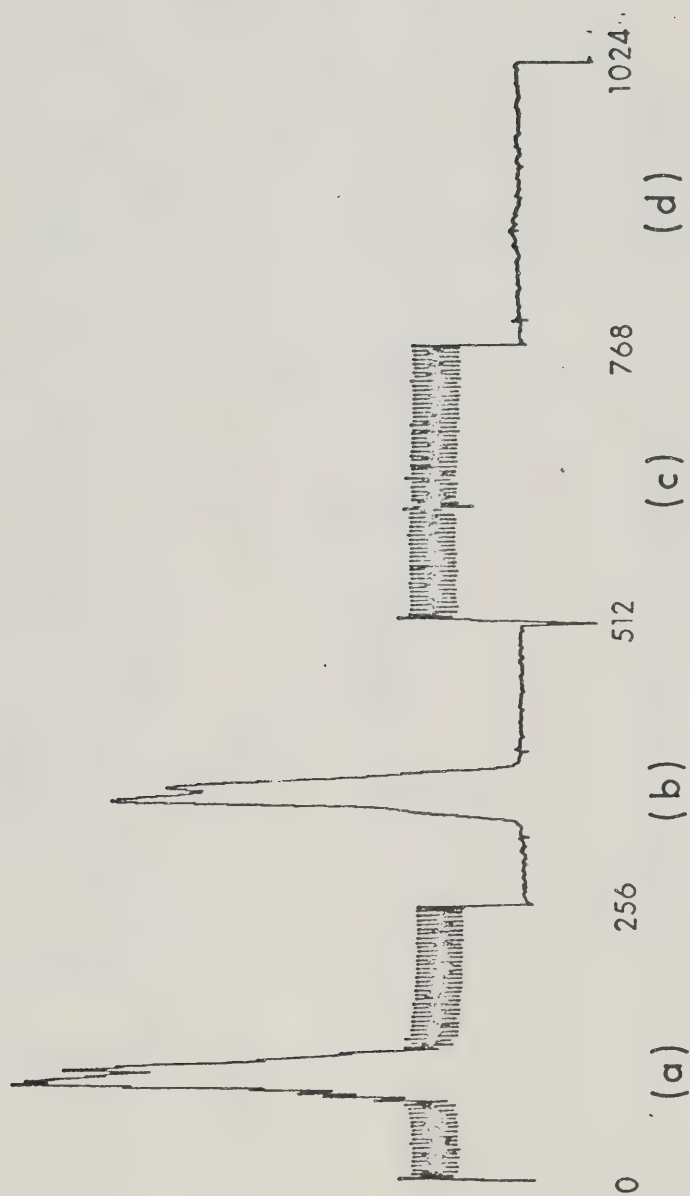


Figure 23. Chart recorder output illustrating memory subtraction and background subtraction capability. See text for discussion.

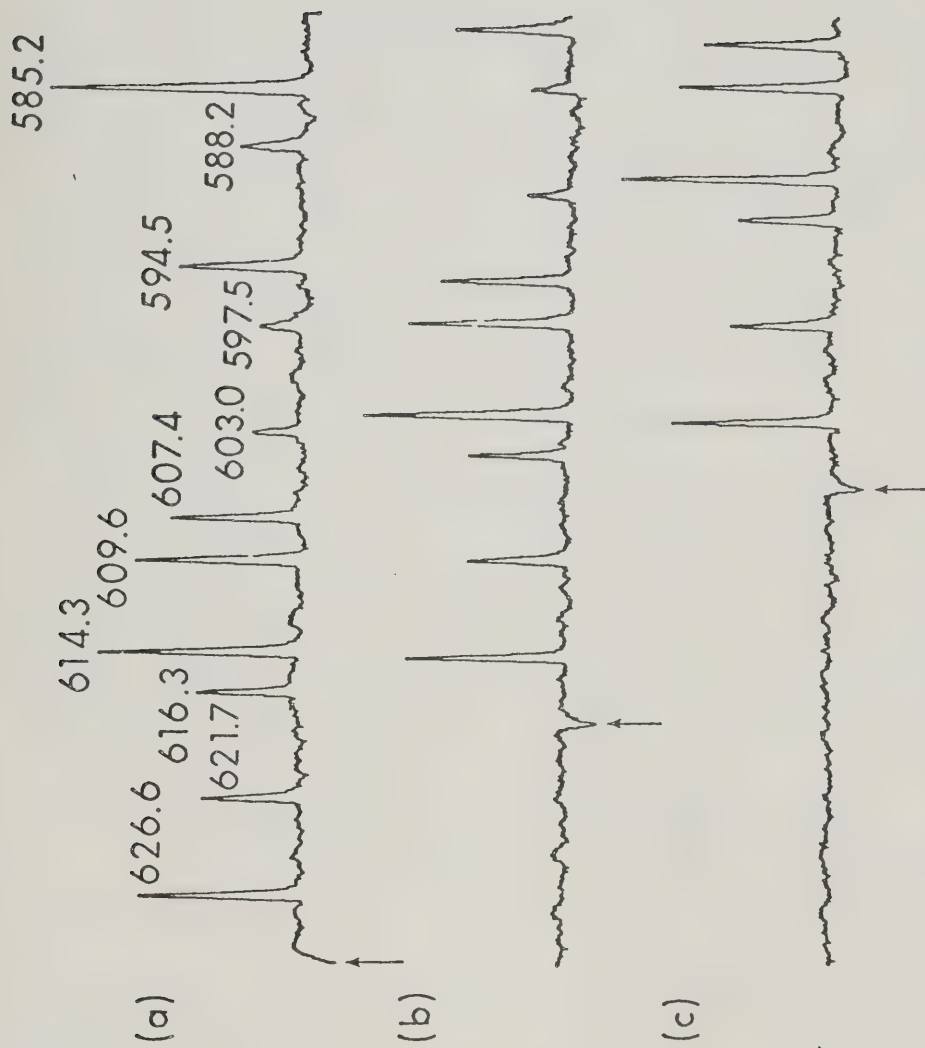


Figure 24. Output signal (neon spectrum) from a photodiode array spectrometer as measured with the transient recorder. NORMAL mode (a) and PRETRIGGER mode with 256 (b) and 512 (c) pretrigger delay settings. Arrow indicates the point in time at which the trigger pulse occurs.

small residual in the central part of Figure 23d indicates that intensity drifted between the two measurements of the optical spatial pattern. The signal shown in Figure 24a is a spectrum of neon in the region of 610 nm as measured from a photodiode array spectrometer. It was measured in the NORMAL mode and a total of 1024 points being obtained at a rate of 45 Hz and then output to a chart recorder at 7 points/sec. This spectrum is identical to that obtained from a minicomputer data acquisition system for a single scan without background subtraction. The noisy base line is due to fixed pattern noise and dark current (see reference 37). The PRE-TRIGGER mode is illustrated in Figures 24b and 24c. In these cases 256 and 512 points were acquired before the trigger pulse that initiates the scan of the photodiode array. It should be noted that the transient recorder cannot be simultaneously operated in both the background subtraction and PRETRIGGER modes.

A transient recorder can add considerable flexibility to a variety of data acquisition tasks in the laboratory. Typical applications range from the measurement of transient atomic absorption signals generated by furnace and carbon rod atomization systems to stopped-flow measurements. For many minicomputer systems it can provide a simple off-line oscilloscope refresh system or it can be used to transfer plots to a recorder, freeing

the minicomputer for more important data acquisition or processing tasks. In addition, the transient recorder is a fundamental building block for more sophisticated instrumentation. Systems with dual memories or even two transient recorders combined with analog components such as multipliers, dividers, difference amplifiers, log modules, and log-ratio modules can perform a large variety of data processing tasks, as can the single memory system presented here with synchronized feedback. In fact, the modification of this transient recorder to perform hardware cross-correlations is exceedingly simple. Finally, it is interesting to note that the recent development of analog shift registers in integrated circuit form is sure to have an impact on transient recorder instrumentation (34). These devices offer the potential of replacing the major functional blocks of the transient recorder (ADC, digital memory, and DAC) with a single 16 pin integrated circuit and in fact the construction of a high speed transient recorder using a serial analog delay line integrated circuit has already been reported (38).

Experimental

Inductively coupled plasma. A commercially available ICP (Plasma-Therm Inc., Rte. 73, Kresson, N.J. 08053) was used as a source of emission spectra. The torch output was imaged with a circular lens onto the entrance

slit of the photodiode array spectrometer. The diode array used contained 1024 elements and provided about 50 nm of wavelength coverage.

Operating conditions for the ICP and spectrometer are given in Table II, and are not necessarily optimum.

Chemicals. Stock solutions (1000 ppm) were made of reagent-grade metal salts. Standard solutions were prepared as required by dilution and used immediately.

Instrumentation. The transient recorder/hardware correlator was breadboarded using a Heath EU-801 Analog-Digital Designer. Standard Heath cards were used for the correlator module except for the sample-and-hold amplifier (model SHA4), which was obtained from Analog Devices.

A schematic of the correlator is shown in Figure 25. Circuit operation is based on the 1024-point transient recorder (TR) with background subtraction capability already described. The TR was used in the NORMAL mode without memory subdivision, i.e. all 1024 points from the diode array were stored for the reference. The array clock is used to control both data acquisition and data recirculation so that these two processes will be precisely synchronized. In order to load the reference, the most concentrated of the standards to be run was aspirated into the plasma and the TR was ARMED. When a spectrum had been acquired, a water blank was aspirated and background subtraction was performed. Multiplication

TABLE II

Operating Conditions of ICP and Spectrometer

RF frequency	27.125 MHz
RF power	1.9-2.0 kW
Coolant flow	14-15 lpm
Nebulizer pressure	32 psi Ca; 36 psi Cr
Observation height (above top of coil)	22 mm Ca; 25 mm Cr
Array center (nominal)	407.5 nm Ca; 420.0 nm Cr
Slit width	100 μ m

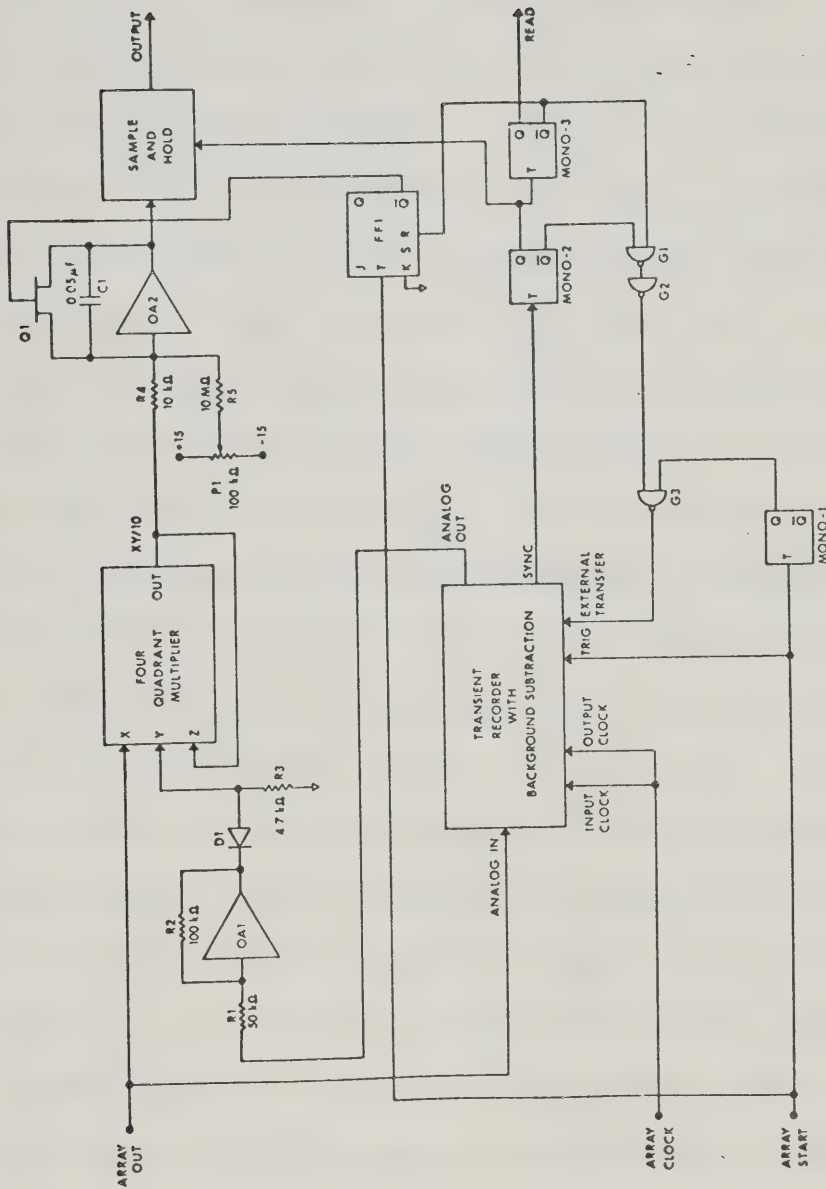


Figure 25. Circuit diagram of hardware correlator.

and integration were performed with a simplified version of the circuitry used in Chapter III.

In order for the correlation to proceed correctly, the TR must be operated in the TRANSFER mode. The reference spectrum will then be stored with the first point available at the TR output. A sample or standard is then aspirated into the plasma and its emission detected. A START pulse from the array toggles mono-1, beginning recirculation of the reference spectrum. The TR output is amplified and inverted by OA1 and clipped by diode D1 and resistor R3 to provide noise immunity. The multiplier output is thus the product of the raw sample spectrum and the clipped, background-subtracted reference spectrum. Simultaneously with the start of spectral multiplication, FF1 is toggled, opening Q1 and allowing integration of the multiplier output by R4 and C1. When reference recirculation is complete, the SYNC pulse from the TR toggles mono-2, causing the sample and hold amplifier to acquire the integrator output. The falling edge of mono-2 toggles mono-3, which resets FF1, closing Q1 and resetting the integrator. The falling edge of mono-3 may also be used to trigger a readout device such as a digital voltmeter. Gates G1, G2, and G3 ensure that the TR cannot recirculate until all sequencing has been terminated.

Potentiometer P1 may be used either to ensure that

integrator output is constant between peaks or to adjust the sampled voltage to be zero when a blank is aspirated.

Readout System. Output voltages were measured with a digital voltmeter (DANA Model 5400) and sent by a SERDEX interface (53) to a teletype for printing. Details of the SERDEX interface are given in Appendix I. Additional circuitry allowed printout of ten successive values on command.

An alternative approach would be to low-pass filter the SHA output to be measured on a chart recorder, as was done with the SAM (35).

The linearity of the correlator was determined with a sine wave generator with $R_2 = 100 \text{ k}\Omega$, $R_4 = 100 \text{ k}\Omega$, and D_1 and R_3 not in circuit. The resulting data are shown in Figure 26.

For a 10-V p-p reference at 45 Hz with a clock rate of 45 KHz, a plot of output versus input for inputs of 0.5 to 15 volts p-p yielded a correlation coefficient of 0.999919 on a linear plot and a slope of 0.9994 ± 0.0041 on a log-log plot. Operated in this manner the correlator acts essentially as a lock-in amplifier. If, however, a large number of cycles of the reference waveform are stored in the TR, then the Q of the circuit will be so high that output instability will result unless either both the input frequency and the

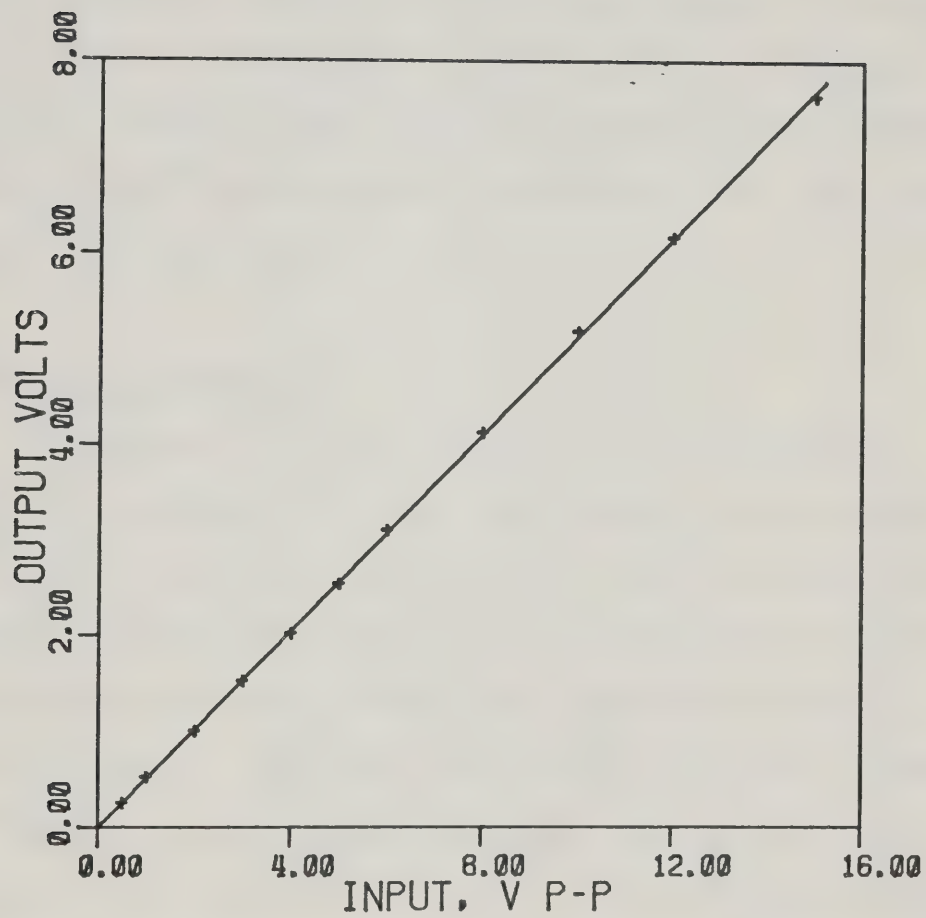


Figure 26. Output vs input of circuit of Figure 25 for sine wave signals.

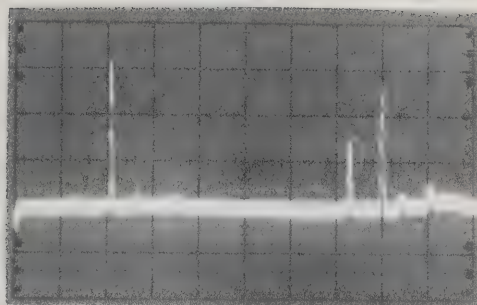
clock frequency are extremely stable or they are synchronized by some means. In the correlation of diode array spectra, clock pulses are synchronized with diode position, so the correlator output is stable with respect to clock drift. If the correlator was to be used as a lock-in amplifier, stabilization could be ensured by multiplying the sine-wave frequency by a phase-locked loop (10) to obtain the clock signal.

Results and Discussion.

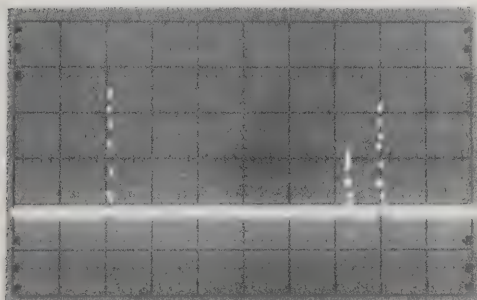
Operation of the correlator is illustrated in Plate 4 for calcium. The raw (unfiltered) array output for 10 ppm Ca is shown in Plate 4a. This is stored in the TR and background subtracted as described to yield the reference spectrum, Plate 4b. Multiplier output is shown in Plate 4c, and the integral in Plate 4d. Clearly, contribution to the integral is made only by the three Ca lines (422.7, 396.8, 393.4 nm) and the output voltage contains a contribution from all the peaks. Since the raw array output is not background subtracted, there will be a blank caused by array dark current and the argon continuum, plus any overlapping lines. The value of the blank will depend on array integration time and efficiency of cooling, height of observation in the plasma, wavelengths observed, plasma operating conditions, and element under investigation, and can be quite sig-

Plate 4. Oscilloscope photographs illustrating correlator operation for calcium determination. (a) Raw diode array spectrum of 10 ppm calcium showing lines at 422.7, 396.8 and 393.4 nm. (b) Background subtracted reference. (c) Multiplier output. (d) Integrator output.

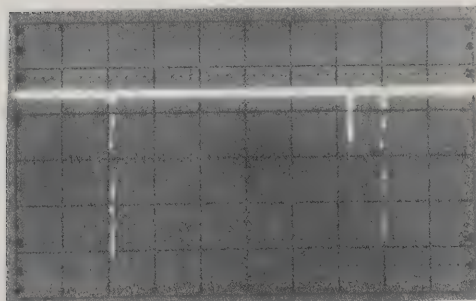
(a)



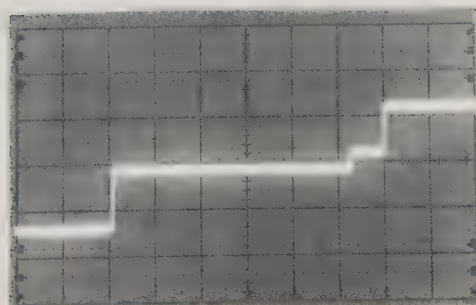
(b)



(c)



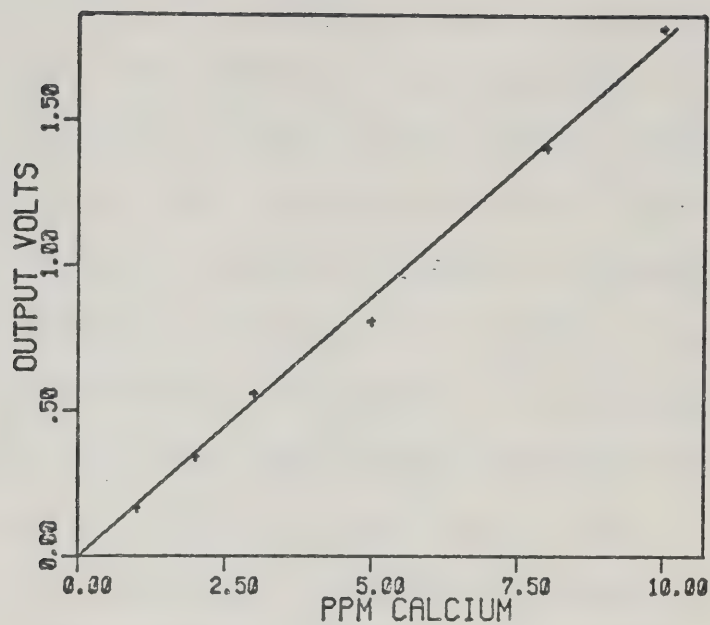
(d)



nificant (0.1±1 volt) with potentiometer P1 adjusted so that integrator output is constant between peaks, as in Plate 4d.

The use of the correlator to determine calibration curves for standard solutions of calcium is illustrated in Figure 27. Figure 27a is a plot of net correlator output in volts versus ppm Ca for solutions from 1-10 ppm. Each point is the mean of 10 measurements. The emission lines used were at 422.7, 396.8, and 393.4 nm with an array integration time of 4.32 sec. A least squares treatment of the data yielded a regression line with a slope of 0.1810 ± 0.0057 V/ppm, an intercept of -0.021 ± 0.033 V, and a correlation coefficient of 0.998000. The relative standard deviation of the 10 measurements of the 10 ppm solution was 3.2% and the detection limit based on a S/N of 2 was 0.4 ppm. The same solutions were run by T. Edmonds under the same operating conditions but utilizing a computer based data acquisition system (37) and a software integration to yield the data of Figure 27b. Here, each point is the total of ten successive background-subtracted array scans. A least squares treatment yielded a slope of 169.70 ± 1.26 units/ppm, an intercept of -6.23 ± 7.35 units, and a correlation coefficient of 0.999889. This software calculation is clearly of higher accuracy than the analog treatment.

A



B

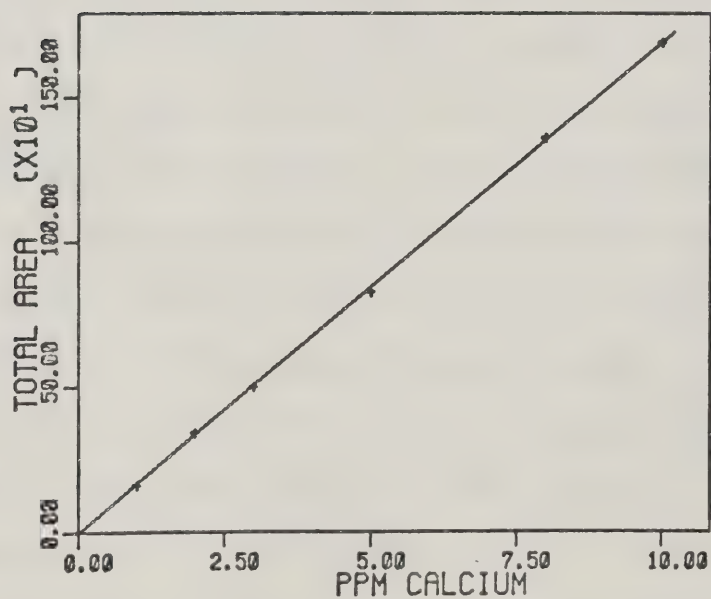


Figure 27. (a) Correlator output vs calcium concentration. (b) Software peak area (arbitrary units) vs calcium concentration. The same solutions were used in both cases.

Calibration curves for chromium are illustrated in Figures 28 and 29. The analysis lines used were at 429.0, 427.5, and 425.4 nm. For a concentration range of 10-100 ppm (Figure 28) an integration time of 2.16 sec was used. A least squares treatment yielded a slope of 0.02994 ± 0.00029 V/ppm, an intercept of -0.062 ± 0.017 V, and a correlation coefficient of 0.999817. The relative standard deviation of the 100 ppm solution was 2.2%, and the detection limit for a S/N of 2 was 4 ppm. The detection limit can be lowered by utilizing a longer integration time. This effect is shown in Figure 29, in which solutions of 1-10 ppm Cr were measured with an integration time of 14.40 sec. A least squares treatment yielded a regression line with a slope of 0.06317 ± 0.00078 V/ppm, an intercept of -0.008 ± 0.005 V, and a correlation coefficient of 0.999693. The relative standard deviation on ten readings of the 10 ppm solution was 1.8%, and the detection limit based on a S/N of 2 was 0.5 ppm. The large decrease in observed output voltage in Figure 29 compared with Figure 28 is due to a decreased net signal intensity from reduction of array dynamic range by increased dark-current pedestal (37).

Actual array output spectra (without background subtraction) are shown in Figure 30 for 10 and 1 ppm Cr with the same operating conditions as used in Figure 29. The large pedestal is clearly visible, as well as the

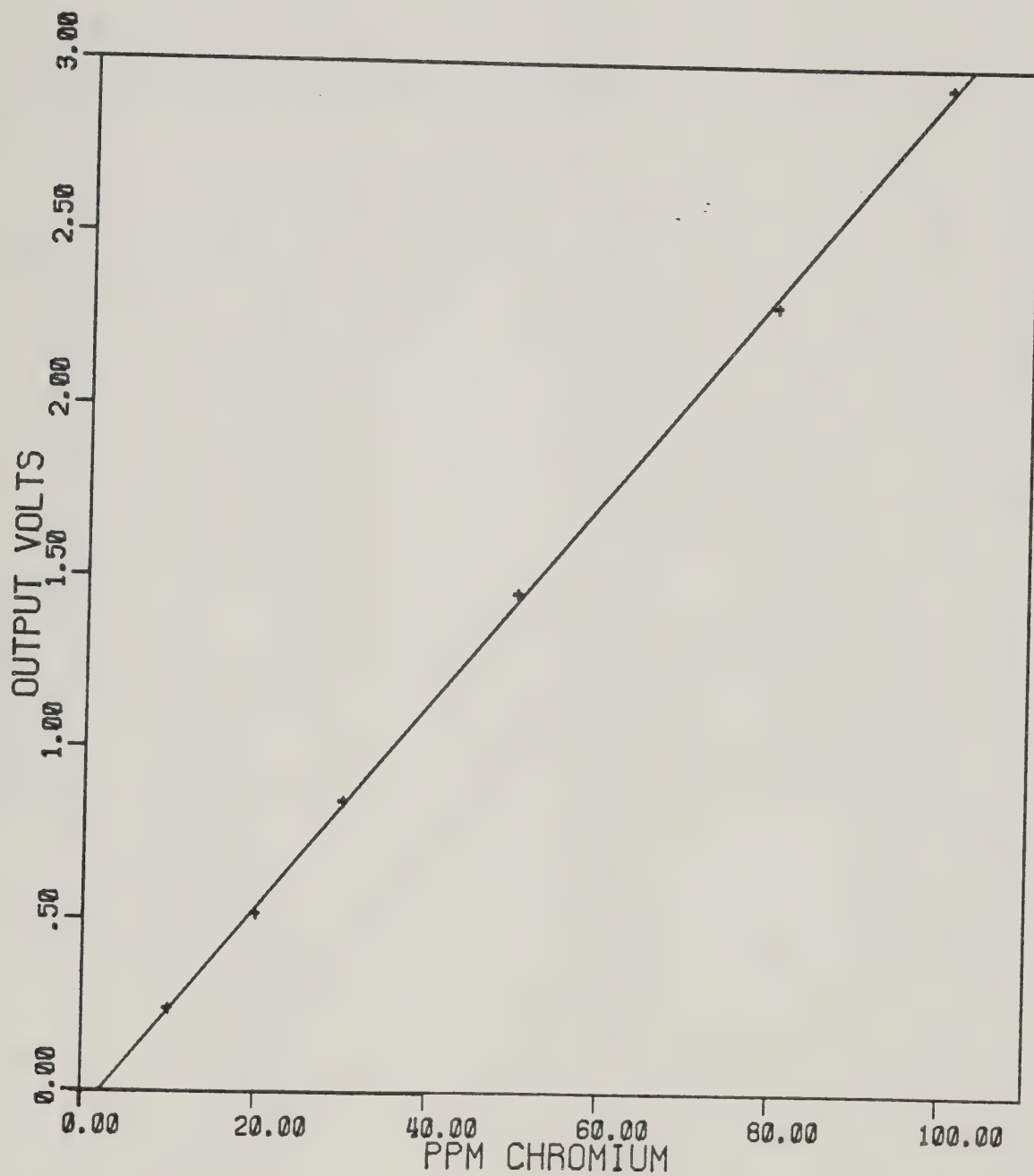


Figure 28. Correlator output vs chromium concentration.
Integration time 2.16 sec.

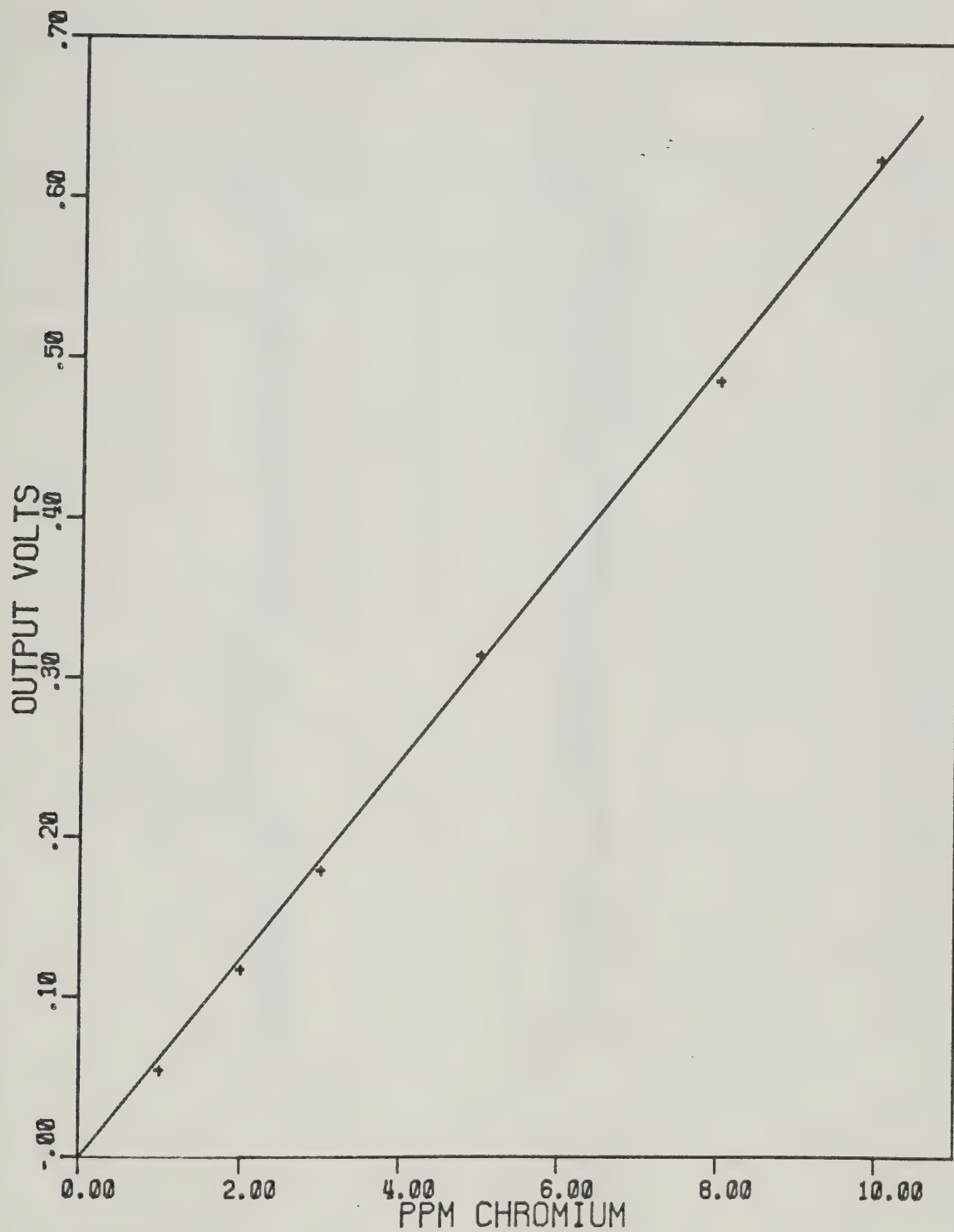


Figure 29. Correlator output vs chromium concentration.
Integration time 14.4 sec.

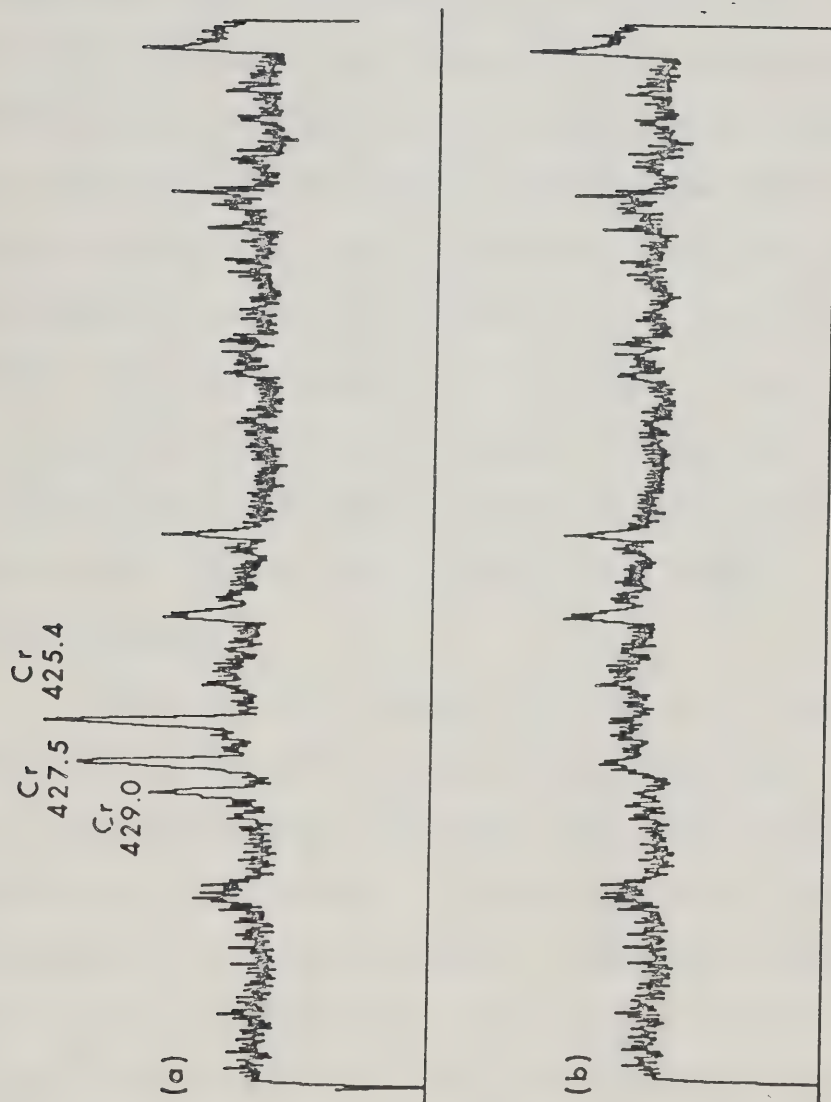


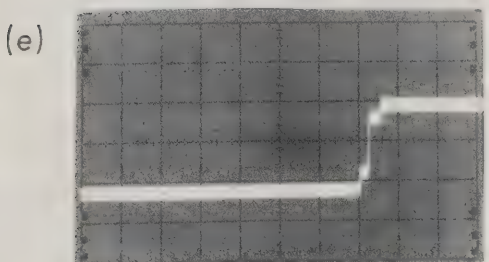
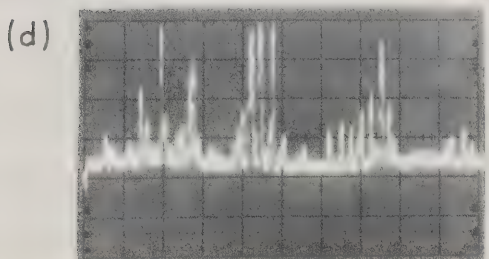
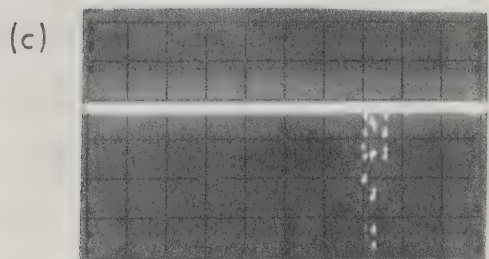
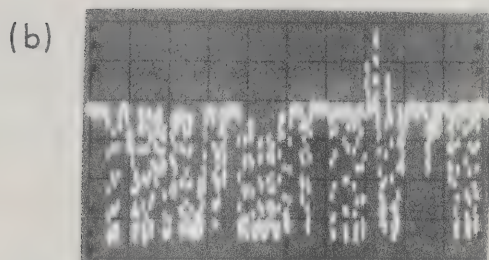
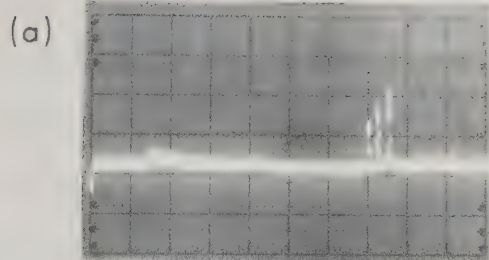
Figure 30. Spectrometer output for solutions containing (a) 10 ppm and (b) 1 ppm chromium under the conditions used to obtain Figure 29.

fixed-pattern noise on the unfiltered array output (37). Discernment of the chromium triplet on the 1 ppm solution is difficult or impossible with the unaided eye.

The background noise level of the multiplier/integrator was determined by grounding the X and Y inputs of the multiplier and sequencing the correlator with the diode array and transient recorder in the normal way. Measurements of the output voltage then gave a standard deviation of 8 mV on ten readings. Standard deviations on the data shown in Figures 27a, 28, and 29 ranged from 66 mV (for 100 ppm Cr) to 11 mV (for 10 ppm Cr at an integration time of 14.40 sec). These data indicate that the major sources of noise do not originate in the correlator itself, but rather in the diode array and/or in the plasma.

Because this approach maximizes sensitivity by determining the total area of all elemental lines in the wavelength region covered, any lines that overlap with any of the lines of the analyte will cause an interference in the determination. A method of eliminating this type of interference is shown in Plate 5. The upper trace (Plate 5a) shows the chromium triplet located at 360.5, 359.3, and 357.9 nm. The right-hand line of the triplet overlaps partially with the weak iron line at 358.1 nm. The iron interference can be reduced or eliminated by a stripping procedure illustrated

Plate 5. Oscilloscope photographs illustrating the use of a stripped reference. (a) Raw diode array spectrum of 10 ppm chromium showing the lines at 360.5, 359.4 and 357.9 nm. (b) Chromium reference after subtraction of spectrum from 1000 ppm iron. (c) Reference spectrum at multiplier input, after inversion and clipping. (d) Raw diode array spectrum of a mixture of 10 ppm chromium and 100 ppm iron. (e) Integrator output for multiplier inputs of (c) and (d).



in photographs b, c, d, and e. The raw chromium spectrum is loaded in the transient recorder in the normal way, but instead of aspirating a water blank for background subtraction a concentrated iron solution (1000 ppm) is employed. When the background subtraction is performed, the trace of Plate 5b results. The higher concentration of iron causes most of the lines to saturate the array and the overlapped (left-hand) portion of the 357.9 nm (right-hand) line is stripped from the reference. Other unoverlapped iron lines become negative, since both the A/D and D/A convertors in the TR are bipolar. This spectrum is then amplified and inverted by OA1 and clipped by D1 and R3, yielding the trace of Plate 5c at the Y-input of the multiplier. The negative iron peaks have now been removed from the reference. Correlation of this stripped reference with the spectrum of a solution containing 10 ppm Cr and 100 ppm Fe, in which the intensity of the overlapped line is clearly out of proportion, yields the integrator output shown in Figure 5e. The largest contribution to the integral is now made by the unoverlapped 359.3 nm chromium line. A plot of correlator output versus iron concentration is shown in Figure 31 for solutions containing 10 ppm Cr and 0, 30, 100, and 250 ppm Fe. Correlation with a normal (unstripped) Cr reference (triangles) yielded a slope of 0.00106 ± 0.00017 V/ppm Fe, an

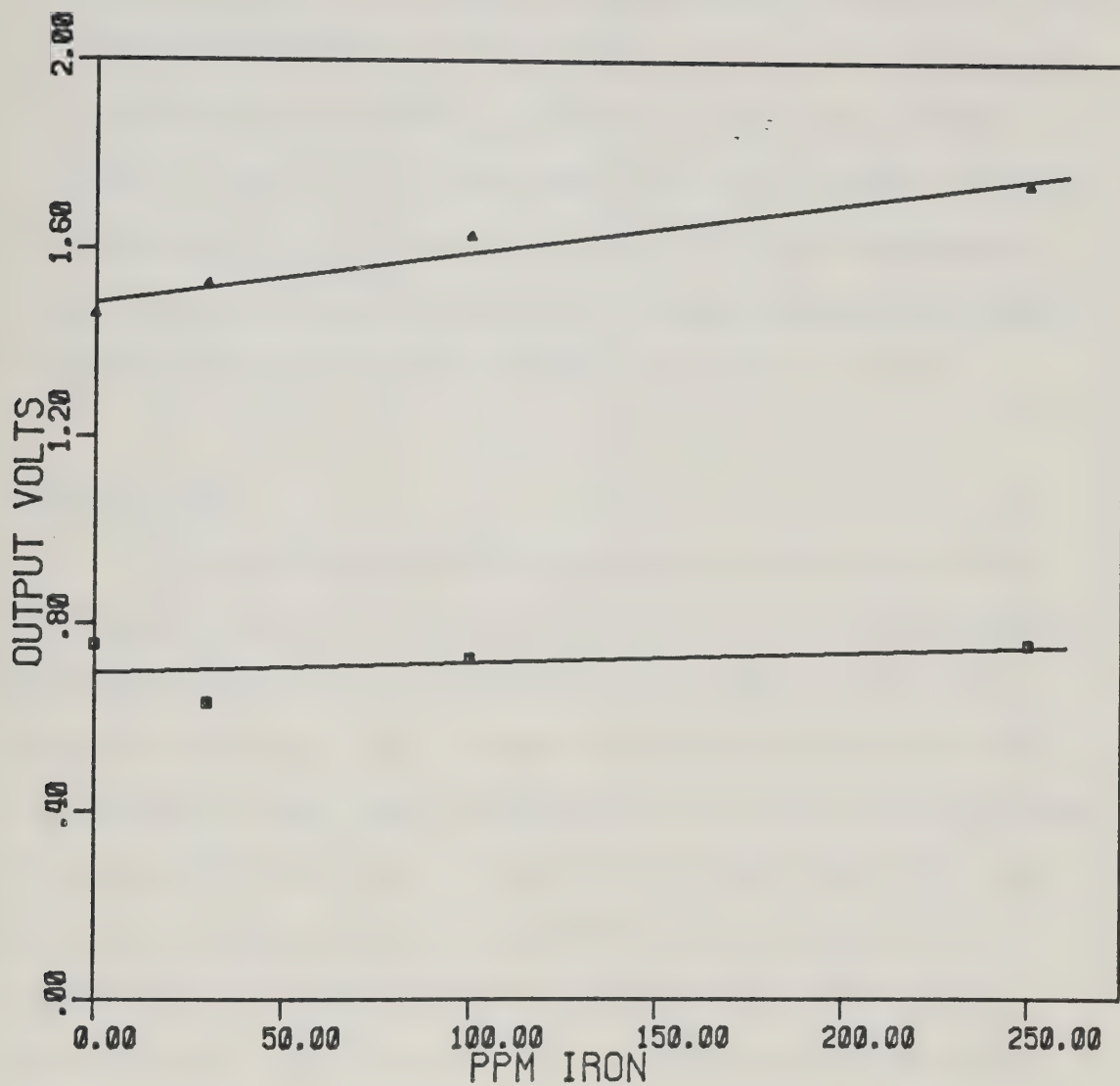


Figure 31. Correlator output vs ppm iron when using an unstripped (triangles) and stripped (squares) chromium reference. See text for discussion.

intercept of 1.486 ± 0.023 V, and a correlation coefficient of 0.976.

A similar treatment of the same solutions but using a stripped reference is also shown in Figure 31 (squares). A least-squares treatment yielded a slope of 0.000217 ± 0.000341 V/ppm Fe, an intercept of 0.697 ± 0.046 V, and a correlation coefficient of 0.410. The iron dependence was therefore reduced markedly by the stripping procedure, although at the cost of halving the output signal.

Conclusions

Hardware correlation provides a fast and highly automated way of reading out the diode array spectrometer. The calculations are performed as quickly as the data can be read out, i.e. 23 msec for 1024 points at 45 kHz. In general, this time period will be so much shorter than the time between scans (integration time) that the data can be regarded as being available instantaneously. Although the instrument as described uses an analog correlation, accuracy could be increased by converting the raw signal to digital form and using the transient recorder output to gate a high-speed binary adder, thereby performing a digital correlation. With such an approach, the transient recorder need only store a logical one at each peak position to gate the binary adder. Therefore, the amplitude resolution required of the

transient recorder need not be as high, and a one-bit analog-to-digital converter, i.e. a comparator, could provide sufficient resolution. This approach would also reduce the number of shift registers needed in the TR memory. Background subtraction could also be performed digitally. While the instrument does not perform τ variation, this could be accomplished either by the circuitry of Chapter III or, perhaps more simply by scanning the monochromator (44).

The correlator has been so designed that a reference can be loaded and results obtained simply by pushing a button; very little operator expertise is required for use of the correlator itself. Although a computer data acquisition and treatment routine could be written that would allow similar ease of operator training, the speed of a software computation would be much less and the cost, at least at present, much greater. The self-aligning nature of the correlation procedure makes monochromator adjustment noncritical, yielding a technique for atomic emission that is as specific as is the use of a particular hollow-cathode lamp for atomic absorption. In addition, correlation provides the opportunity of performing sequential multi-element analysis simply by changing the reference spectrum. The use of hardware correlation for the readout of emission spectra therefore provides a remarkable

degree of flexibility in both design and operation, according to the specific requirements of each individual user.

CHAPTER V

DIGITAL FILTERING

Background

The correlation operations discussed so far involve the direct implementation of the correlation integral. An alternative method that has become popular in recent years is the Fourier transform implementation of correlation, i.e. multiplication of the Fourier transforms of the signal and correlation function and inverse Fourier transformation of the result (54-61). This procedure is illustrated pictorially in Figure 32 (from Reference 3). The original noisy spectrum (Figure 32a) is transformed to yield the Fourier domain representation (Figure 32d). High frequency noise in the Fourier spectrum is eliminated by boxcar truncation (Figure 32e) to give a modified Fourier domain representation (Figure 32f). Inverse transformation of Figure 32f yields the smoothed spectrum (Figure 32c). The same result could be obtained by cross-correlating the original spectrum (Figure 32a) with the time domain representation of the Fourier domain smoothing function, i.e. a sinc function (Figure 32b). Figure 31 is, therefore a pictorial representation of Equations 4 and 5.

In Chapters II, III, and IV, we have discussed the direct application of the correlation integral (Equation 4). In this chapter, we will discuss

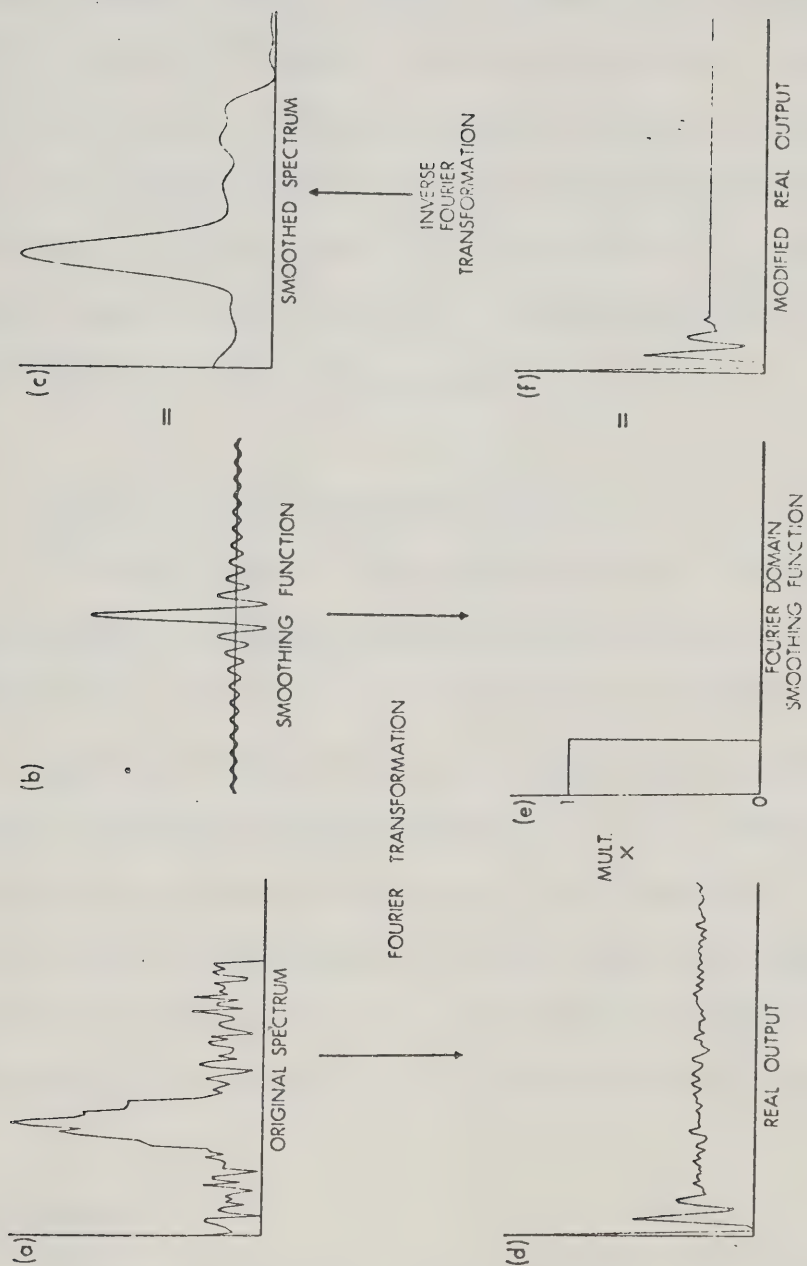


Figure 32. Smoothing of a signal by direct cross-correlation (a,b,c) and by Fourier domain digital filtering (a,d,e,f,c).

the Fourier transform route of Equation 5. The first part of this chapter will deal with the application of a simple Fourier domain digital filter that readily allows various types of signal modification (54). In the second part, the Fourier domain representation of a popular class of digital filters developed by Savitzky and Golay (62) will be presented. The calculations to be discussed were carried out on a PDP8/e computer using a program (DIGFIL) given in Appendix II.

A. The Fourier Transform Route

In this study, the application of a very simple but versatile Fourier domain digital filter is illustrated (54). The filter is based on a simple trapezoid that has been widely used as an apodizing function in Fourier transform spectroscopy (63, 64). When applied to spectral signals this filter is remarkably versatile. Through the manipulation of four numerical indices smoothing, differentiation, resolution enhancement or deconvolution can easily be implemented on a signal.

Experimental

The spectra used to demonstrate the application of the digital filter were measured using a computer-coupled photodiode array spectrometer (37). Sources used included a dc arc and a Mg hollow cathode lamp.

All calculations were carried out in the PDP-8/e computer which is part of the data acquisition system for the photodiode array spectrometer. Programs were written in FORTRAN and run under the OS/8 operating system.

The digital filters were implemented using the Fourier transform route as illustrated by Equations 4 and 5. A Fast Fourier Transform (FFT) (65, 66) was used to carry out the transformation of the spectra and the inverse transformation of the filtered Fourier domain signal. The output of the FFT subroutine consists of two series, $X(J)$ and $Y(J)$, which are the real and imaginary components of the transform. All filtering operations were carried out on the real part of the transform ($X(J)$). Thus $X(J)$ corresponds to $A(f)$ in Equation 5 and will be referred to as the Fourier domain signal.

If the spectrum ($a(x)$) consisted of N digital spectral points, then N values of both the $X(J)$ and $Y(J)$ arrays were calculated using zero filling (67). After filtering (Eq. (5)), the N values of the filtered Fourier domain signal ($C(f)$) were transformed back, again using zero filling, to N values of the real ($X(J)$) and imaginary ($Y(J)$) components of the transform. On this second transform, the N values of the real array are the desired filtered spectral components ($c(x)$) (56).

Zero filling provides interpolation (68) as well as keeping all arrays at the same length, a major convenience in Fourier domain digital filtering operations.

The Fourier domain digital filter $B(f)$ in Equation 5) was a simple trapezoid characterized by four indices (N_1 , N_2 , N_3 , N_4) that define the vertices of the trapezoid. Typical Fourier domain digital filters that can be obtained by manipulation of the integer values of the four indices are shown in Figure 33. The vertical dotted line indicates the position of the first point (0 Hz) of the Fourier domain signal. Digital filtering is implemented simply by multiplying the Fourier domain signal by the appropriate filter function. Signal points between N_1 and N_2 , and N_3 and N_4 are multiplied by the "y" value of the slope, which varies linearly between 0 and 1. Signal points between N_2 and N_3 are not altered, and those less than N_1 and greater than N_4 are set equal to zero. To implement a particular filter the operator simply types in the desired four indices, N_1 , N_2 , N_3 and N_4 at the computer terminal. If N_1 is zero and N_2 is equal to 1, a filter such as that shown in Figure 33a results; whereas setting N_1 negative and N_2 positive (>1) results in the filter shown in Figure 33e. The remaining figures indicate other possible filters obtained by varying the values of the indices.

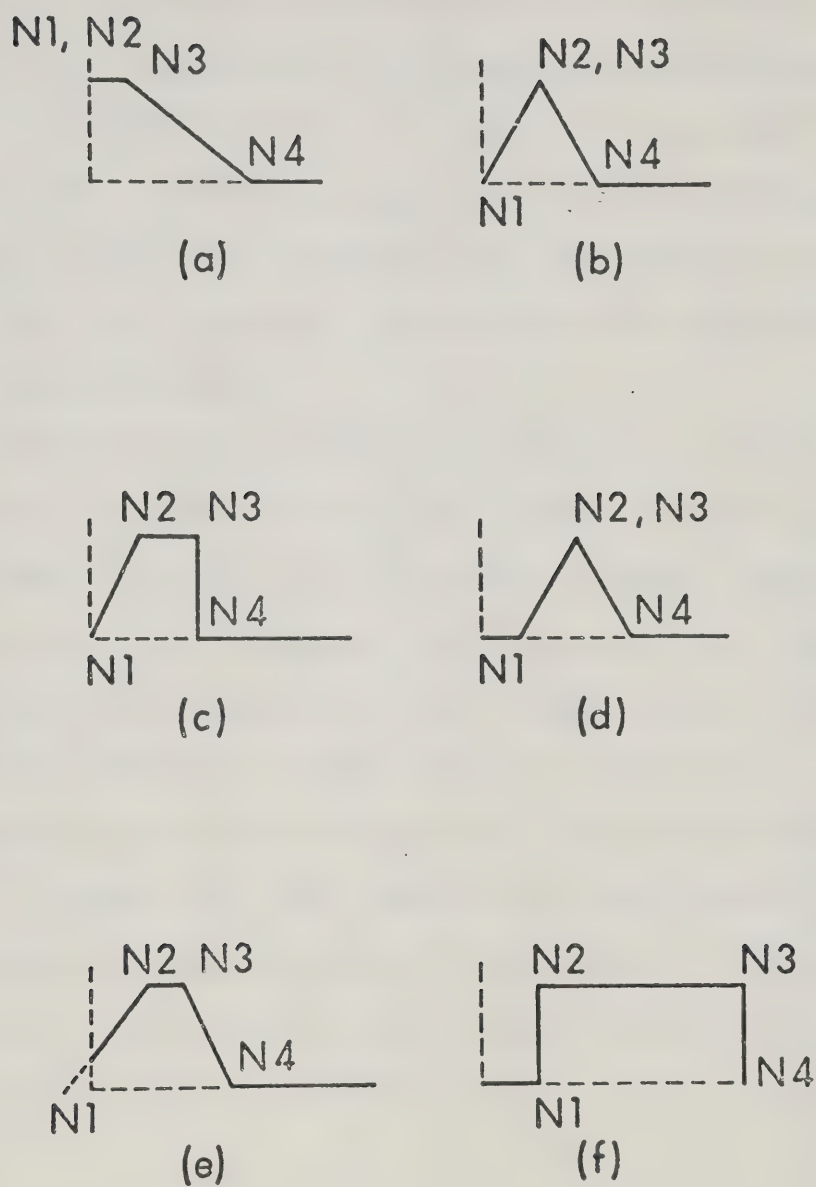


Figure 33. Fourier domain digital filters. See text for discussion.

Additional Fourier domain digital filters can be obtained by successive application of the filters shown in Figure 33. Successive application of the filters shown in Figures 33b and 33c results in the filter shown in Figure 34a. Similarly, the filter shown in Figure 34b results from two successive applications of the filter shown in Figure 33e, once with $N_2=N_3$ and the second time with $N_3=N_4$.

Several signal processing operations can be carried out on spectra using these digital filters. The filter shown in Figure 33a is used for general purpose smoothing and high frequency noise elimination. Diagnosis of noise information is often useful and can be carried out using the filter shown in Figure 33f. Differentiation can be accomplished using the filters shown in Figures 33b, 33c, 33d and 34a and deconvolution can be approximated using the filters shown in Figures 33e and 34b. These operations are all discussed and illustrated in the next section.

Results and Discussion

The distribution of signal and noise information in the Fourier domain representation of a noisy signal is such that signal information tends to be concentrated in the first part of the transformed noisy signal and noise information, particularly if it has high frequency

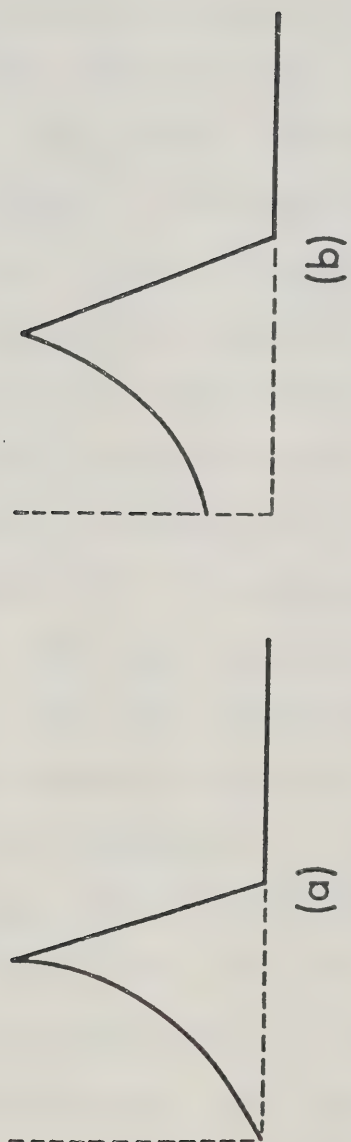


Figure 34. Second derivative (a) and "deconvolution" (b) Fourier domain digital filters.

components that are separated from the signal information, tends to appear in the later part of the transformed noisy signal (55). In such cases, digital filtering can be quite effective in minimizing the noise on a signal. A spectrum is shown in Figure 35a (Mg triplet at 382.2 nm) that contains high frequency noise, particularly on the peaks. This noise was caused by a faulty power supply in the measurement system. The real part of the Fourier transform of this noisy signal (Figure 35b) clearly reveals the presence of excess high frequency noise. The Fourier domain signal shown in Figure 35b is 256 points long. Application of the filter shown in Figure 33a with $N_1=0$, $N_2=1$, $N_3=99$ and $N_4=100$ results in the retransformed spectrum shown in Figure 35c. Note that the majority of the high frequency noise has been removed from the spectrum.

From a diagnostic point of view it may be useful to determine the distribution of the noise in the signal domain. This can be accomplished by using a filter with indices equal to 99, 100, 255, 256 (see Figure 33f). The result of applying such a filter is shown in Figure 35d, which indicates that the noise was concentrated in the region of the spectral peaks.

Further examples of the effectiveness of Fourier domain digital filtering in removing high frequency noise components are shown in Figure 36. The spectrum

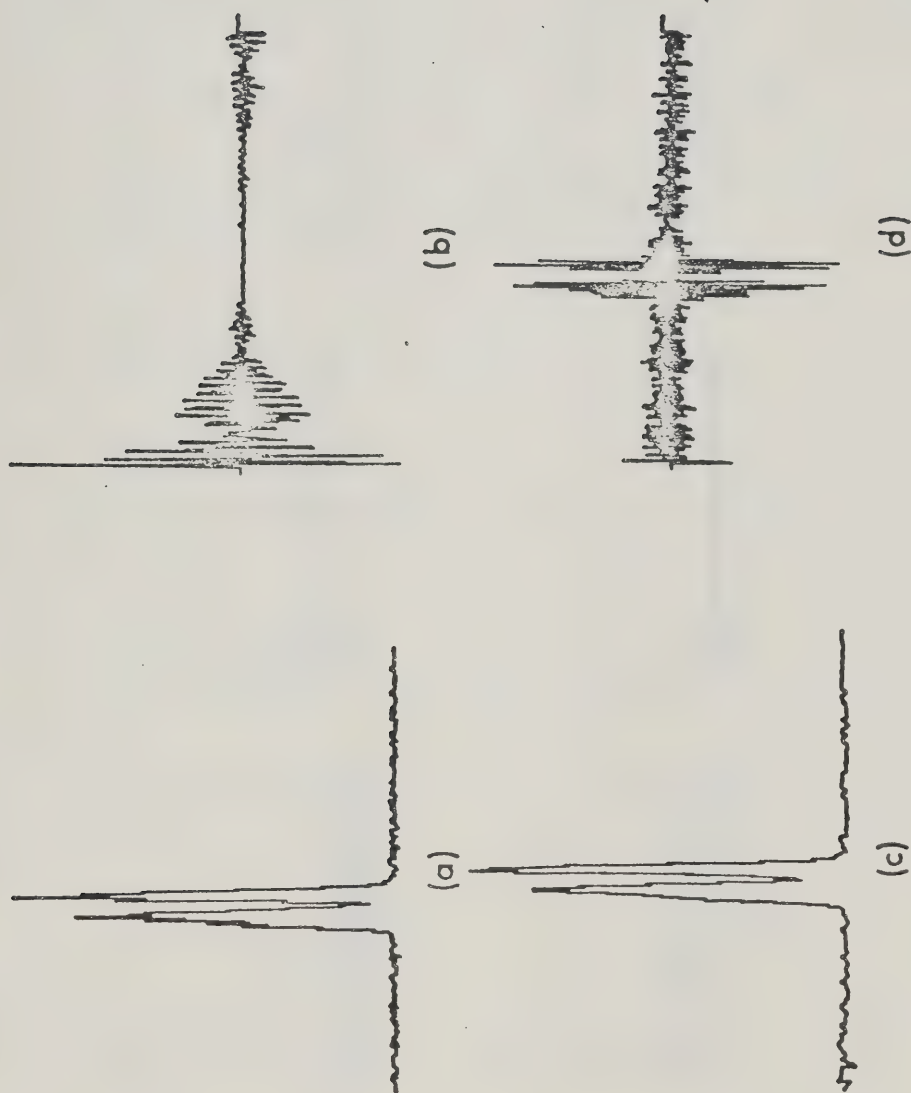


Figure 35. Removal and analysis of high frequency noise on a signal. See text for discussion.

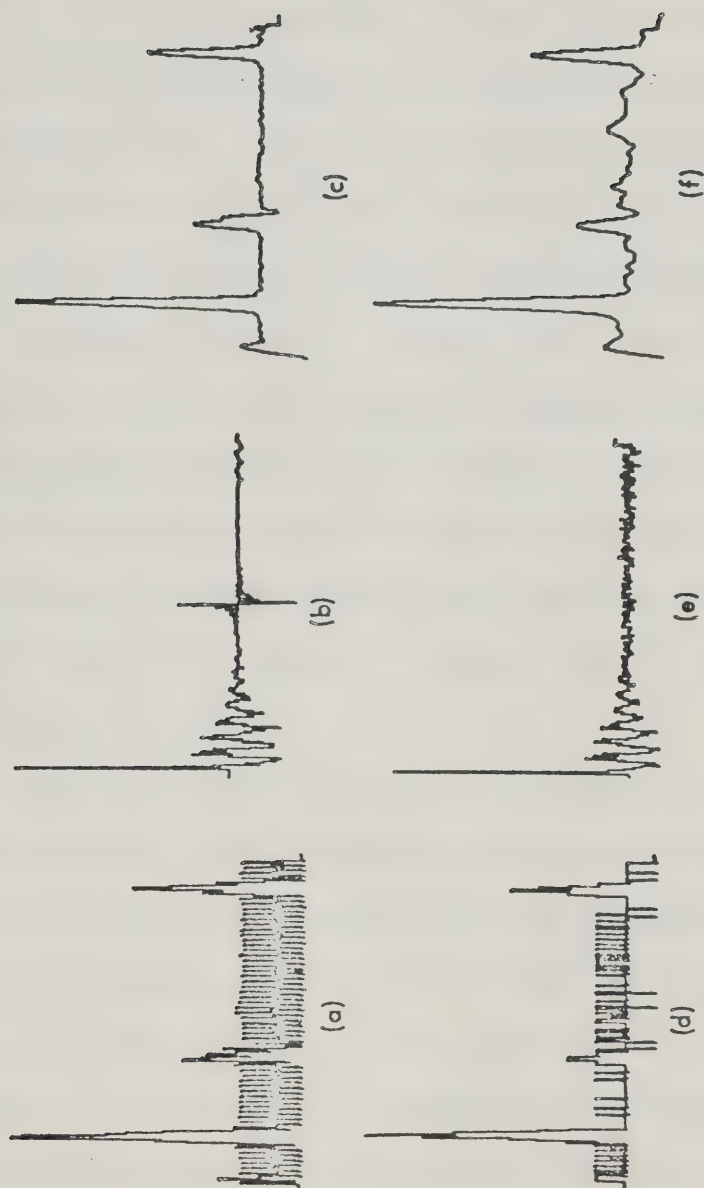


Figure 36. Removal of fixed frequency noise (a,b,c) and minimization of quantizing noise (d,e,f) by Fourier domain digital filtering.

shown in Figure 36a contains an intense fixed frequency noise component. Its transform (Figure 36b) indicates that the noise is concentrated at about the 125th word. A filter with indices equal to 0, 1, 99, 100 easily removes this narrow-band high-frequency noise component (see Figure 36c). Also, if desired, a software notch filter could be set up for noise of this type.

With low level signals quantizing noise can become serious as shown in Figure 36d. Quantizing noise has considerable high frequency components as shown by the transform of this signal (Figure 36e). Application of a digital filter with indices equal to 0, 1, 2, 100 and retransformation yields the spectrum shown in Figure 36f, in which the effects of quantization noise are considerably reduced.

The derivative theorem of Fourier transforms (69) states that if the imaginary part of the Fourier transform of a function is multiplied by a linear ramp starting at the origin, the result is the real part of the Fourier transform of the first derivative of the original function. In practice a linearly decreasing ramp is often combined with the increasing ramp to avoid undue accentuation of high frequency noise (55, 70). Such a digital filter can easily be set up using the trapezoid indices as shown in Figure 33b. The first derivative is perhaps of minimal use in processing peak type signals

although it has found application in detecting peak locations by use of the zero crossing value. However, if the filter shown in Figure 33b is applied instead to the *real* part of the Fourier transform of the signal and the resulting function (which now is the imaginary part of the Fourier transform of the first derivative of the signal) is retransformed, a resolution-enhanced signal is obtained. This is illustrated in Figure 37, in which the real part of the Fourier transform (Figure 37b) of the spectral signal shown in Figure 37a is multiplied by the digital filter shown in Figure 33b with indices equal to 1, 125, 125, 250. Note that the signals and transform in Figure 5 are all 512 points long. The resulting resolution-enhanced signal is shown in Figure 37c.

Higher derivatives of a signal have been used to obtain further peak sharpening (71-73). A second derivative may be obtained by two successive applications of the filters shown in Figure 33b and 33c resulting in the overall filter shown in Figure 34a. It was found that very similar results could be obtained with a single application of the filter shown in Figure 33d. The resolution enhanced signal obtained using this filter (Figure 33d) with indices equal to 25, 125, 125, 250 is shown in Figure 37d. Resolution enhancement is greater than that obtained in Figure 37c although the negative sidelobes, characteristic of second derivative

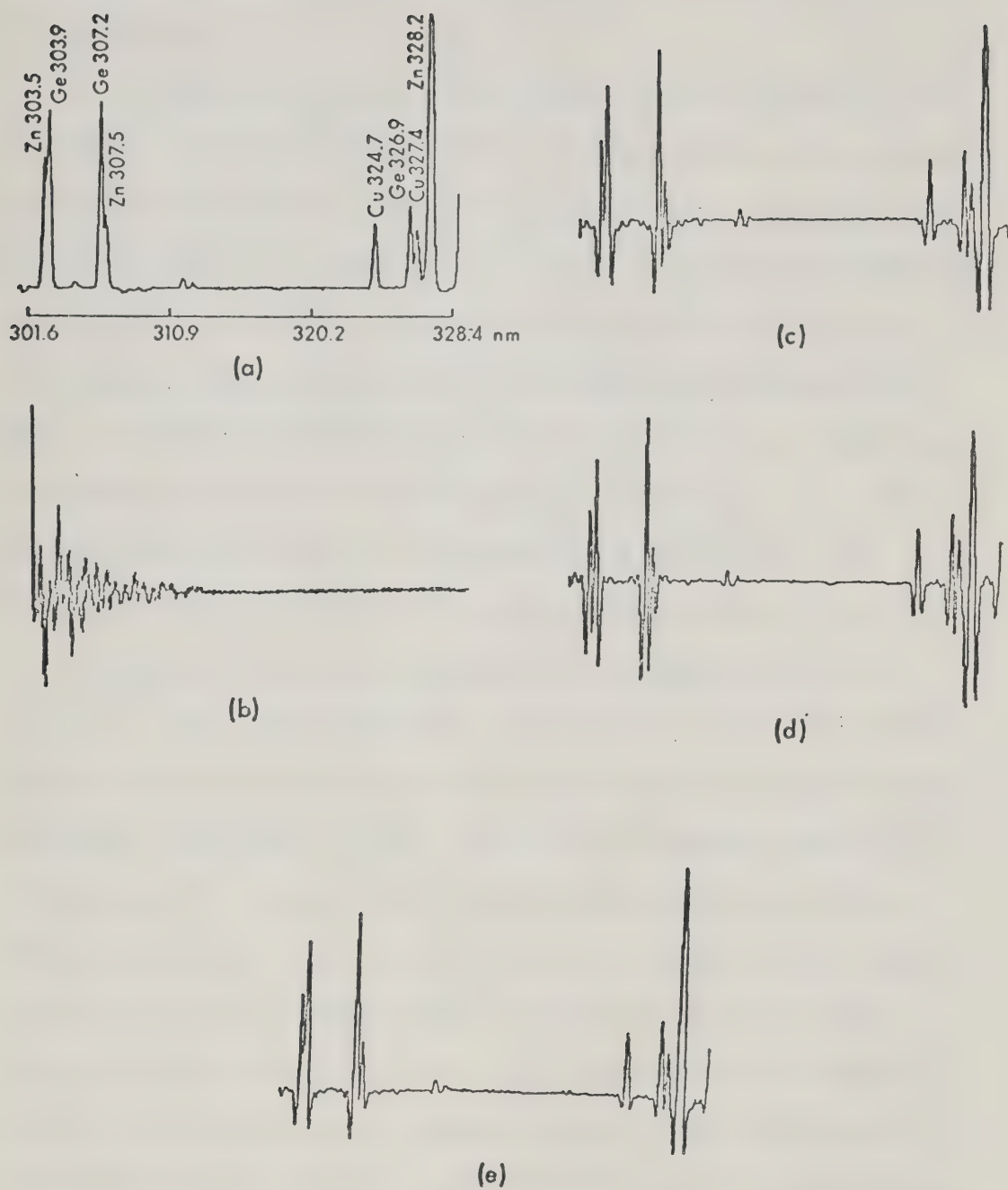


Figure 37. Resolution enhancement using "differentiation" and "deconvolution" Fourier domain digital filters.

resolution enhancement procedures, are also increased in magnitude.

Finally it is also possible, using filters such as those shown in Figure 33e and Figure 34b, to approximate deconvolution resolution enhancement techniques. Deconvolution, in the Fourier domain, is accomplished by dividing the Fourier transform of the observed signal by the Fourier transform of the response function (69, 74). In spectroscopy the signal is a spectrum and the response function is the resolution function. If the resolution function is assumed to be $\sin^2 x/x^2$, its Fourier transform will be a linear truncation function of a form similar to a filter with indices equal to 0, 1, 1, N4. Deconvolution amounts to multiplying the Fourier transform of the signal by the reciprocal of the Fourier transform of the resolution function which in this example would be an increasing hyperbola with a finite value at 0Hz in the Fourier domain. Thus, application of the filters shown in Figures 33e and 34b approximates deconvolution. The main value of these filters for resolution enhancement is that with less attenuation of the low-frequencies there is less generation of negative sidelobes. The spectrum resulting from the application of the filter shown in Figure 33 with indices -25, 125, 125, 250 is shown in Figure 37e. Resolution enhancement is not quite as great as that shown

in Figures 37c and 37d but sidelobe generation is reduced.

These examples illustrate the power and ease of Fourier domain digital filtering. With the simple functions shown in Figures 33 and 34 a number of rather sophisticated signal processing operations can be carried out readily. In addition, an important aspect of Fourier domain digital filtering is that it is, in most cases, considerably easier to design a digital filter in the Fourier domain than it is in the signal domain, i.e. in the frequency domain rather than the time domain. For example, the form of a Fourier domain notch filter is intuitively clear from Figure 36b while the form of a notch filter that could be directly applied to the signal (Figure 36a) via the correlation equation is not readily apparent. Thus the Fourier domain approach to digital filtering considerably enhances an experimenter's capability in developing unique digital filters for specific signal processing needs.

In conclusion, a major point that often bothers many who would like to use digital filtering techniques is the question of signal distortion. What must be kept in mind is that often the goal of digital filtering is optimization of the measurement of a particular signal parameter. If the desired parameter is peak height, then the matched filtering techniques discussed in Chapter IV can be used (39-43). Although matched filtering dis-

torts peak shape, it optimizes the signal-to-noise ratio (peak height/rms base line noise) for peak height measurement. In contrast, the goal of resolution enhancement is optimization of the measured peak position. This is often achieved by techniques, such as those presented in this chapter, that generate narrower spectral peak shapes, at times with significant distortion of the peak shape, in order to optimize the precision of the peak position measurement. In addition, resolution enhancement is usually achieved at the expense of amplitude signal-to-noise ratio. However, optimal processing of the spectral information for both peak height and peak position cannot be simultaneously achieved using a single filtering operation. Unique digital filters would also be necessary for the optimal measurement of other peak parameters such as area and width. Realization of this important concept facilitates intelligent and effective utilization of digital filtering techniques.

B. Frequency Response of Savitzky-Golay Filter Functions

In 1964, an important class of correlation functions for processing chemical signals were made popular by Savitzky and Golay (62, 75). Use of these functions represents the direct implementation of Equation 2 by means of a digital computer. A total of eleven different types of functions of various lengths were calculated,

allowing various degrees of signal-to-noise ratio enhancement, resolution enhancement, or differentiation. In light of the simplicity of the Fourier transform route of correlation, it is particularly useful to know the Fourier domain response of these functions, i.e. their frequency response (76-78). This was determined by Fourier transformation of the functions (by program DIGFIL) and determination of their amplitude spectra, i.e. the root sum-of-squares of the real and imaginary portions of the FFT output series.

The frequency response characteristics of all eleven 7 and 21 point Savitzky-Golay filter functions are shown in Figures 38 and 39. Plots of the functions are shown in columns a and c of both figures with the frequency response plots shown in columns b and d. The vertical axis is the amplitude of the Fourier transform, and the horizontal axis is frequency. Both axes are linear. The frequency axis extends from 0 Hz (dc) to one-half of the sampling frequency, i.e. the full unaliased range. Thus if a filter function was used to process a signal that was sampled at 0.01 sec intervals (100 Hz sampling rate) the corresponding frequency response plot of the filter is interpreted as extending from 0 Hz to 50 Hz.

In all cases the roman numeral designations of the filters correspond to those in the original tables

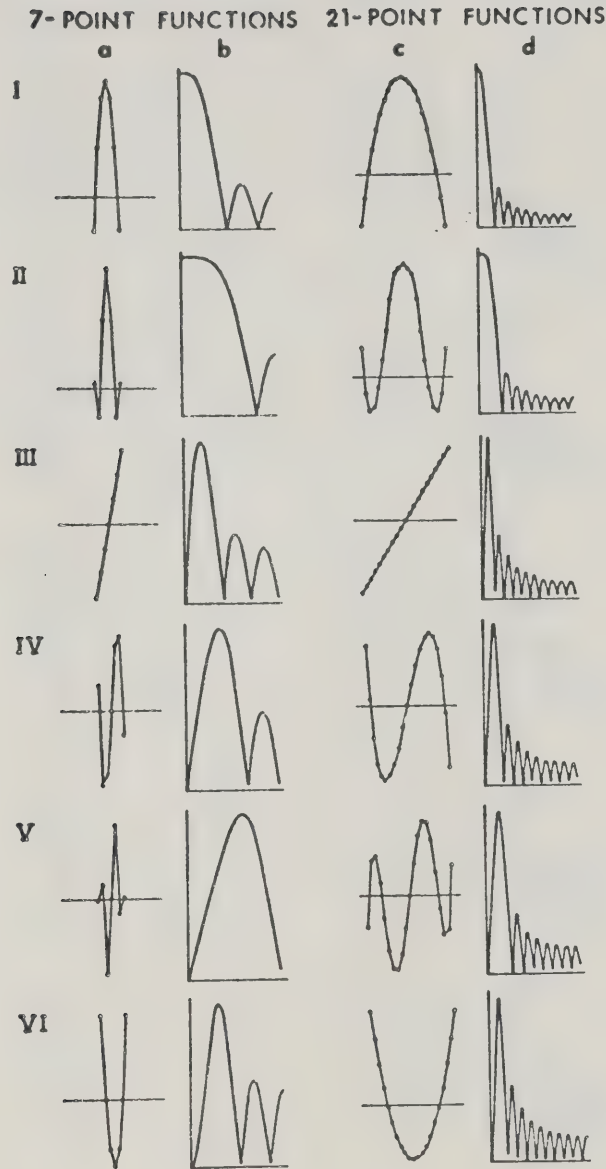


Figure 38. Seven and twenty-one point Savitzky-Golay filter functions (columns a and c) with their corresponding frequency responses (columns b and d). Filters I to VI.

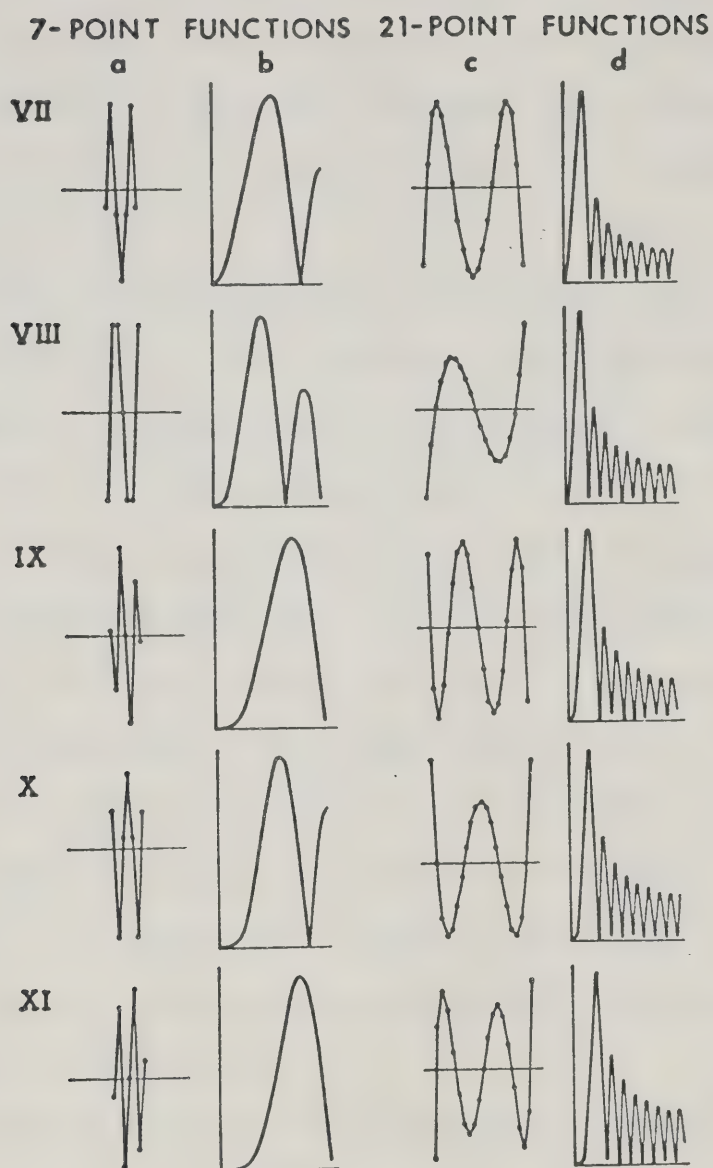


Figure 39. Seven and twenty-one point Savitzky-Golay filter functions (columns a and c) with their corresponding frequency responses (columns b and d). Filters VII to XI.

of Savitzky and Golay (62). The corrected tables of Steiner, Termonia, and Deltour (79) have been used where appropriate. This was necessary for filter IV (21 point function) and both functions for filters V, VII, IX, X, and XI.

As one scans the figures, it becomes clear that the interpretation of the action of each individual filter is aided by a knowledge of its frequency response. Filters I and II perform smoothing with filter II having a somewhat higher frequency cutoff. The low pass nature of these filters is apparent as is the significantly lower cutoff of the 21 point functions as compared to the 7 point functions. For comparison a larger scale figure of the frequency response plot of filter I (7 point) is shown in Figure 40 along with the corresponding plot for a conventional single stage RC low pass filter. The two filters have equivalent 3 dB points and hence cross at this point.

All the remaining filters perform differentiation. Filters III, IV, and V take a first derivative, filters VI and VII a second, filters VIII and IX a third, filter X a fourth, and filter XI a fifth. As discussed earlier, multiplication of the Fourier transform of a signal by a linear ramp is equivalent to taking its first derivative (69). As can be seen in Figure 38 for filters III, IV, and V, this is exactly the response in the

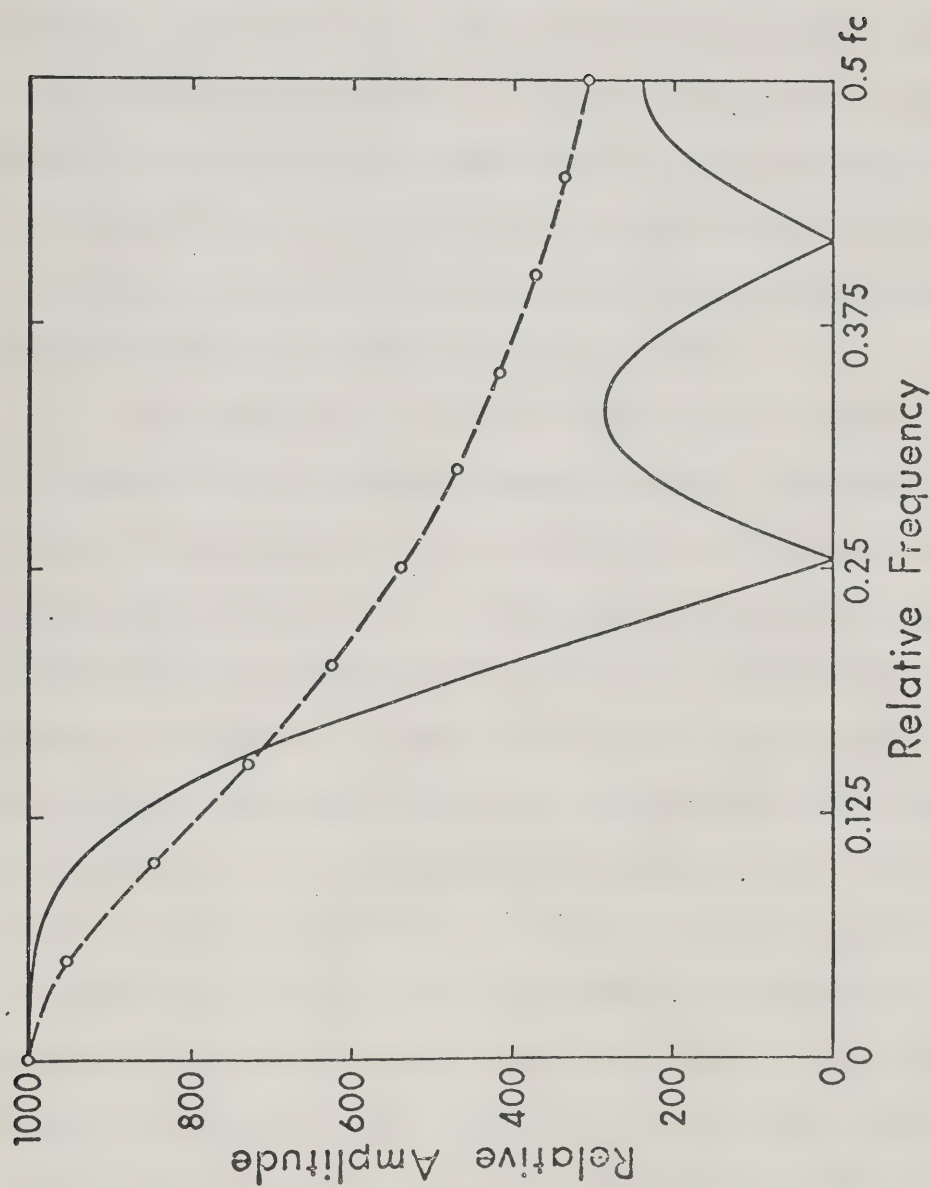


Figure 40. Frequency response plots of Filter I (7 point) (solid line) and an RC low pass filter (dashed line) with equivalent 3 dB points. f_c is the clocking or sampling rate.

Fourier domain with subsequent low pass rolloff in order to suppress high frequency noise. The different initial slopes of these three filters is analogous to different RC time constants for analog first derivative (single stage high pass) filters. Higher derivatives simply have increasing power dependence in the rising portion of their slope, i.e. f^2 for a second derivative; f^3 for a third, and so on. This follows from the Fourier domain representation of differentiation (69).

In order not to unduly complicate Figures 38 and 39, phase response plots have not been included. However, a knowledge of a filter's phase response is necessary along with its frequency response in order to completely characterize the filter. Fortunately the phase responses of these filters are very simple. In all cases the phase angle is constant between successive nodes in the frequency response plots. The initial phase is 0° for filters I, II and X; $+90^\circ$ for filters III, IV, V, and XI; $+180^\circ$ for filters VI and VII, and -90° for filters VIII and IX. After the initial lobe, the phase angle undergoes a 180° shift at each node. For example, the phase spectrum for the seven-point function for filter III, which performs a first derivative, is initially $+90^\circ$ through the first lobe, then -90° through the second lobe, and again $+90^\circ$ through the final lobe.

It is interesting to compare the plots of Figures 38 and 39 with those presented earlier in Figures 33 and 34. Although the detailed shapes of the transforms of the Savitzky-Golay filters are clearly much different than those of Figures 33 and 34, there is an overall very strong resemblance between the first lobes in Figures 38 and 39 and certain of the forms resulting from one or more applications of the trapezoid of Figure 33. This strong resemblance must hold, since low-pass filtering, differentiation, and so on all have a very specific Fourier domain representation. For example, the first derivative performed by Filter Va possesses a Fourier domain response almost identical to the triangle of Figure 33b; i.e. a linearly increasing ramp from the origin followed by low-pass filtering to reduce the effect of high-frequency noise. Similarly, the Fourier domain representation of the first lobe of Filter VIIb, which takes a second derivative, closely resembles the filter of Figure 34a, i.e. a parabolic increase from the origin with subsequent low-pass filtering. Although Savitzky and Golay present a total of 116 different filter functions, the effects of these functions can clearly be approximated by specifying only four integers in the Fourier domain.

The type of data presented in Figures 33, 34, 38, and 39 is quite useful in interpreting exactly

what effects can be imposed by a given filtering operation. In Chapter VI we will see how these digital filtering operations may be implemented in real time by an analog-based hardware correlation based on a tapped analog delay line.

CHAPTER VI

CROSS-CORRELATION II: THE TAPPED ANALOG DELAY LINE.

Background

As originally developed, correlation filters such as those of Savitzky and Golay (62) were applied to stored chemical signals by a software calculation using a digital computer, either directly or by the Fourier transform route of Chapter V. Direct implementation of these or other correlation filters by analog means, although well-known under the name of transversal filtering (80), has been difficult because it requires that a short section of the analog signal be temporarily stored and made available in parallel form. The development of tapped analog delay lines in simple integrated circuit packages (34, 81) that are similar in concept to the SAM of Chapter III has overcome this problem, and allows input chemical signals to be correlated with a weighting function in real time. In particular, ready application of the Savitzky-Golay and other correlation filters is now possible.

The nature of a correlation filter as constructed from a tapped analog delay line is shown in Figure 41. Note that the output signal is the weighted sum of several sequential signal values that are simultaneously available at the parallel outputs (taps) of the analog delay line. The correlation function may therefore be

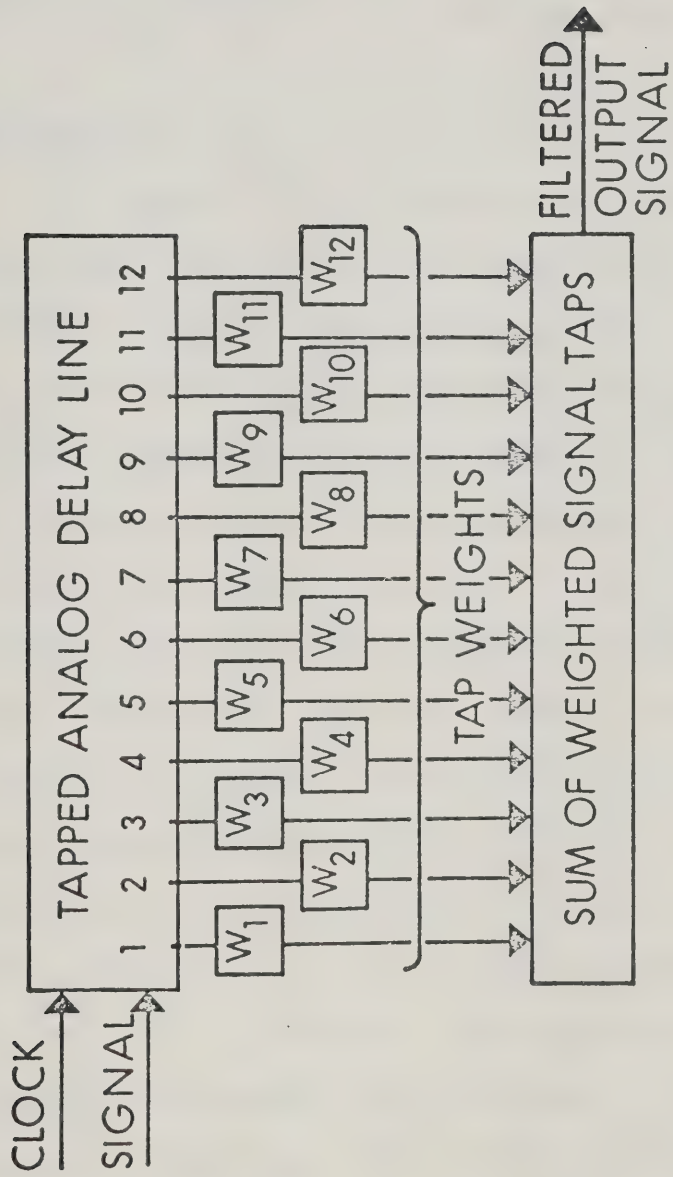


Figure 41. Transversal (correlation) filter.

selected simply by choosing the weighting function, and the correlation operation is performed by clocking the analog input signal through the delay line. Since this operation may be performed very rapidly, a cross-correlation may readily be obtained in real time.

Experimental

The tapped analog delay line (TAD-12) was obtained from Reticon Corporation, 910 Benicia Ave., Sunnyvale, CA. 94086. It is a MOS circuit based on silicon diode array architecture (34) and is contained in a standard 22 pin IC package. The organization of the TAD is shown in Figure 42a. There are twelve independent delay lines with delays of 1,3,5...21,23 clock pulses. The delay lines are all loaded and clocked simultaneously. Thus, the "taps" are really the outputs of the 12 analog delay lines. The tapped values are summed using an operational amplifier with the tap weights proportional to the reciprocal of the resistor value (see Figures 42b and 42c). The minimum recommended resistor value is 10 k Ω . A circuit evaluation card (TC-12) is available from Reticon that contains an operational amplifier as well as a TTL to MOS interface that produces the two-phase clock required by the TAD-12 from a single TTL clock. This circuit card was modified to allow resistors to be plugged in from any tap to either the

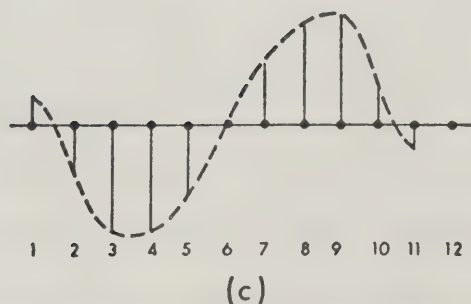
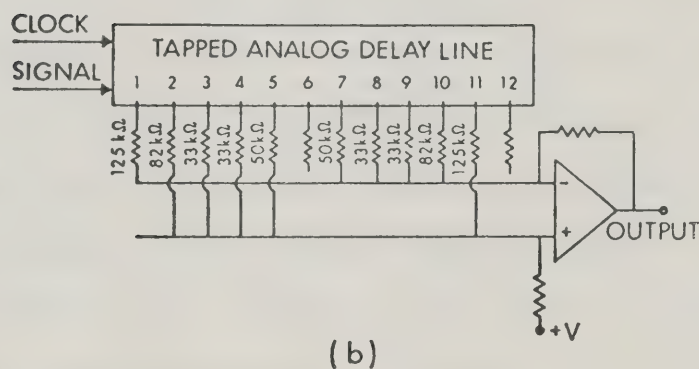
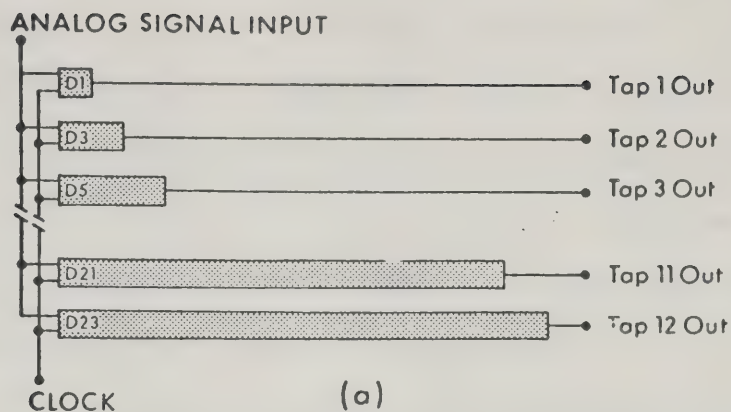


Figure 42. (a) Organization of TAD-12. (b) Implementation of a transversal filter with TAD-12, weighting resistors and operational amplifier. (c) Tap weights for Figure 2b.

inverting or noninverting inputs. Thus the weighting function could be changed quickly and easily.

The TAD-12 has a specified maximum clock rate of 5 MHz, retention time of 40 msec, analog signal bandwidth of 2 MHz, signal-to-noise ratio of 40 dB and acquisition time of 25 nsec. When utilized with the TC-12 evaluation card power is required at +5 V and ± 15 V.

The linearity of the TAD was determined by measuring the input and output amplitudes of a 1 kHz sine wave for the twelfth tap, which would be expected to exhibit the worst linearity. These data are shown in Figure 43. A least-squares treatment of the data for inputs in the range of 0.12-6.0 volts peak-to-peak yielded a slope of 0.5874 ± 0.007175 , an intercept of 0.0321 ± 0.0229 V, and a correlation coefficient of 0.999478.

Results and Discussion

With a conventional low pass filter most weight is given to the most recent signal value with exponentially decreasing weight given to past signal values. In their original paper (62) Savitzky and Golay discussed the fact that such a filter introduces distortion into the filtered signal because future signal values have no influence. They went on to indicate that a symmetrical exponential function would make a more ideal low pass filter as both past and future signal values

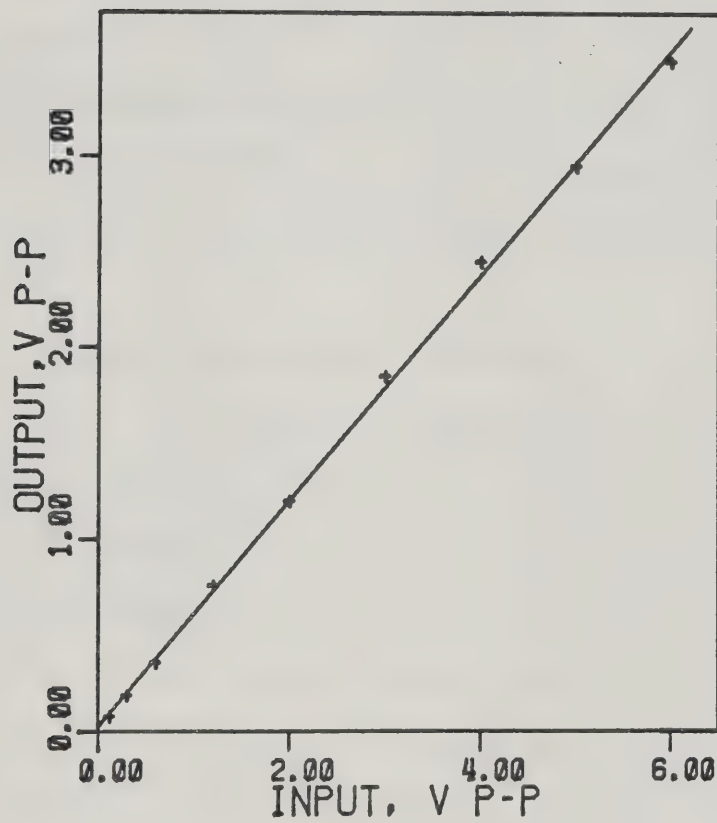
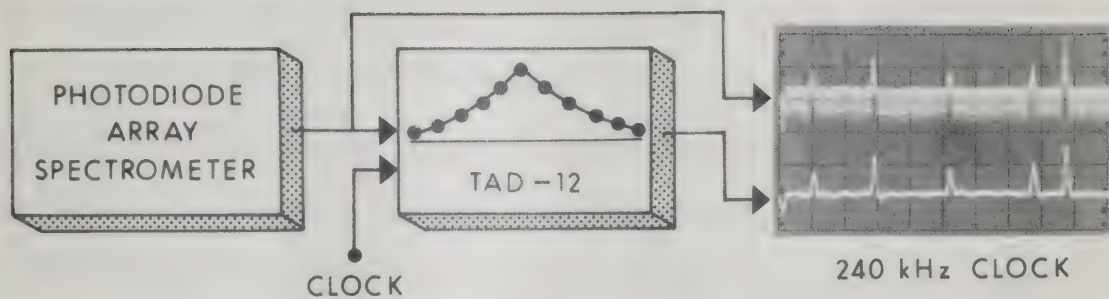


Figure 43. Output vs input of the twelfth tap of the TAD for a sine wave signal.

would be used in determining the output. The real time implementation of such a filter response is essentially impossible with conventional techniques and such filters are normally implemented on a signal stored within a digital computer. However, a low pass filter with a symmetrical exponential weighting can easily be implemented on an analog signal in real time using a tapped analog delay line transversal filter. This is illustrated in Plate 6.

The signal source was a photodiode array spectrometer (37). The present analog filters in the measurement system were by-passed and the raw output signal fed directly to the TAD. As can be seen in the upper trace of Plate 6a this raw signal is highly corrupted with a 45 kHz fixed pattern noise from the photodiode array readout clock. The symmetrical exponential low pass filter is very effective in removing this fixed pattern noise (See lower trace of Plate 6a).

A key variable in the utilization of the TAD is its clock rate. For the lower trace of Plate 6a the TAD clock rate was 240 kHz, which seemed to provide the "best looking" output signal. By varying the clock rate the width of the filtering function can be adjusted relative to the signal information, in this case the spectral peak. What this amounts to, in other terms, is that the clock rate provides a very easy and effective



(a)

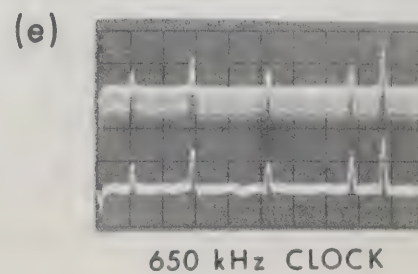
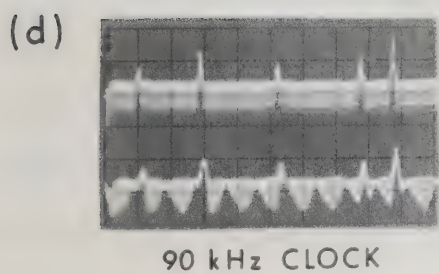
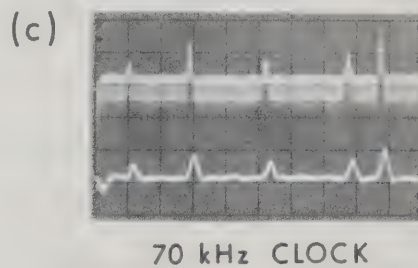
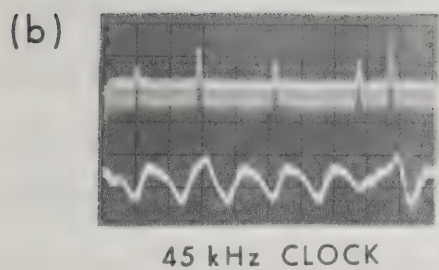


Plate 6. Application of a symmetrical exponential TAD transversal filter.

way to control or set the high frequency cutoff (i.e. 3 dB point) of the low pass filter. In addition, since the TAD is a sampled data processor the aliasing aspect of the clock must also be considered. These aspects of the clock are illustrated in Plates 6b through 6e.

At a TAD clock frequency of 45 kHz (Plate 6b), there is essentially complete destruction of all signal information because 45 kHz fixed pattern noise associated with the photodiode array output signal is aliased into the passband of the filter. When the TAD clock is increased to 70 kHz (Plate 6c) the array signal is rather heavily low pass filtered with the spectral peaks significantly broadened. This illustrates the situation where the filter function is too broad (i.e. 3 dB point too low) relative to the signal information. In conventional terms, the "time constant" is too long. However, note that the peaks remain symmetrical even with such heavy low pass filtering. With a comparable time constant a conventional low pass filter would have significantly skewed the spectral peaks. A 90 kHz TAD clock frequency again results in aliasing of the fixed pattern noise into the filter passband (Plate 6d). Finally, increasing the TAD clock to 650 kHz (Plate 6e) results in a weighting function that is too narrow. The peaks remain sharp but the fixed pattern noise is only partially removed. This series of photographs

clearly illustrates the unique importance of the clock as a variable for optimizing and controlling the characteristics of a TAD transversal filter.

In interpreting the action of a weighting function as a filter it is particularly useful to know the frequency response characteristics of the filter. The theoretical frequency response of the symmetrical exponential weighting function is shown in Figure 44. It was calculated by taking the Fourier transformation of the eleven tap weights with program DIGFIL. Note that the frequency axis extends from 0Hz (dc) to only one-quarter of the TAD clock frequency. One would expect that the frequency response plot should extend to one-half the TAD clock frequency as that would be the full unaliased range. The confusion arises here because the output delays in the TAD are separated by two clock pulses. Thus, in terms of units of clock time, the TAD actually has another 11 taps, each with a weight of zero, interleaved with the existing 12 taps. When a symmetrical exponential weighting function with interleaved zeros is transformed the frequency response plot shown in Figure 45 results which now extends to one-half the TAD clock frequency. In general we have worked with frequency response plots such as those shown in Figure 44 but it must always be remembered that the full unaliased range has a response of the type shown in

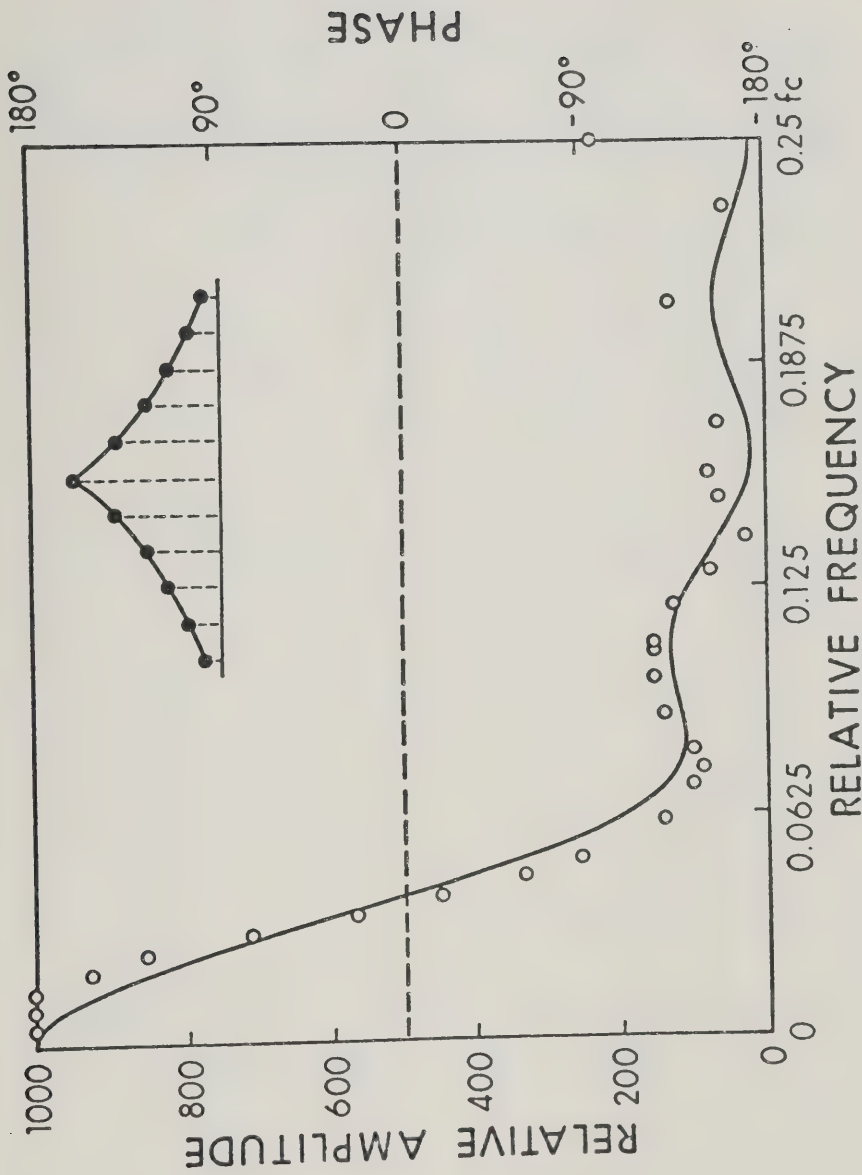


Figure 44. Frequency (solid line) and phase (dashed line) response plots for the symmetrical exponential function. Circles represent experimental values for the frequency response.

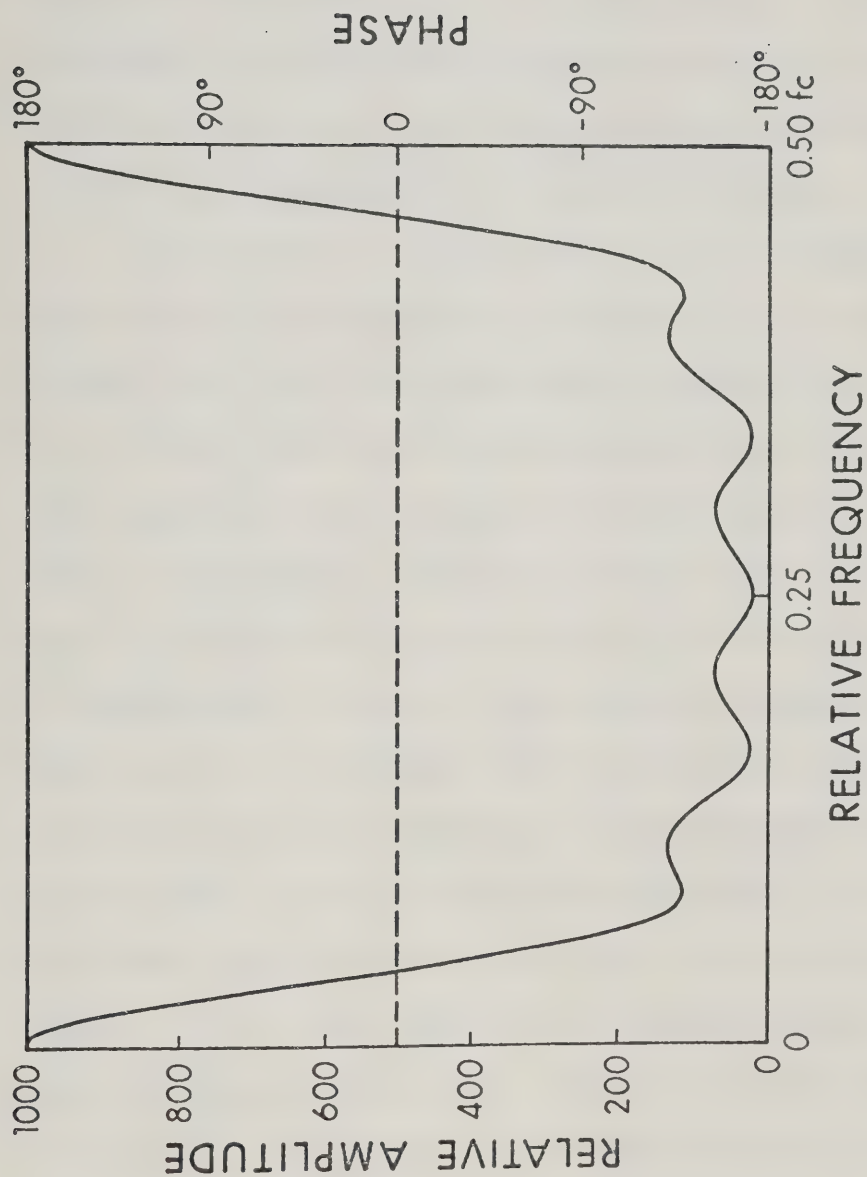


Figure 45. Frequency (solid line) and phase (dashed line) response plots for the full unaliased TAD transversal filter with the symmetrical exponential weighting.

Figure 45.

The experimentally determined frequency response is also shown in Figure 44. It was determined using a sine wave generator as the signal source. Note that the agreement is quite reasonable even though no attempt was made to accurately trim the weighting resistors to exactly fit the symmetrical exponential function.

As shown in Figures 44 and 45, the symmetrical exponential TAD transversal filter is an example of a filter that does not introduce any phase shift. This is, in fact, the key characteristic that allows peak like signals to be low pass filtered without introducing skew. In addition, this is a filter characteristic that is essentially impossible to achieve with active or passive RC filters. The frequency response and phase plots of a single-sided exponential weighting function which approximates a conventional single stage RC low pass filter is shown in Figure 46. In this case the phase response varies through the passband of the filter. It is this phase shift characteristic that can generate asymmetrical peak distortion and displacement. If, however, the decaying exponential shown in Figure 46 is reversed so that the twelfth tap has the most weight, the frequency response is unaffected but the phase response is inverted. This suggests that the TAD can be used with exponentially increasing tap weights to correct

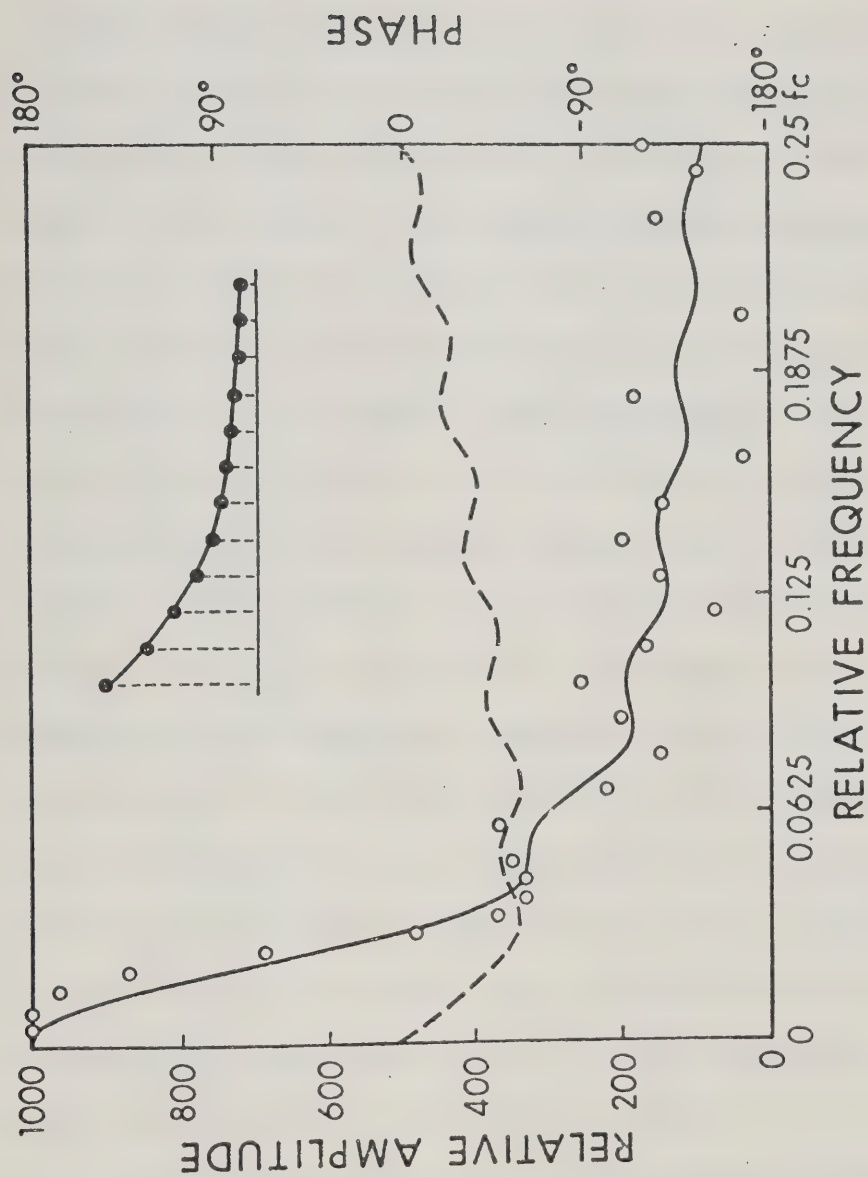


Figure 46. Frequency (solid line) and phase (dashed line) response plots for the one-sided exponential weighting function. Circles represent experimental values for the frequency response.

for peak asymmetry produced by excess RC filtering and perhaps, in more general terms, be set up to correct for any signal distortions induced by an instrumental response function. A simple feasibility example of such an application is shown in Figure 47. Heavy RC filtering was applied to the output signal from the photodiode array spectrometer and the TAD was used to resymmetrize the peaks. The computer data acquisition system associated with the photodiode array spectrometer was used for background subtraction and plotting of the digitized array signal. With moderately heavy RC filtering and the TAD out of the circuit, skewing of the spectral peaks is evident (Figure 47a). However, with the TAD in the circuit peak symmetry is restored (Figure 47b). In particular, the small peak in the middle of the spectrum is better resolved from the skewed edge of the large peak. In this example the TAD can be thought of as a high speed analog preprocessor to the digital data acquisition system. Since it acts in real time it performs the resymmetrization cross-correlation operation at the 45 kHz data rate or in about 20 msec for a 1000 point signal.

Differentiation of a signal may be accomplished by using one of several functions presented by Savitzky and Golay. Some results of using an eleven point first-derivative TAD transversal filter (Table III of reference

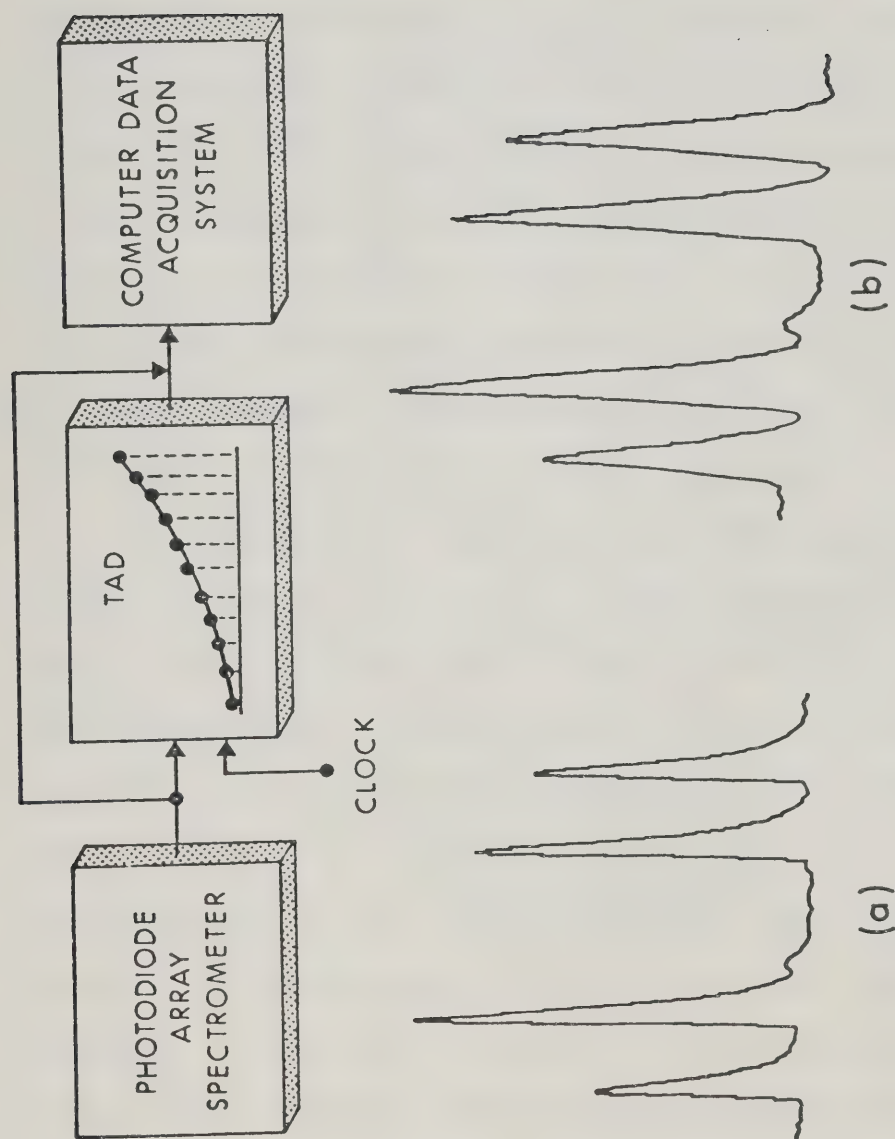


Figure 47. Use of a TAD transversal filter to correct phase shifts introduced by heavy RC filtering.

62) to differentiate a square wave are shown in Plate 7. The TAD clock frequency was 200 kHz for all measurements. The application of a 100 Hz square wave results in the output of sharp positive and negative spikes from the TAD, i.e. the square wave is differentiated. When the square wave frequency is increased to 500 Hz the spikes are still present, but are considerably less sharp. An input square wave of 6000 Hz is output as a sine wave and input of a 10,000 Hz square wave results in integration of the square wave and thus a triangular wave output. This behavior is easily explained by referring to the frequency response plot shown in Figure 48.

It can be seen that the TAD differentiator is really a bandpass filter with a peak response at about 6000 Hz and its first node at about 13,000 Hz. When the input square wave frequency lies low on the rising portion of the curve (point a \approx 100 Hz), a good differential results because all the lower harmonics also lie on the rising portion of the curve. When the input square wave frequency is increased to 500 Hz (point b), only the harmonics to the 11th (5500 Hz) lie on the rising portion of the curve and the quality of the differential is not as high. An input square wave of 6000 Hz (point c) falls at the maximum of the bandpass and is therefore output as a sine wave. Square wave signals such as 10,000 Hz (point d) occurring on the falling side of the bandpass

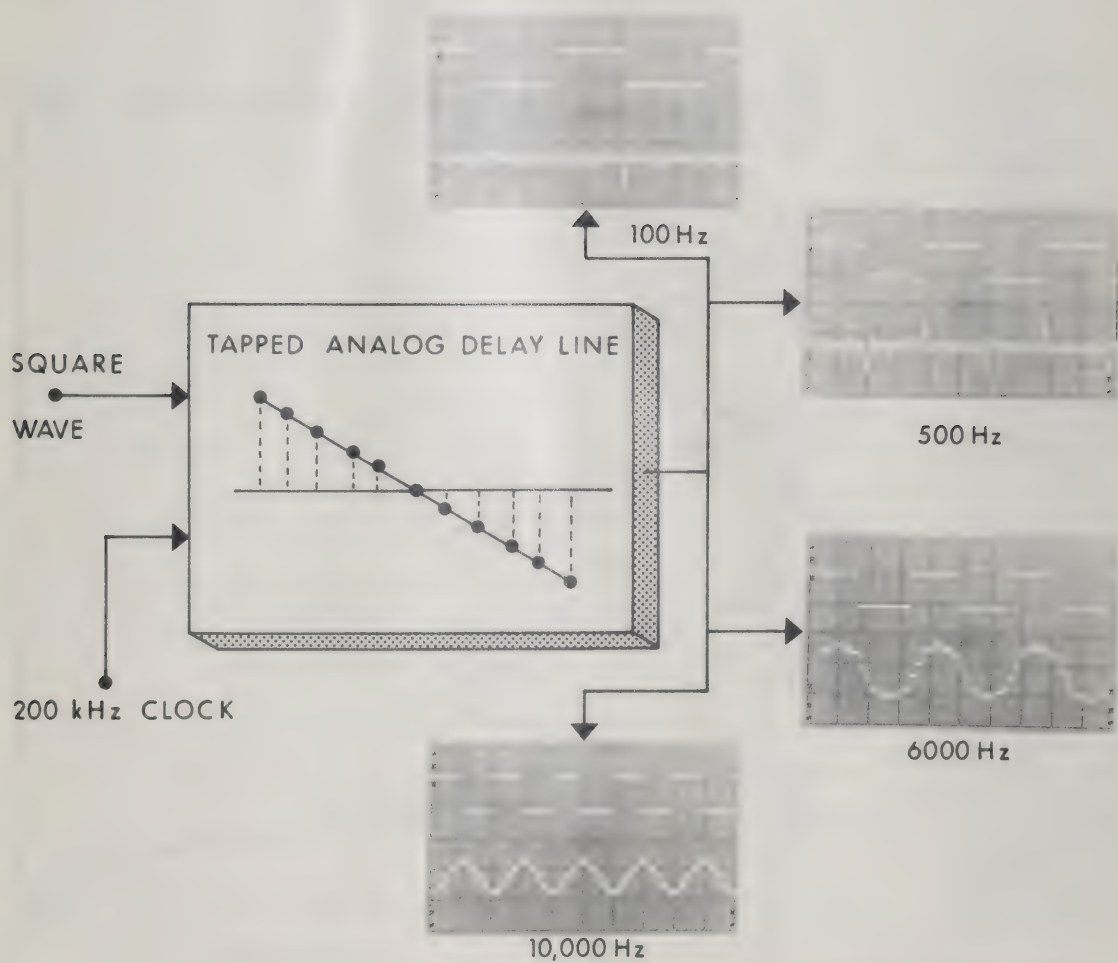


Plate 7. Application of a TAD transversal filter to "differentiation" of a square wave.

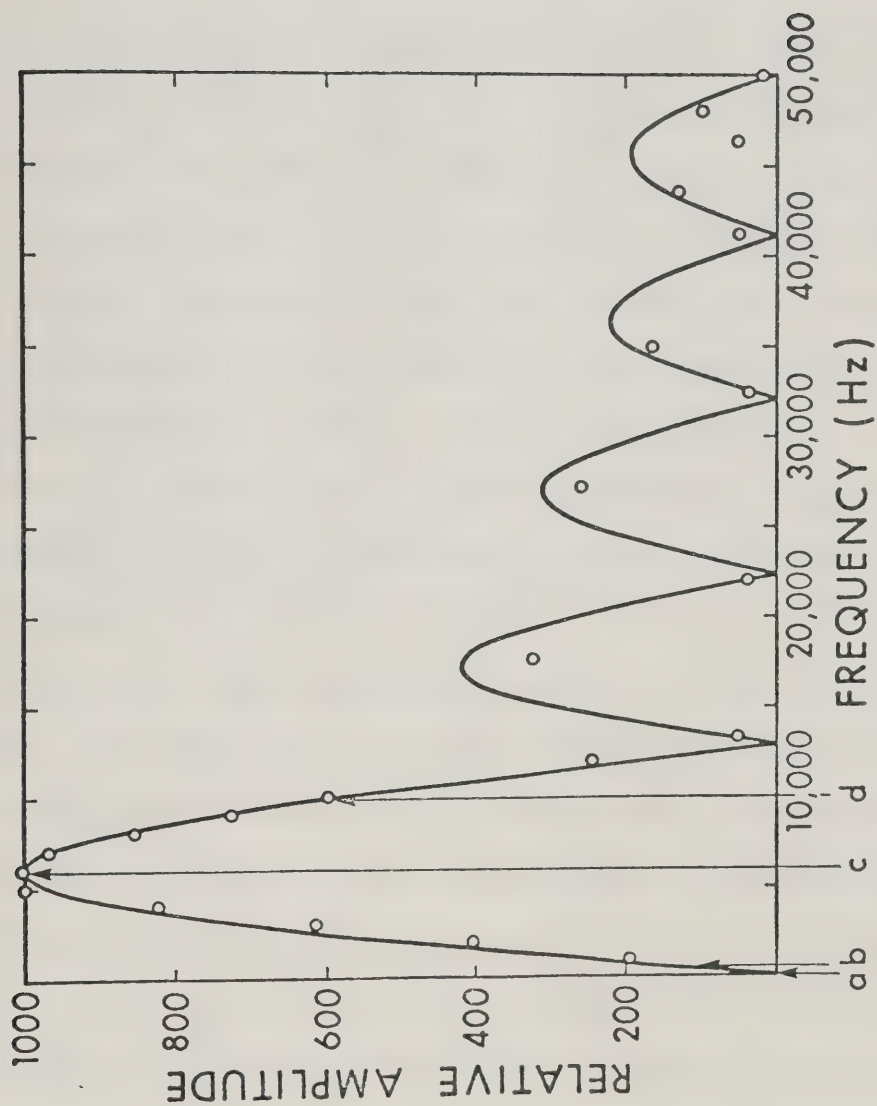


Figure 48. Frequency response plot for the TAD transversal filter shown in Plate 7 showing the location of (a) 100, (b) 500, (c) 6000, and (d) 10,000 Hz square waves. Circles represent experimental values for the frequency response.

are integrated. Clearly the frequency response plots obtained by Fourier transformation of the weighting functions are quite useful in understanding the characteristics of the cross-correlation operation.

Resolution enhancement of peak type signals can be carried out by taking the second derivative of the signal. A TAD transversal filter was set up with an eleven point Savitzky-Golay second derivative weighting function (Table VI of reference 62 and Table III of this thesis) in order to test its utility for resolution enhancement. It was used in inverted form so as to give positive peaks. The test signal was a dc arc spectrum of Cu and Ge in a ZnO-graphite matrix previously acquired with a photodiode array spectrometer and computer system, and stored on DEC tape. This signal is the same as that given in Figure 37a (Chapter V). In order for it to be processed by the TAD second derivative filter it was output from the computer through a DAC at a rate of 50 kHz (signal is 512 points long). Photographs of expanded scope traces of the first (column I) and last (column II) sections of the signal as outputted from the DAC are shown in Plate 8a and as processed by the TAD in Plate 8b. The TAD clock rate was 120 kHz.

The theoretical frequency and phase responses of the Savitzky-Golay 11-point second derivative filter

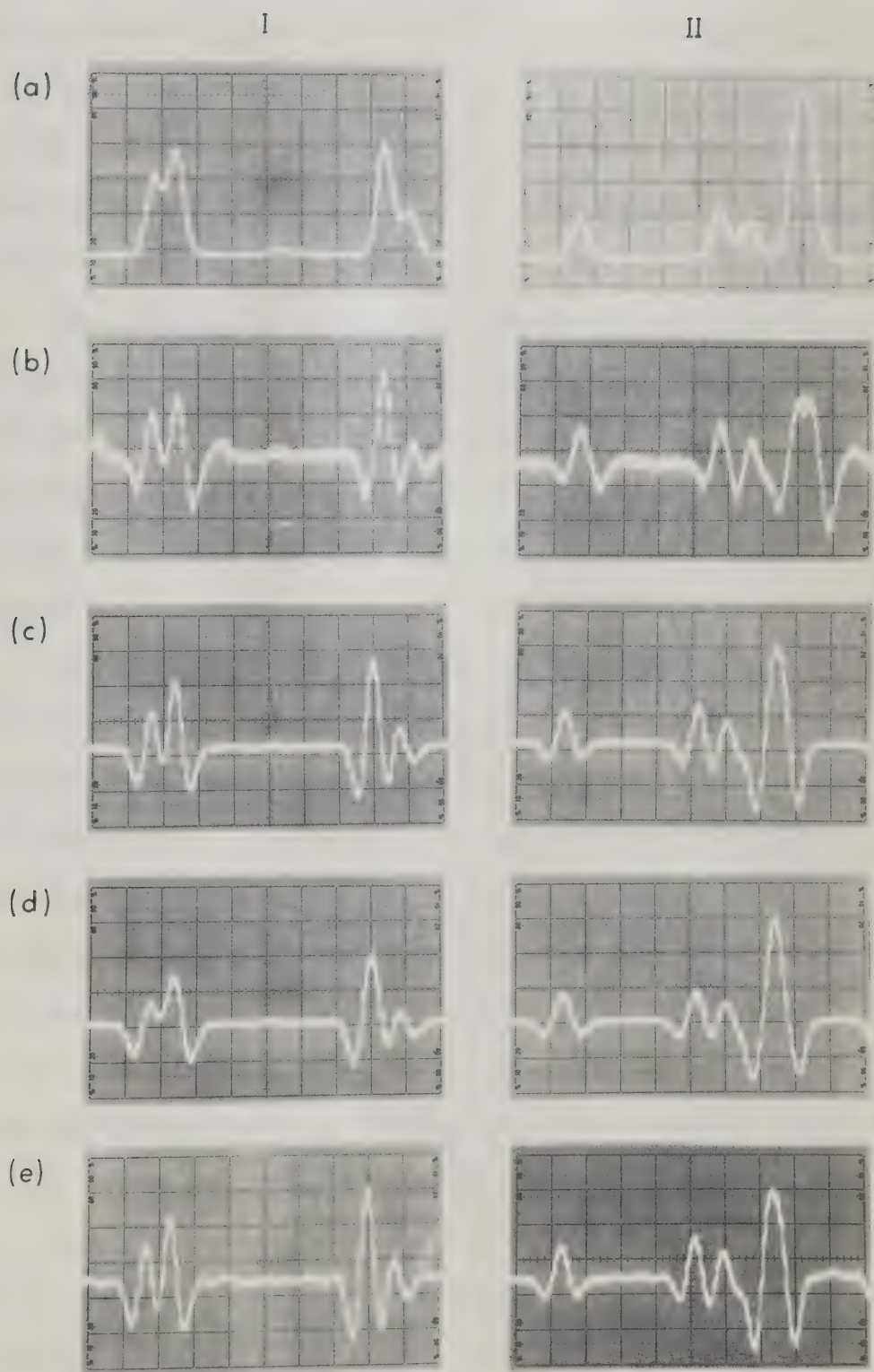
TABLE III

Generation of TAD Resistor Values from Savitzky

Golay Weights (11 Point Second Derivative)

<u>Raw S-G</u> <u>Weights</u>	<u> 1/ Weights </u> <u>Smallest scaled</u> <u>to 10.0</u>	<u>Nearest Resistor</u> <u>Value (k ohms)</u>
15	10.0	10
6	25.0	27
-1	150	150
-6	25.0	27
-9	16.6	18
-10	15.0	15
-9	16.6	18
-6	25.0	27
-1	150	150
6	25.0	27
15	10.0	10

Plate 8. Second derivative resolution enhancement.
(a) Signal, (b) TAD 11 point filter,
(c) software 9 point filter, (d) software
11 point filter, and (e) Fourier domain
digital filter. See text for discussion.



are shown in Figure 49a. However, the resistor weights actually used did not correspond exactly to the theoretical weights (see Table III). When the Fourier transformation of the actual resistor weights is taken the frequency and phase responses shown in Figure 49b result. Now there is a small response at dc and a low frequency lobe. The reason for the small response at dc is the fact that our resistor weights did not sum to zero while the true Savitzky-Golay weights do. The experimental points shown in Figure 49b verify a small response at dc but the low frequency node was not observed.

The responses shown in Figure 49 illustrate that relatively small mismatches in resistor weights to theoretical weights can significantly alter the filter characteristics. This was also observed for several other TAD filters where, in particular, the position and relative amplitude of side lobes was altered by small resistor mismatches. However, with the Fourier transform program of Appendix II it is easy to type in any particular set of tap weights and thereby calculate the frequency and phase responses to be expected.

Finally, it is useful to briefly compare the resolution enhancement capabilities of the TAD second derivative filter to two other methods: (1) the conventional software application of a Savitzky-Golay filter

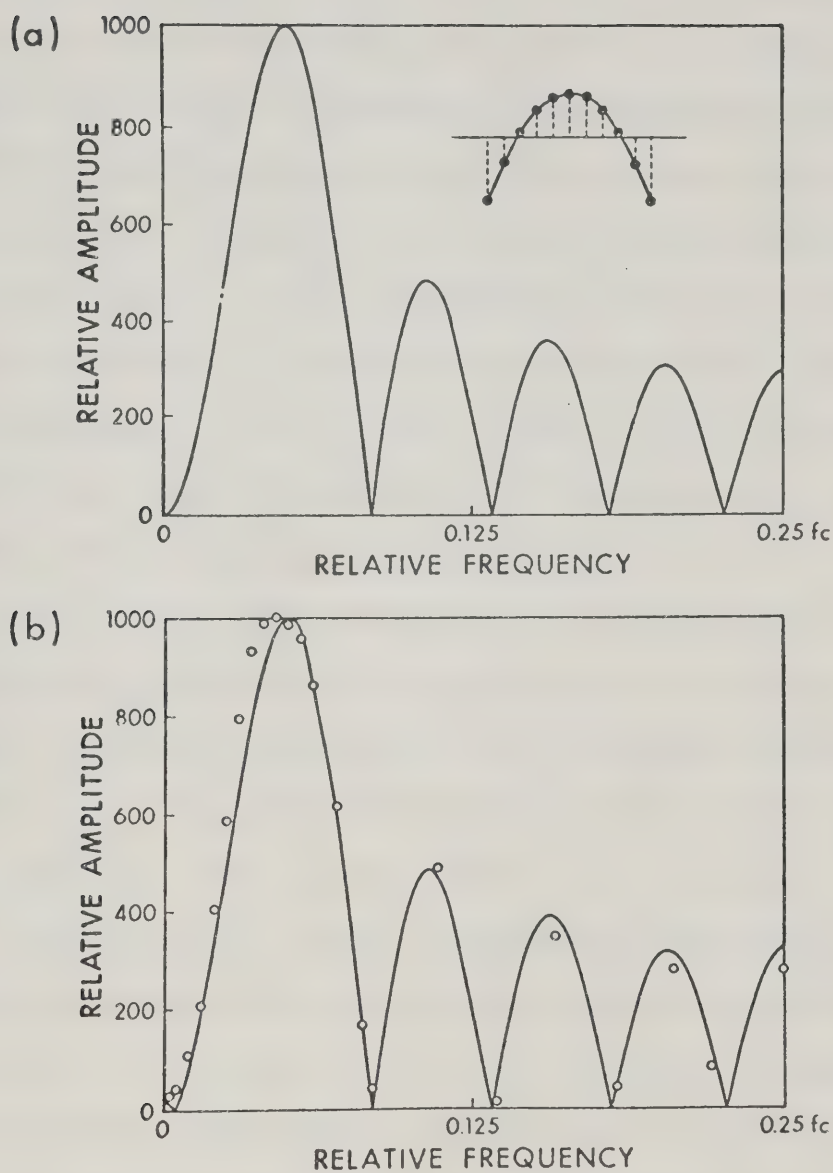


Figure 49. Frequency responses for the theoretical (a) and actual (b) tap weights of the TAD second derivative filter. Circles in (b) represent experimental values for the frequency response.

and (2) The Fourier domain digital filter of Chapter V. The test signal is the dc arc spectrum shown in Figure 37a and the results are presented in Plates 8c through 8e. Results obtained by the software application of 9 and 11-point Savitzky-Golay second derivative functions to the dc arc spectrum are shown in Plates 8c and 8d. It is important to note that it is the results shown in Plate 8c for the 9 point function that are most similar to those shown in Plate 8b for the 11 point TAD implementation. The reason for this is that the TAD allows independent control over the width of the filter function through the TAD clock. Recall that for Plate 8b the signal was clocked out of the DAC at 50 kHz and the TAD was clocked at 120 kHz. Because there are two clock pulse delays between taps the effective clock rate with respect to the taps is 60 kHz. Thus the TAD 11 point weighting function is slightly narrower relative to the signal information than when it is applied directly by software. Based on the relative differences in the clock rates (50 kHz signal and 60 kHz filter) it would be expected that the 11 point TAD would achieve resolution enhancement more comparable to that of a 9-point filter as indicated by the photographs in Plate 8. This control adds considerable flexibility to the TAD implementation in that the width of the filter can be fine tuned to the desired

performance by varying the clock frequency.

The results obtained using the Fourier domain digital filter of Chapter V that approximates second derivative resolution enhancement are shown in Plate 8e. The filter used was that shown in Figure 32d of Chapter V with indices equal to 25, 125, 125 and 250. Again very similar results to those obtained with the TAD are achieved. However, it is important to note that the TAD resolution enhancement was carried out in real time or in about 10 msec for the 512 point signal presented at a rate of about 50 kHz. The direct software application of the Savitzky-Golay filter took about 20 sec and the Fourier domain digital filter about 2 min, both programmed in FORTRAN and run on a PDP 8/e minicomputer.

Conclusions

Clearly the TAD is a remarkably versatile device for implementing cross-correlation in real time. Only some of its many capabilities (37) have been illustrated here. Also the present device is among the first of this type of circuit to become available. The characteristics and capabilities of tapped analog delay lines may be expected to improve with further advances in solid-state technology. Already Reticon has announced a 32 tap device with a 60 dB dynamic range. One can envision tapped analog delay line transversal filters

being incorporated in a wide variety of scientific instrumentation as flexible analog data processors. A simple combination that we have found effective is to use a TAD as an output processor for a transient recorder. Thus, once a signal is acquired, it can be recirculated and hence processed in any number of different ways with the TAD.

CHAPTER VII

SUMMARY

In the foregoing chapters, we have seen how correlation instrumentation of varying levels of complexity can be used to manipulate chemical data in a large number of ways. The simple block diagram presented in Figure 4 represents a variety of uniquely powerful instruments that can be applied to a large number of different measurements. Future developments in integrated-circuit technology will simplify even further the application of correlation techniques. For example, progress can be expected both in digital filtering techniques with the development of microprocessors and their support circuitry, and in analog methods of correlation with further development of devices based on bucket-brigade, charge-coupled device, or diode array technology. Performance of these devices will be enhanced and costs will drop as fabrication procedures improve and yields increase. Therefore, more and more sophisticated instrumentation will become available in future years.

Two different paths of development can be discerned in the use of correlation instrumentation. First, high density fabrication procedures for logic circuitry have allowed the development of single-chip microprocessors such as the eight bit Intel 8080A and Motorola 6800, the twelve bit Intersil 6100, and the sixteen bit TMS 9000.

A large variety of different support chips are also becoming available that allow relatively simple expansion of these basic microprocessors into microcomputers. Since direct implementation of Savitzky-Golay filter functions is possible with a programmable desk calculator (82), as the price of microcomputers drops and the level of performance increases, applications such as digital filtering will become more and more facile.

Simultaneously with the improvement in digital circuitry has come further development in analog circuit design (34). Later generation SAMs and TADs will contain more storage elements and provide a much improved dynamic range. Therefore, the ease of analog-based correlation operations will also improve in coming years.

In conclusion, we have also seen in the foregoing chapters that correlation methods can be used both to enhance the ease of measurement and to modify selectively the characteristics of the information obtained. Therefore, the approach to measurement from a correlation viewpoint can often yield new insight into factors involved in the measurement process.

BIBLIOGRAPHY

1. Y. W. Lee, T. P. Cheatham, Jr., and J. B. Wiesmer, Proc. IRE. 38, 1165 (1950).
2. Y. W. Lee, "Statistical Theory of Communication," John Wiley and Sons, New York, N.Y. (1960).
3. Gary Horlick and Gary M. Hieftje in "Computers in Chemical and Biochemical Research," Vol. 3, C. Klopfenstein and C. L. Wilkins, Eds., Academic Press, New York, N.Y. (in press).
4. Raymond Annino, "Signal and Resolution Enhancement Techniques in Chromatography," in press.
5. G. M. Hieftje, Anal. Chem. 44(6), 81A (1972).
6. G. M. Hieftje, Anal. Chem. 44(7), 69A (1972).
7. G. M. Hieftje, R. I. Bystroff, and R. Lim, Anal. Chem. 45, 253 (1973).
8. Gary Horlick, Anal. Chem. 45, 319 (1973).
9. Gary Horlick and Keith R. Betty, Anal. Chem. 47, 363 (1975).
10. H. V. Malmstadt, C. G. Enke, S. R. Crouch, and Gary Horlick, "Optimization of Electronic Measurements," W. A. Benjamin, Inc., Menlo Park, CA., 1974.
11. T. C. O'Haver, J. Chem. Educ. 49(3), A131 (1972).
12. T. C. O'Haver, J. Chem. Educ. 49(4), A211 (1972).
13. Ronald F. Evilia and A. James Diefenderfer, Anal. Chem. 39, 1885 (1967).

14. M. Moresco and E. Zilli, Rev. Sci. Instrum. 46, 1582 (1975).
15. D. K. Morgan, RCA Application Note ICAN-6101, in "COS/MOS Digital Integrated Circuits," RCA Solid State, Somerville, N.J. 08876, 1973, p. 360.
16. "Signetics Digital, Linear, and MOS Applications," Signetics, 811 East Arques Avenue, Sunnyvale, Calif., 94086, 1974, p. 6-1.
17. H. V. Malmstadt, C. G. Enke, and S. R. Crouch, "Digital and Analog Data Conversions," W. A. Benjamin, Inc., Menlo Park, CA., 1973, p. 182.
18. Y. H. Pao, R. N. Zitter, and J. E. Griffiths, J. Opt. Soc. Amer., 56, 1133 (1966).
19. J. Cleary, J. Opt. Soc. Amer. 57, 841 (1967).
20. J. E. Griffiths and Y. H. Pao, J. Chem. Phys. 46, 1679 (1967).
21. R. R. Alfano and N. Ockman, J. Opt. Soc. Amer. 58, 90 (1968).
22. R. Anderson and J. Cleary, J. Opt. Soc. Amer. 60, 531 (1970).
23. H. Z. Cummins and H. L. Swinney, "Light Beating Spectroscopy" in "Progress in Optics," Vol. 8, E. Wolf, Ed., North-Holland Publishing Company, Amsterdam, 1970, p. 135.
24. B. J. Berne and R. Pecora, Ann. Rev. Phys. Chem. 25, 233 (1974).

25. H. Z. Cummins and E. R. Pike, Eds., "Photon Correlation and Light Beating Spectroscopy," Plenum Press, New York, N.Y. (1974).
26. B. R. Ware and W. H. Flygare, Chem. Phys. Lett. 12, 81 (1971).
27. E. E. Uzigris, Opt. Commun. 6, 55 (1972).
28. E. E. Uzigris, Rev. Sci. Instrum. 45, 74 (1974).
29. P. N. Pusey, D. E. Koppel, P. W. Schaefer, R. D. Camerini-Otero, and S. H. Koenig, Biochemistry 13, 952 (1974).
30. A. Mole and E. Geissler, J. Phys. E.: Sci. Instrum. 8, 417 (1975).
31. S. H. Chen, W. B. Veldkamp, and C. C. Lai, Rev. Sci. Instrum. 46, 1356 (1975).
32. G. Feher and M. Weissman, Proc. Nat. Acad. Sci. USA 70, 870 (1973).
33. E. L. Elson and D. Magde, Biopolymers 13, 1 (1974).
34. Gary Horlick, Anal. Chem. 48, 783A (1976).
35. K. R. Betty and Gary Horlick, Anal. Chem. 48, 1899 (1976).
36. P. W. Fry, J. Phys. E. Scientific Instruments, 8, 337 (1975).
37. Gary Horlick, Appl. Spectrosc. 30, 113 (1976).
38. T. A. Last and C. G. Enke, submitted to Anal. Chem.
39. G. L. Miller, J. V. Ramirey, and D. A. H. Robinson, J. Appl. Phys. 46, 2638 (1975).

40. G. L. Turin, IRE Trans. Information Theory, IT-6, 311 (1960).
41. C. W. Helstrom, "Statistical Theory of Signal Detection," Pergamon Press, Oxford, 1968.
42. W. L. Root, Proc. IEEE 58, 610 (1970).
43. D. C. Champeney, "Fourier Transforms and Their Physical Applications," Academic Press, London, 1974.
44. Gary Horlick and Edward G. Coddling, Anal. Chem. 45, 1749 (1973).
45. P. J. Jurs, B. R. Kowalski, T. L. Isenhour, and C. N. Reilly, Anal. Chem. 41, 691 (1969).
46. S. L. Grotch, Anal. Chem. 42, 1214 (1970).
47. E. G. Coddling and G. Horlick, Appl. Spectrosc. 27, 366 (1973).
48. G. Beech, Anal. Chim. Acta. 83, 133 (1976).
49. K. R. Betty and Gary Horlick, Anal. Chem., in press.
50. V. A. Fassel and R. N. Krisely, Anal. Chem. 46, 1110A, 1155A (1974).
51. N. E. Korte and M. B. Denton, Chemical Instrumentation 5(1), 33 (1973-74).
52. P. N. Daum and Peter Zamie, Anal. Chem. 46, 1347 (1974).
53. W. L. Switzer, Anal. Chem. 48, 1003A (1976).
54. K. R. Betty and Gary Horlick, Appl. Spectrosc. 30, 23 (1976).

55. Gary Horlick, Anal. Chem. 44, 943 (1972).
56. J. W. Hayes, D. E. Glover, D. E. Smith, and M. W. Overton, Anal. Chem. 45, 277 (1973).
57. D. E. Smith, Anal. Chem. 48, 221A (1976).
58. C. Allen Bush, Anal. Chem. 46, 890 (1974).
59. M. Caprini, S. Cohn-Sfetcu, and A. M. Manof, IEEE Trans. Audio Electroacoustics AU-18, 389 (1970).
60. T. Inouye, T. Harper, and N. C. Rasmussen, Nucl. Instrum. Meth. 67, 125 (1969).
61. D. W. Kirmse and A. W. Westerberg, Anal. Chem. 43, 1035 (1971).
62. A. Savitzky and M. J. E. Golay, Anal. Chem. 36, 1627 (1964).
63. L. Mertz, Infrared Phys. 7, 17 (1967).
64. Edward G. Coddington and Gary Horlick, Appl. Spectrosc. 27, 85 (1973).
65. R. S. Singleton, IEEE Trans. Audio Electroacoustics AU-17, 166 (1969).
66. L. Mertz, Appl. Opt. 10, 386 (1971).
67. P. R. Griffiths, Appl. Spectrosc. 29, 11 (1975).
68. G. Horlick and W. K. Yuen, Anal. Chem. 48, 1643 (1976).
69. R. Bracewell, "The Fourier Transform and its Application," McGraw-Hill, New York, N.Y., 1965.
70. F. R. Stauffer and H. Sakia, Appl. Opt. 7, 61 (1968).

71. A. E. Martin, *Spectrochim. Acta.* 14, 97 (1959).
72. L. C. Allen, H. M. Gladney, and S. H. Glarum, *J. Chem. Phys.* 40, 3135 (1964).
73. P. C. Kelly and G. Horlick, *Anal. Chem.* 45, 2130 (1974).
74. G. Horlick, *Appl. Spectrosc.* 26, 395 (1972).
75. C. G. Enke and T. A. Nieman, *Anal. Chem.* 48, 705A (1976).
76. K. R. Betty and G. Horlick, *Anal. Chem.*, in press.
77. H. Tominaga, M. Dojyo, and M. Tanaka, *Nucl. Instrum. Meth.* 98, 69 (1972).
78. R. L. LaFara, "Computer Methods for Science and Engineering," Hayden Book Co., Rochelle Park, N.J., 1973, pp. 184-188.
79. Jean Steinier, Yves Termonia, and Jules Deltour, *Anal. Chem.* 44, 1906 (1972).
80. H. E. Kallman, *Proc. IRE* 28, 302 (1940).
81. K. R. Betty and Gary Horlick, *Anal. Chem.*, 48, 2248 (1976).
82. Jean-Jacques Pireaux, *Appl. Spectrosc.* 30, 219 (1976).
83. D'Arcy H. Lorimer and Alexis T. Bell, *Ind. Eng. Chem. Fundam* 15, 71 (1976).
84. "SERDEX User's Guide," Analog Devices, P.O. Box 280, Norwood, Mass. 02062.

APPENDIX I

The voltage output of the correlator of Chapter 4 was digitized with a digital voltmeter and printed on a teletype by means of a SERDEX SERIAL Data EXchange Module (53, 83-84). These modules allow communication of a DVM or other device using parallel BCD output code with a teletype a computer that utilizes serial ASCII (American Standard Code for Information Interchange) code.

A block diagram of the SERDEX module is shown in Figure 50. A signal from a teletype is received in the isolated current-loop receiver and converted from serial to parallel ASCII. A decoder then recognizes either a question mark (?) or one of six control characters (% , \$, = , ' , * , !) and outputs a pulse if one of these characters has been received. All other characters are ignored. The question mark can be used to trigger an analog-to-digital conversion. The completion of this conversion (as indicated by a change in STATUS) then loads the BCD output of the ADC into the SERDEX and initiates data transmission. The BCD digits are then loaded word serially into a parallel to ASCII converter, and sent to the teletype via the isolated current loop transmitter.

A full schematic of the SERDEX module as connected to a teletype and DVM (DANA Model 5400 modified

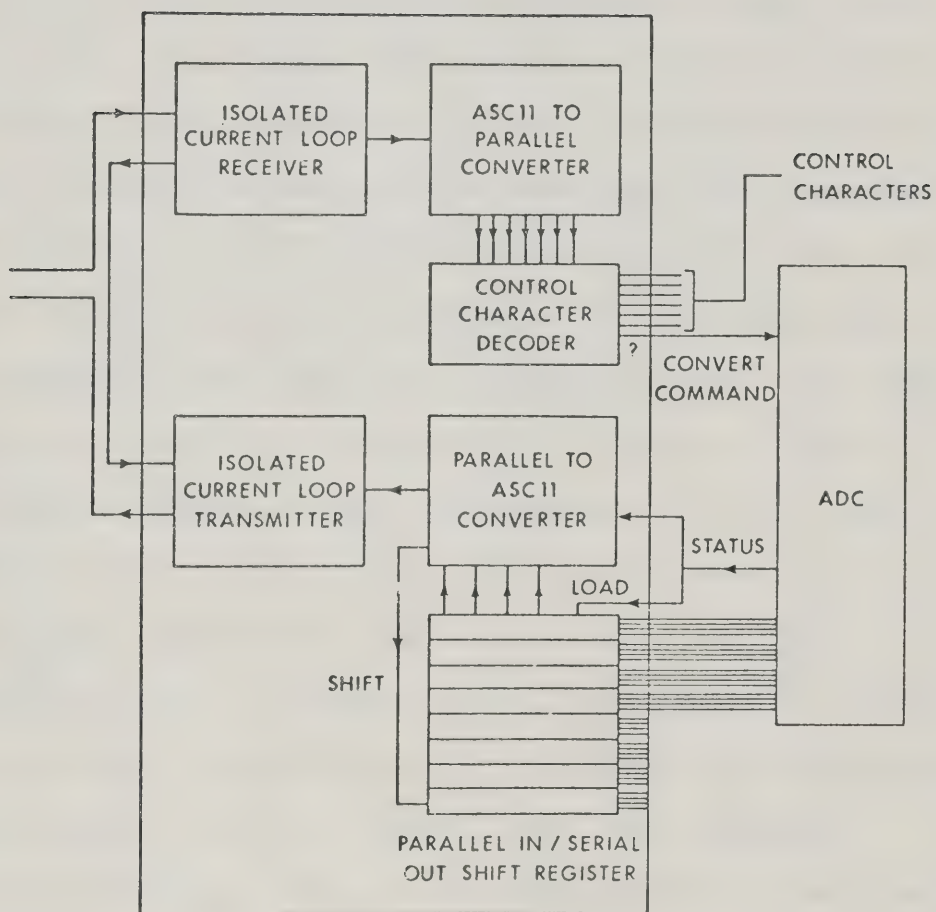


Figure 50. Block diagram of the SERDEX module.

to be TTL compatible) is shown in Figure 51. The teletype is connected via a twisted wire pair to an active 20 ma current source formed by Q1, D1, R1 and R2 and thence to the isolated current loop transmitter and receiver, which are connected in the half duplex mode (84). The clock driver (SCL 1006) is wired to provide operation of the SERDEX at 110 baud transmission rates. Control inputs are wired for 8 data bits per character with no stop bits and without parity verification. The connection of the serial inputs to the receiver register outputs allows the user to type an eight digit test message and verify its reception by typing a slash (/), causing the system to echo the message. In the implementation shown, the control character outputs and the convert command (?) are not used; rather, the experiment itself initiates A-to-D conversion. A valid BCD output is indicated by a 0→1 on the PRINT line; this toggles Mono-1 (set for about 1 sec) and initiates data transmission. A total of eight words can be transmitted without external expansion of the SERDEX. The first word is used to indicate the voltage polarity: if positive (POLARITY = 0) it will be 0000; if negative (POLARITY = 1) it will be 1100. The addition of the remaining bits of the eight-bit ASCII code make these numbers 10110000 and 10111100 respectively. These are printed by the teletype as "0" for positive voltages or

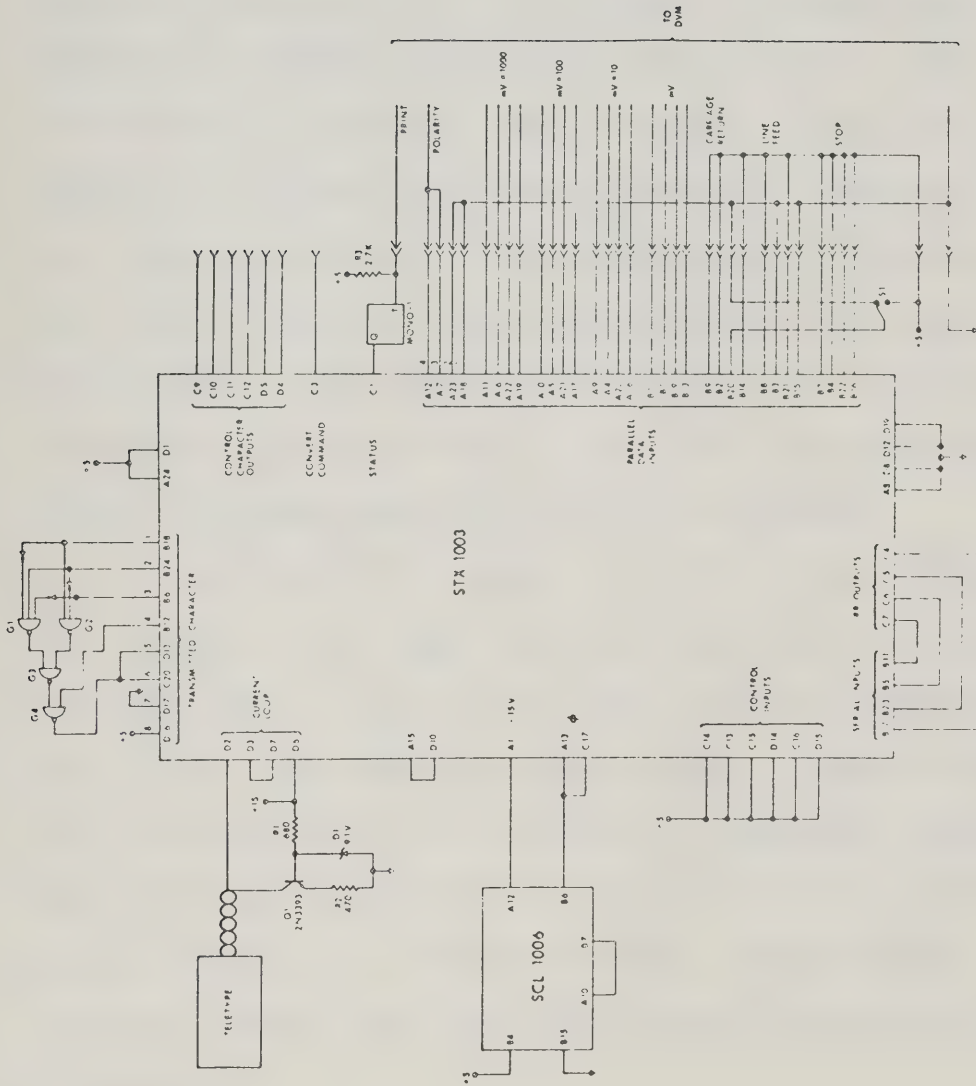


Figure 51. Circuit diagram of the connection of the SERDEX module to a digital voltmeter and teletype.

"<" for negative voltages. The reason for not indicating negative voltages with a minus sign (-) will be discussed later.

After the sign character has been transmitted, the four BCD digits for the voltage (in millivolts) are converted to ASCII and transmitted in order. The sixth word is wired as 1101 (S1 open) or 1111 (S1 closed), whereas the seventh and eighth words are wired as 1010 and 1111 respectively. The SERDEX module recognizes 1111 as a command to cease transmission; hence the seventh and eighth words may or may not be printed depending on the position of S1. The stop character itself, although transmitted, is not printed.

The function of gates G1 to G4 is to recognize the four-bit words 1101 and 1010 and change the fifth and sixth ASCII bits so that they will be transmitted as 10001101 and 10001010 respectively. They are therefore interpreted by the teletype as carriage return and line feed respectively. Thus, S1 can be used to control whether or not the teletype automatically carriage returns and line feeds after the printing of a voltage.

It was mentioned earlier that a negative voltage was indicated by an ASCII "<" rather than a minus sign. Examination of a table of the ASCII code shows that a minus sign is indicated by 10101101. The last four

bits of this word (1101) are exactly those interpreted by gates G1 to G4 as carriage return; hence, the above circuit could not distinguish between the two. This limitation may be corrected by employing a flip-flop to change the state of bit 5 (D13) to 0 when the first word is transmitted (84).

APPENDIX II

The data presented in Chapter 5 and 6 were largely obtained by a computer program called DIGFIL. This program was written in FORTRAN II for a DEC PDP 8/e mini-computer with a DECTape based OS/8 operating system and 16 K of core.

DIGFIL is a general-purpose Fourier transform program using the Fast Fourier Transform (FFT), and is an extensive modification of an earlier program (FFATOD) written by E. G. Coddington. DIGFIL will accept input either from teletype or DECTape, and will allow output to teletype, DECTape, an oscilloscope, or a chart recorder. The Fourier transformation section allows apodization either by the trapezoid of Chapter 5, or by a function stored earlier on DECTape. Output of the FFT section may be either the real, or imaginary series, or the amplitude spectrum. The phase spectrum may also be calculated if desired. The amplitude spectrum may also be phase corrected versus a reference stored in IPR: this feature allows calculation of phase-corrected amplitude spectra of interferograms obtained with a Michelson interferometer.

For proper operation, SUBROUTINE COOLTK is required. This subroutine is a modification by G. Horlick of a program written by Singleton (65) that allows

calculation of the FFT based on the Cooley-Tukey algorithm.

```

C
C      PROGRAM DIGFIL
C
COMMON X,Y,NP,N2POW,IPR
DIMENSION X(512),Y(512),J(512),IPR(512)
SOPDEF KCF      6030
SOPDEF DBCO     6505
SOPDEF DBSO     6506
C
C      DATA INPUT BEGINS
C
3      WRITE(1,502)
502    FORMAT ('INPUT:  TTY:1; DTA1:2')
      READ (1,503) NO
      IF (NO-1) 141,141,142
141    WRITE (1,540)
540    FORMAT('ENTER NO. POINTS TO READ, TOTAL NO., POWER OF 2, 313')
      READ (1,501) N,NP,N2POW
501    FORMAT (3I3)
      DO 1 I=1,NP
1      J(I)=0
      WRITE (1,503)
503    FORMAT ('ENTER DATA, 15')
      READ (1,500) (J(I),I=1,N)
500    FORMAT (15)
      GO TO 80
142    WRITE (1,541)
541    FORMAT ('ENTER NO. OF POINTS AND POWER OF 2, 213')
      READ (1,501) NP,N2POW
      WRITE (1,510)
      READ (1,511) C
      CALL IOPEN ('DTA1',C)
      READ (4,505) (J(I),I=1,NP)
80     DO 81 I=1,NP
81     X(I)=FLOTT(J(I))
S      CLA
S      TAD      \NP      /ENTER NO. OF POINTS
S      CIA      /NEGATE NP
S      DCA      POINT    /STORE IN POINT
S      CLA CLL
      JO=1
C
C      SCALING OF X ARRAY
C
33     S=X(1)
      DO 17 I=2,NP
      IF(X(I)-S)17,17,18
18     S=X(I)
17     CONTINUE
      C=X(1)
      DO 19 I=2,NP
      IF(X(I)-C)26,19,19
20     C=X(I)
19     CONTINUE
      S=1000./ (S-C)
      C=C*S
      WRITE(1,514)S,C
514    FORMAT('THE SCALING FACTOR IS 'F12.4' MINIMUM SCALED VALUE'F12.4)
      DO 28 I=1,NP
28     J(I)=S*X(I)-C

```



```

C
C      GENERAL OUTPUT BRANCHING
C
16      WRITE(1,508)
508     FORMAT('TTY:1; DTA1:2; SCOPE:3; RECORDER:4; CONTINUE:5; FFT:6; IFR:7')
      READ(1,509)NO
509     FORMAT(I3)
      IF (NO-7) 130,130,16
130     IF (NO-1) 16,131,131
131     GO TO(21,22,23,24,3,26,27)NO
C
C      FOURIER TRANSFORM SECTION
C
26      IF (JO) 72,70,72
72      WRITE(1,520)
520     FORMAT('SUBTRACT AVERAGE VALUE, Y OR N')
      JO=1
      READ(1,507)NO
      IF(NO-1632)54,56,54
56      S=0.0
      DO 55 I=1,NP
55      S=X(I)+S
      S=S/FLOAT(NP)
      DO 57 I=1,NP
57      X(I)=X(I)-S
C
C      APODIZATION SECTION
C
54      WRITE (1,530)
530     FORMAT ('APODIZATION, Y OR N')
      READ (1,5: ') NO
      IF (NO-1632) 99,90,99
90      WRITE (1,536)
536     FORMAT ('TTY:1, DTA1:2')
      READ (1,509) NO
      IF (NO-1) 91,91,135
C
C      TRAPEZOIDAL APODIZATION
C
91      WRITE (1,531)
531     FORMAT ('ENTER N1,N2,N3,N4: 4I3')
      READ (1,532) N1,N2,N3,N4
532     FORMAT(4I3)
      S=1./FLOAT(N2-N1)
      IF (N1) 94,94,92
92      NO=N1
      DO 93 I=1,N1
93      X(I)=0.
      GO TO 95
94      NO=1
95      DO 96 I=NO,N2
96      X(I)=X(I)+S*FLOAT(I-N1)
      S=1./FLOAT(N4-N3)
      DO 97 I=N3,N4
97      X(I)=X(I)+S*FLOAT(N4-I)
      DO 98 I=N4,NP
98      X(I)=0.
      GO TO 99
C
C      APODIZATION FROM STORED ARRAY (DTA1)
C
135     WRITE (1,510)
      READ (1,511) C
      CALL IOPEN ('DTA1',C)
      READ (4,505) (J(I),I=1,NP)
      DO 136 I=1,NP
136     X(I)=X(I)*FLOAT(J(I))
99      WRITE(1,525)
525     FORMAT('HAPPY? Y OR N')
      READ(1,507)NO
      IF(NO-1632)33,62,33

```



```

C
C      LOADING OF ARRAYS FOR FFT
C
62      NO=NP/2
        DO 52 I=1,NO
          Y(I)=X(2*I)
52      X(I)=X(2*I-1)
        DO 51 I=1,NO
          Y(I+NO)=0
51      X(I+NO)=0.
C
C      FOURIER TRANSFORMATION
C
        CALL COOLTK
        JOC=1
        JO=0
        WRITE (1,526)
526      FORMAT ('PHASE SPECTRUM.  Y OR N?')
        READ (1,507) NO
        IF (NO-1632) 70,71,70
C
C      CALCULATION OF PHASE SPECTRUM
C
71      WRITE (1,590)
590      FORMAT ('IMAX = ?  13')
        READ (1,509) N1
        N1=N1-1
        DO 710 I=1,NP
          S=ABS(Y(I))/X(I)
          PZ=ATAN(S)
          IF (Y(I)) 701,702,702
          IF (X(I)) 703,707,707
702      PZ=3.1415927-PZ
703      GO TO 707
          IF (X(I)) 705,706,706
701      PZ=3.1415927+PZ
705      GO TO 707
706      PZ=6.2831853-PZ
707      CONTINUE
          S=(3.1415927/FLOAT(NP))*FLOAT(I-1)*FLOAT(N1)
          PZ=PZ+S+3.1415927
          IF (PZ) 711,712,712
711      C=1.0
          GO TO 713
712      C=0.0
713      PZ=ABS(PZ)/6.2831853
          NO=IFIX(PZ)
          S=FLOAT(NO)
          J(I)=ABS(PZ-S-C)*1000.0
710      CONTINUE
        WRITE (1,550)
550      FORMAT ('PHASE CORRECT?  Y OR N?')
        READ (1,507) NO
        IF (NO-1632) 16,152,16
C
C      PHASE CORRECTION VERSUS REFERENCE PHASE IN IPR
C
152      DO 153 I=1,NP
        S=FLOAT(J(I)-IPR(I))*0.0062831853
        S=COS(S)
        Y(I)=S*Y(I)
        X(I)=X(I)*S
        IPR(I)=IPR(I)+10
        IF (S) 160,153,153
160      IPR(I)=-IPR(I)
153      CONTINUE
        JOC=0
        GO TO 16

```



```

C
C      FFT OUTPUT BRANCHING
C
70      WRITE(1,521)
521      FORMAT('X:1; Y:2; A:3; RETRANSFORM:4')
      READ(1,509)NO
      IF (NO-4) 132,132,70
132      IF (NO-1) 70,133,133
133      GO TO (33,75,59,72) NO
C
C      SWITCHING OF X AND Y FOR Y OUTPUT
C
75      DO 76 I=1,NP
      C=X(I)
      X(I)=Y(I)
76      Y(I)=C
      GO TO 33
C
C      CALCULATION OF AMPLITUDE SPECTRUM
C
59      DO 61 I=1,NP
61      X(I)=SQRT(X(I)*X(I)+Y(I)*Y(I))
      IF (J0C) 161,161,164
161      DO 162 I=1,NP
      IF (IPR(I)) 163,163,162
163      IPR(I)=-IPR(I)
      X(I)=-X(I)
162      IPR(I)=IPR(I)-10
      GO TO 33
164      S=X(1)
      DO 165 I=2,NP
      IF(X(I)-S)165,165,166
166      S=X(I)
165      CONTINUE
      S=1000 /S
      DO 167 I=1,NP
167      J(I)=S*X(I)
      GO TO 16
C
C      STORAGE OF PHASE REFERENCE IN IPR
C
27      DO 154 I=1,NP
      NO=IPR(I)
      IPR(I)=J(I)
154      J(I)=NO
      GO TO 16
C
C      TELETYPE PRINTOUT
C
21      WRITE(1,505)(J(I),I=1,NP)
505      FORMAT(10(15,1X))
      GO TO 16
C
C      OUTPUT TO DECtape STORAGE (DTR1)
C
22      WRITE(1,510)
510      FORMAT('ENTER FILE NAME, A6')
      READ(1,511)C
511      FORMAT(A6)
      CALL OPEN('DTR1',C)
      WRITE(4,505)(J(I),I=1,NP)
      CALL CLOSE
      GO TO 16

```



```

C
C      OSCILLOSCOPE OUTPUT SECTION
C
23      J(NP+1)=500
          J(NP+2)=1023
          J(NP+3)=500
          NO=NP+3
S      CLA CLL
S      TAD      \NO
S      CIA
S      DCA      POIN
SSET,   CLA
S      TAD      POIN      /GET NO. OF POINTS
S      DCA      10        /SET POINT COUNTER
S      TAD      K0177     /GET STARTING ADDRESS
S      DCA      11        /SET STARTING ADDRESS
SPLOT,  CLA CMA
S      DBCO      /CLEAR OUTPUT BUFFER
S      CLA
S      TAD      I  11      /GET DATA POINT
S      TAD      K2000      /SET OUTPUT FLAG
S      DBCO      /SET OUTPUT BUFFER
S      KSF      /CHECK FOR STOP FROM KEYBOARD
S      JMP      CONT
S      KCF      /CLEAR KEYBOARD BUFFER
S      JMP      \16      /EXIT
SCONT,  ISZ      10        /CHECK POINT COUNTER, SKIP IF ZERO
S      JMP      PLOT      /GET NEXT POINT
S      JMP      SET       /START OVER
C
C      RECORDER OUTPUT SECTION
C
24      WRITE(1,512)
512      FORMAT('ENTER DELAY, 13')
          READ(1,509)NT
S      CLA CLL
S      TAD      POINT      /GET NO. OF POINTS
S      DCA      10        /SET POINT COUNTER
S      TAD      K0177     /GET STARTING ADDRESS
S      DCA      11        /SET STARTING ADDRESS
31      DO 32      I=1,NT
32      NO=1*1
S      CLA CMA
S      DBCO      /CLEAR OUTPUT BUFFER
S      CLA
S      TAD      I  11      /GET DATA POINT
S      TAD      K2000      /SET OUTPUT FLAG
S      DBCO      /SET OUTPUT BUFFER
S      CLA
S      ISZ      10        /CHECK POINT COUNTER, SKIP IF ZERO
S      JNP      \31
          GO TO 16
SK2000, 2000
SP0IN,  0000
SP0INT, 0000
SK0177, 0177
507      FORMAT (A1)
4      CALL EXIT
          END

```



```

C      SUBROUTINE COOLTK      SOURCE:  G. HORLICK
C      THIS SUBROUTINE PERFORMS A FAST FOURIER TRANSFORM
C      BASED ON THE COOLEY-TUKEY ALGORITHM.  AN INPUT
C      ARRAY OF REAL DATA OF LENGTH NP (2**N2POM) MUST
C      FIRST BE SORTED SO THAT THE ORIGINAL ODD-NUMBERED
C      POINTS APPEAR IN THE FIRST NP/2 ELEMENTS OF X AND
C      THE ORIGINAL EVEN-NUMBERED POINTS APPEAR IN THE
C      FIRST NP/2 ELEMENTS OF Y.  THE REMAINING ELEMENTS
C      OF X AND Y ARE FILLED WITH NP/2 ZEROES APIECE.
C      THE OUTPUT CONTAINS NP POINTS OF THE
C      REAL TRANSFORM IN X AND NP IMAGINARY POINTS IN Y.
C

```

```

      SUBROUTINE COOLTK
      COMMON X,Y,NP,N2POM,IPR
      DIMENSION X(512),Y(512),IPR(512)
      DIMENSION L(13)
      N=NP
      NTHPOM=3**N2POM
      N4POM=N2POM/2
      IF(N4POM)60,63,60
60      DO 61 IPASS=1,N4POM
      NXTLTH=2**((N2POM-3)+IPASS)
      LENGTH=4*NXTLTH
      SCALE=6.3831653/FLOAT(LENGTH)
      DO 61 J=1,NXTLTH
      ARG=FLOAT(J-1)*SCALE
      C1=COS(ARG)
      S1=SIN(ARG)
      C2=C1*C1-S1*S1
      S2=C1*S1+C1*S1
      C3=C1+C3-S1+S2
      S3=C3*S1+S2+C1
      DO 61 ISOL00=LENGTH,NTHPOM,LENGTH
      J1=ISOL00-LENGTH+J
      J2=J1+NXTLTH
      J3=J2+NXTLTH
      J4=J2+NXTLTH
      R1=X(J1)+X(J3)
      R2=X(J1)-X(J3)
      R3=X(J2)+X(J4)
      R4=X(J2)-X(J4)
      FI1=Y(J1)+Y(J3)
      FI2=Y(J1)-Y(J3)
      FI3=Y(J2)+Y(J4)
      FI4=Y(J2)-Y(J4)
      X(J1)=R1+R3
      Y(J1)=FI1+FI3
      IF(J-1)64,62,64
64      X(J3)=C1*(R2+FI4)+S1*(FI2-R4)
      Y(J3)=-S1*(R2+FI4)+C1*(FI2-R4)
      X(J2)=C3*(R1-R3)+S2*(FI1-FI3)
      Y(J2)=-S2*(R1-R3)+C3*(FI1-FI3)
      X(J4)=C3*(R2-FI4)+S3*(R4+FI2)
      Y(J4)=-S3*(R2-FI4)+C3*(R4+FI2)
      GO TO 61
62      X(J3)=R2+FI4
      Y(J3)=FI2-R4
      X(J2)=R1-R3
      Y(J2)=FI1-FI3
      X(J4)=R2-FI4
      Y(J4)=R4+FI2
61      CONTINUE
63      IF(N2POM-2*N4POM)65,66,65
65      DO 67 J=1,NTHPOM,2
      R1=X(J)+X(J+1)
      R2=X(J)-X(J+1)
      FI1=Y(J)+Y(J+1)
      FI2=Y(J)-Y(J+1)
      X(J)=R1
      Y(J)=FI1
      X(J+1)=R2
67      Y(J+1)=FI2

```



```

66      DO 68 J=1,13
          L(J)=1
          IF(J-N2P0N)69,69,68
69      L(J)=2**((N2P0N+1-J)
68      CONTINUE
          IJ=1
          L1=L(13)
          NTHP0N=L(12)
          ISOLOC=L(11)
          J=L(10)
          N2P1=L(9)
          N2=L(8)
          NP2MJ=L(7)
          L8=L(6)
          N2P0=L(5)
          N4P0N=L(4)
          LENGTH=L(3)
          NXTLTH=L(2)
          IPASS=L(1)
          DO 601 J1=1,L1
              DO 601 J2=J1,NTHP0N,L1
                  DO 601 J3=J2,ISOLOC,NTHP0N
                      DO 601 J4=J3,J,ISOLOC
                          DO 601 J5=J4,N2P1,J
                              DO 601 J6=J5,N2,N2P1
                                  DO 601 J7=J6,NP2MJ,N2
                                      DO 601 J8=J7,L8,NP2MJ
                                          DO 601 J9=J8,N2P0,L8
                                              DO 601 J10=J9,N4P0N,N2P0
                                                  DO 601 J11=J10,LENGTH,N4P0N
                                                      DO 601 J12=J11,NXTLTH,LENGTH
                                                          DO 601 J1=J12,IPASS,NXTLTH
                                                              IF(IJ-J1)610,610,601
610                      R=X(IJ)
                          X(IJ)=X(J1)
                          X(J1)=R
                          FI=Y(IJ)
                          Y(IJ)=Y(J1)
                          Y(J1)=FI
601                      IJ=IJ+1
                          ARG=3.1415927/FLOAT(N)
                          C1=COS(ARG)
                          S1=-SIN(ARG)
                          C1JX=1
                          S1JX=0.
                          N2=N/2
                          N2P1=N2+1
                          DO 70 J=2,N2P1
                              NP2MJ=N+2-J
                              SORR1=X(J)+X(NP2MJ)
                              SORF1=Y(J)-Y(NP2MJ)
                              R=C1JX
                              C1JX=C1JX+C1-S1JX+S1
                              S1JX=R+S1+S1JX+C1
                              SORR2=X(J)-X(NP2MJ)
                              SORF2=Y(J)+Y(NP2MJ)
                              SORR3=C1JX+SORR2-S1JX+SORF2
                              SORF3=C1JX+SORF2+S1JX+SORR2
                              Y(J)=0.5*(SORF1-SORR3)
                              X(J)=0.5*(SORR1+SORF3)
                              IF(J-N2P1)71,70,71
71                      Y(NP2MJ)=0.5*(-SORF1-SORR3)
                          X(NP2MJ)=0.5*(SORR1-SORF3)
70      CONTINUE
          X(1)=X(1)+Y(1)
          Y(1)=0.
          RETURN
          END

```


B30174